NASA CR-72979
Bell Model 8606

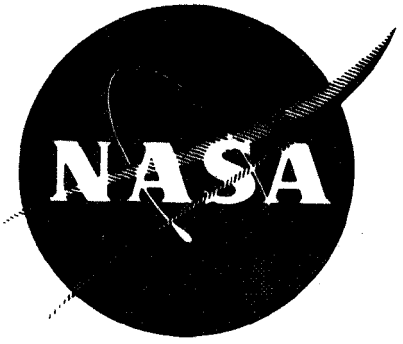

EVALUATION OF METALLIC POSITIVE EXPULSION BELLOWS OPERATING PARAMETERS WITH CRYOGENIC PROPELLANTS

by

R. L. Lange

and

J. T. Hughes

Bell Aerospace Company
A Division of Textron

prepared for

NATIONAL AERONAUTICS AND SPACE ADMINISTRATION

NASA Lewis Research Center
Contract NAS 3-13327
Rudy Grey, Project Manager

NOTICE

This report was prepared as an account of Government-sponsored work. Neither the United States, nor the National Aeronautics and Space Administration (NASA), nor any person acting on behalf of NASA:

A.) Makes any warranty or representation, expressed or implied, with respect to the accuracy, completeness, or usefulness of the information contained in this report, or that the use of any information, apparatus, method, or process disclosed in this report may not infringe privately-owned rights; or

B.) Assumes any liabilities with respect to the use of, or for damages resulting from the use of, any information, apparatus, method or process disclosed in this report.

As used above, ''person acting on behalf of NASA'' includes any employee or contractor of NASA, or employee of such contractor, to the extent that such employee or contractor of NASA or employee of such contractor prepares, disseminates, or provides access to any information pursuant to his employment or contract with NASA, or his employment with such contractor.

Requests for copies of this report should be referred to

National Aeronautics and Space Administration
Scientific and Technical Information Facility
P. O. Box 33
College Park, Md. 20740

NASA CR-72979
Bell Model 8606

FINAL REPORT

EVALUATION OF METALLIC POSITIVE EXPULSION BELLOWS OPERATING PARAMETERS WITH CRYOGENIC PROPELLANTS

by

R. L. Lange

and

J. T. Hughes

Bell Aerospace Company,
A Division of Textron

Post Office Box One
Buffalo, New York 14240

prepared for

NATIONAL AERONAUTICS AND SPACE ADMINISTRATION

July 26, 1971

Contract NAS 3-13327

NASA Lewis Research Center

Cleveland, Ohio

Rudy Grey, Project Manager

Propulsion Section, Liquid Rocket
Technology Branch

FOREWORD

The research described herein was conducted at the Bell Aerospace Company, a Division of Textron, under NASA Contract NAS 3-13327 with Mr. Rudy Grey, Propulsion Section, Liquid Rocket Technology Branch, NASA-Lewis Research Center, as Project Manager.

ABSTRACT

This report describes the work performed to meet the program objective of determining any change in the ability of Metallic Positive Expulsion Bellows to react the damage mechanisms of vibration, fatigue, storage and buckling while containing liquid hydrogen or liquid oxygen. The results of the test program were compared to the results of a previously conducted similar test program at ambient temperature. The results of the program have shown that metallic bellows are suitable for positive expulsion of liquid hydrogen and liquid oxygen. The data obtained has been used to correct analytical techniques for predicting wear, cycle life, buckling pitch and strain distribution patterns.

SUMMARY

This report describes the work performed in accordance with NASA-Lewis Research Center Contract NAS 3-13327 to evaluate the effects of cryogenic propellants on Metallic Positive Expulsion Bellows operating parameters in a simulated mission duty cycle environment.

The program objective was to determine any change in the ability of the bellows to react the damage mechanisms of vibration, expulsion, high strain fatigue, storage and incipient buckling, while containing liquid hydrogen or liquid oxygen. A second objective was to revise design and computer data, as required, to account for any changes in design criteria required by these propellants.

The program scope encompassed a test program, the results of which were compared to the results of a previously conducted test program at ambient temperature, and an analytical program using material property data for cryogenic temperatures for prediction of the test program results. The test program subjected three convolute bellows test specimens to a series of vibration, storage, expulsion cycling and incipient buckling in a liquid hydrogen and liquid oxygen environment.

The bellows test specimens were designed and fabricated by Bell Aerospace Company, a division of Textron. The bellows cores were fabricated by DK Aerospace Company from a seamless tube fabricated by Rollmet Inc. The specimens were dynamically tested in a unique apparatus capable of vibratory motion in two mutually perpendicular axis while maintaining a cryogenic environment. The remaining tests were conducted in a multi-purpose; cycling, storage, and buckling apparatus capable of monitoring bellows motion while maintaining a cryogenic environment.

The analytical evaluation techniques used for predicting wear, cycle life, buckling pitch and strain distribution patterns were corrected for propellant effects and correlated to the test results. The program has shown that metallic bellows are suitable for positive expulsion of liquid hydrogen and liquid oxygen exhibiting greater wear resistance and higher cycle life than bellows tested at ambient conditions.

GLOSSARY OF TERMS

Abrasion - wear resulting from oscillatory motion of mating surfaces which breaks down any natural protective film causing the material to adhere and break away at each oscillation. Those particles broken away are usually work hardened and act as an abrasive to the mating parts.

Buckle - localized deformation caused by compressive strains within the convolution (annular ring) resulting in an unstable strain state.

Convolution - one of a set of identical annular rings forming a bellows. One convolution is composed of one root, one crest and two sidewalls.

Core - a full set of convolutions forming the bellows.

Cryoforming - the process of metal forming at cryogenic temperatures resulting in increased mechanical strength properties.

Cryostat - a vacuum insulated chamber.

Crippling (buckle) - a convolution crest deformation of sufficient severity to prevent normal bellows operation.

Crest - the tightly formed radius on the convolute forming the bellows maximum (outside) diameter.

Dewar - a double walled cryogenic vessel with a vacuum space between walls.

Expulsion Cycle - the bellows motion required to progress from the nested position to the extended position and back to the nested position.

Extended Pitch - the fully loaded bellows pitch at maximum temperature.

Free-Side (Bellows) - the unrestrained side of the test specimen

Free Length - the bellows core length at pressure equilibrium

Incipient - for the purposes of this report incipient is synonymous with visually detectable.

Impact - wear which results from a collision of two surfaces

Life Cycle - the number of complete expulsion cycles before failure.

Leaf - that portion of the convolution between the root and crest. In this report the terms leaf and sidewall are used interchangeably

Mission Duty Cycle - a complete spectrum of all the damage mechanisms a device would be exposed to in service.

Nested Pitch - the minimum allowable collapsed bellows pitch

Oscillation - a single sweep from one extreme limit to the other in a vibrating body.

Oscillogram - a motion record of an oscillating body

Pitch - axial distance from a point on one convolution to an identical point on an adjacent convolution.

Root - the tightly formed radius on the convolution forming the bellows minimum (inside) diameter.

Sidewall - see leaf

Span - the radial distance between the convolution inside (root) radius and outside (crest) radius.

Wear - metal removal as a result of vibratory motion.

TABLE OF CONTENTS

LIST OF FIGURES

LIST OF TABLES

INTRODUCTION

The complex mission duty cycle requirements of spacecraft have led to the development of propellant positive expulsion devices for either reaction control systems or main tank propellant positioning. In recent years, several highly efficient devices have been designed for this purpose. Pistons, flexible membranes, metal bellows and surface tension apparatus have been used to separate the pressurizing gasses from the propellants. The device selected for any particular mission is dependent upon the requirements of the specific application.

The metallic positive expulsion bellows has found common acceptance where long-term storage, multiple cycles and propellant compatibility are of prime importance. A metal bellows is a cylindrically shaped device with accordion-like convolutions along the outside which provide its extension capability. The convolutions are made by either welding annular rings together at the inside and outside diameters or by hydroforming them from tubes. The selection of either welded or formed bellows is dependent upon the requirements of a specific application.

Metal bellows have been successfully used as positive expulsion devices for several years with earth storable propellants at ambient conditions. With an extension of this application to cryogenic propellants, however, many questions have been raised regarding the ability of metallic positive expulsion bellows to react the loads imposed during a typical mission duty cycle while at cryogenic temperatures.

These questions were primarily concerned with the effects of the known changes in the bellows material properties of strength, crack propagation, fatigue, strain hardening and elastic modulus at these low temperatures relative to bellows operation.

The program objective described by this report was to determine any change in the ability of the bellows to react the damage mechanisms of vibration, expulsion cycle - high strain fatigue, storage and incipient buckling, while containing liquid hydrogen (LH_2) and liquid oxygen (LO_2). A second objective was to revise design and computer data, as required, to account for any changes in design criteria required by these propellants.

The bellows configuration selected for this program was designed by Bell Aerospace Company (BAC). The bellows core design is identical to that developed for the Minuteman program and subsequently used on a Bell Aerospace Company Independent Research and Development (IR&D) evaluation. The cores were fabricated at DK Aerospace (Division of MSL Industries, Inc.) from seamless tubes fabricated by the Rollmet Company (A Division of Wyman-Gordan, Inc.)

The approach to this program was a parametric comparison of the results of the cryogenic test program to a similar test program previously conducted at room temperature where the only variable is the test fluid, LH_2 and LO_2. The room temperature data base was the result of the Minuteman Development Program and the Bell Aerospace IR&D Program which studied the effects of wear and impact on bellows life. Using these comparisons, new formula constants and design criteria were developed along with qualitative data from results which were not general in nature. Although the data is developed for one specific design, it can be applied to any design by determining the scaling effects or influence factors for the new design.

BELLOWS DESIGN AND FABRICATION

The design of bellows for positive expulsion tanks has evolved from an empirical evaluation of available bellows configurations to the use of highly sophisticated, computerized, analytical design techniques for the prediction of strain patterns, cycle life, buckling pitch, wear and fatigue for configuration definition. The bellows tested in this program is the configuration designed and developed for the Minuteman III Program and was chosen because of the large data base available with which to compare the test results.

The Minuteman seamless formed bellows configuration is a single sweep leaf design. (Refer to Figure 1). The root and crest bend radius minimizes nested height but is large enough to prevent crack initiation sites. The number of convolutes and diameter is a function of volume required and space limitations. The span and pitch dimensions are the result of optimizing stiffness requirements, maximum efficiency and adequate margin below incipient buckling pitch.

With this design which simulated the Minuteman bellows tanks materials, fabrication procedures, surface finishes and circumferential dimensions, the bellows test specimens were subjected to a test program simulating the most significant damage mechanisms to which bellows are exposed in service.

Test Specimen Design

The bellows test specimen assembly consists of a three-convolute bellows core welded to end plate closures with provisions for cryogen flow, mounting and instrumentation attachment. (Refer to Figures 2 and 3). The bellows core to end plate weld is a semi-butt automatic TIG weld of .007 inch (.01778 cm) bellows core to a .010 inch (.0254 cm) weld land. Both parts are 347 stainless steel. The end plates have provisions for instrumentation blocks at the particular test position, for stud mounted accelerometers. Also mounted to each end plate is a trunnion which has a dual role of specimen support and motion transmission. One end plate has ports to allow access to the internal volume of the specimen. The ports, along with the instrumentation mounting studs, were positioned with one vent port at the top and one set of studs at the bottom for any of three test positions.

A three-convolute bellows core was chosen for two reasons: first, the center convolute strain pattern is typical of that in any but end convolutions for multiple convolute bellows and, second, by positioning only the center convolution on the simulated tank shell very close control was obtainable during vibration testing.

Results provided by the Reference 5 computer program show that

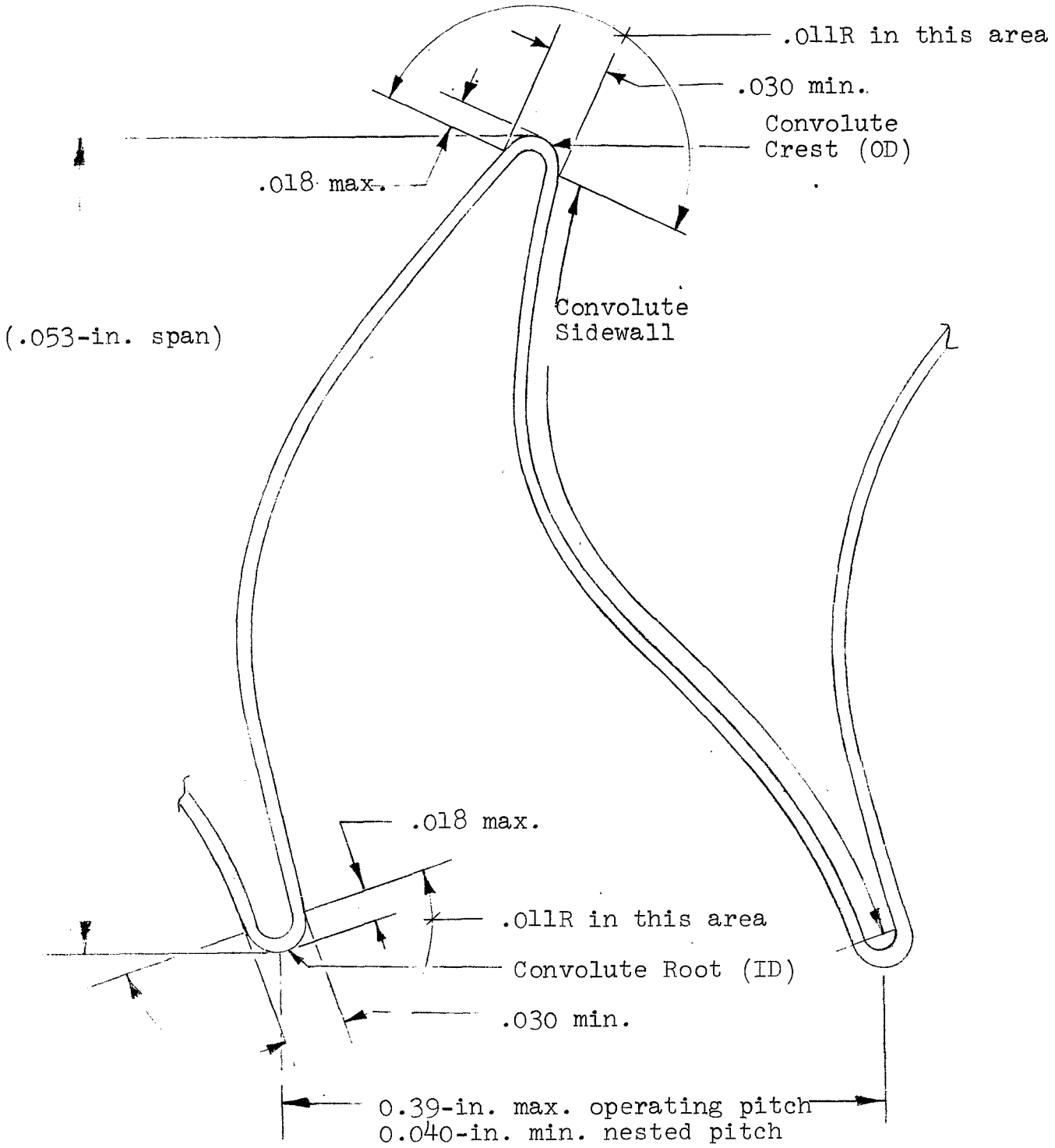

TEST SPECIMEN

FIGURE 1 BELLOWS CONVOLUTE CONFIGURATION

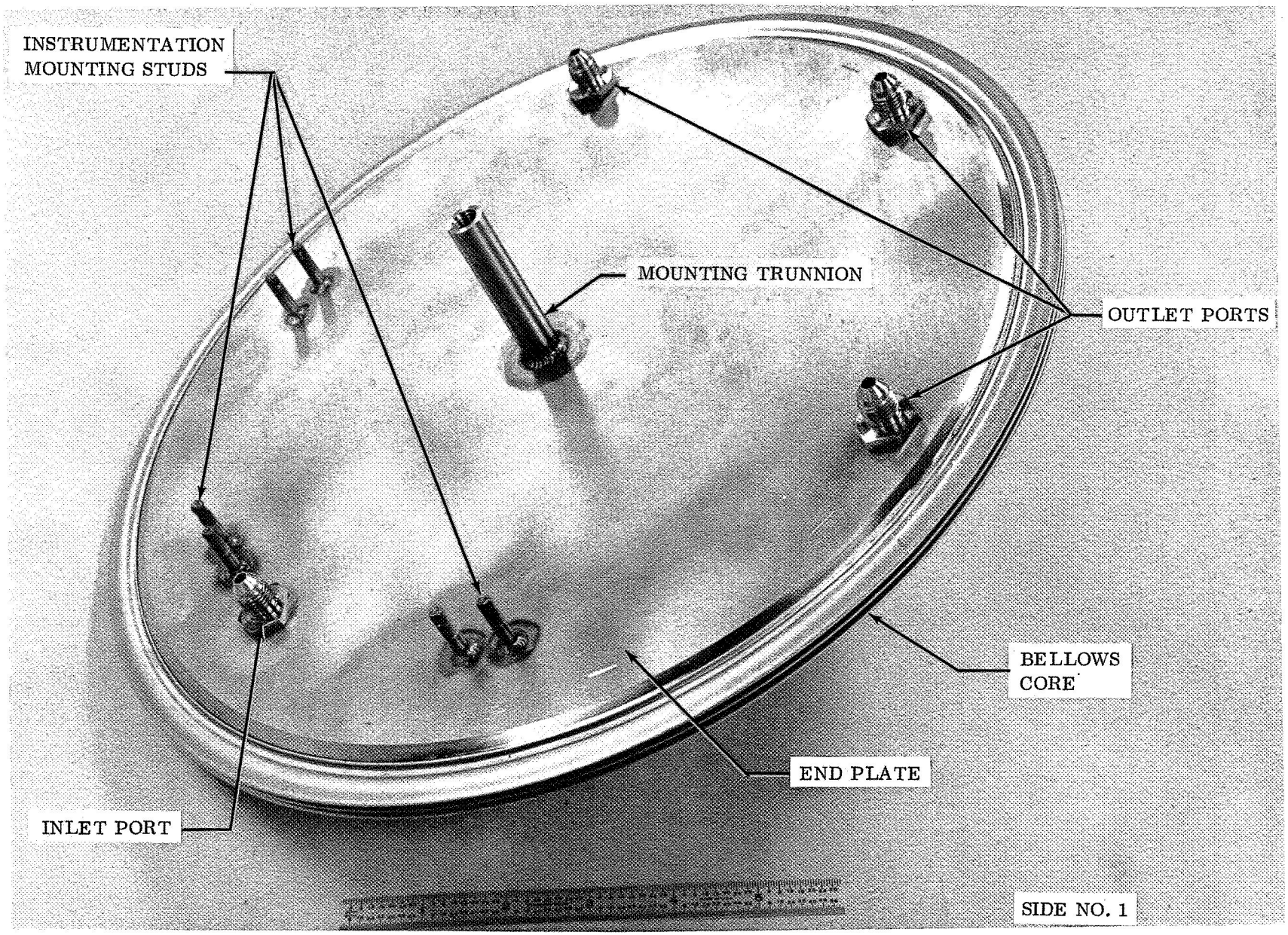

FIGURE 2. PORT SIDE BELLOWS TEST SPECIMEN ASSEMBLY

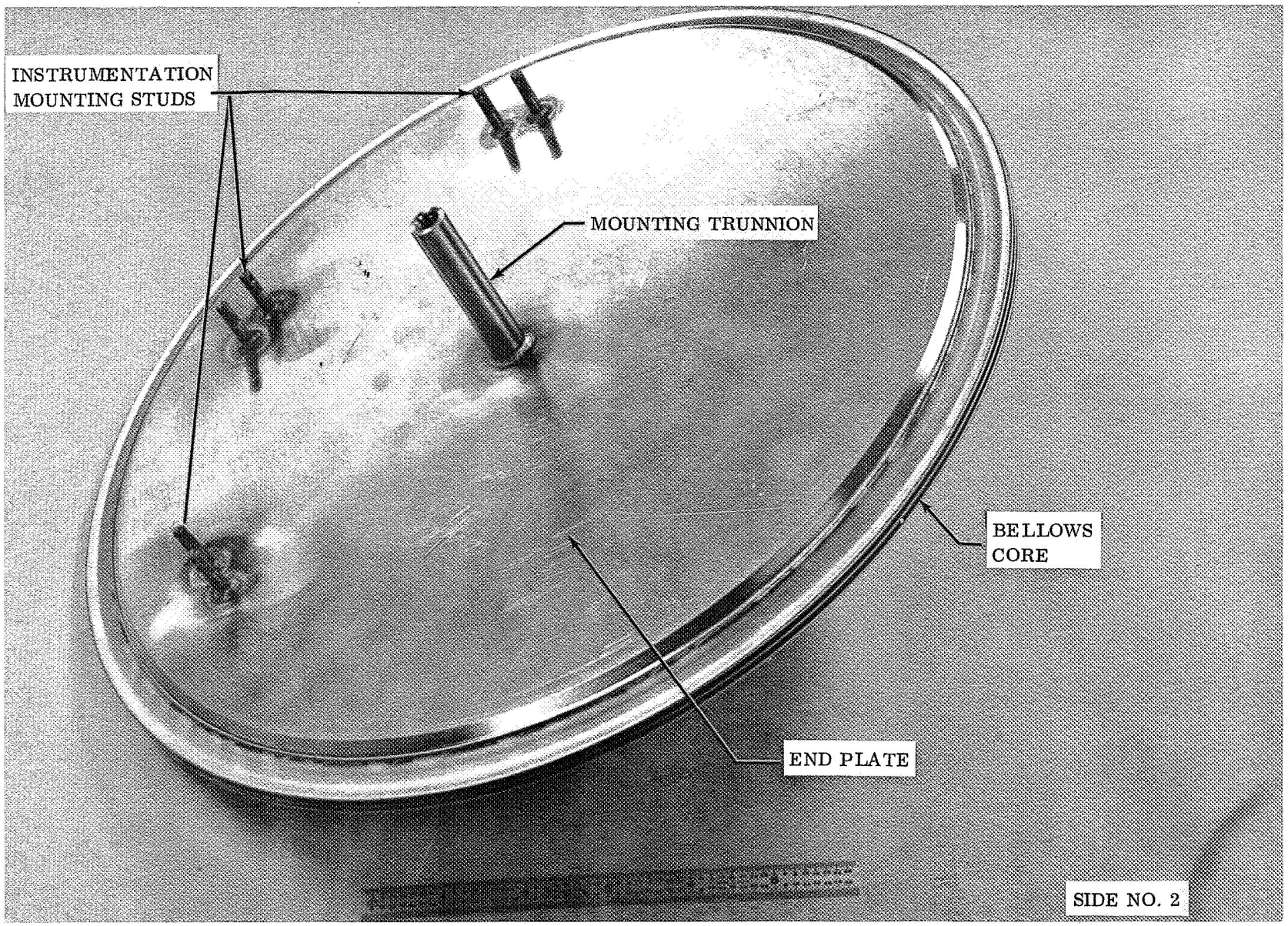

FIGURE 3. CLOSED SIDE BELLOWS TEST SPECIMEN ASSEMBLY

the stress-strain pattern due to the end attachment stiffening effects, during extension and nesting, are completely damped out within the first full convolute. Two computer runs were made with different end restraints, but otherwise identical bellows geometric configuration and loading. The results are presented in Figure 4. In one case the ends were assumed fully clamped, while in the other, the ends were simply supported. The strains become essentially equal within 1/3 of a convolute and become identical within 3/4 of a convolute. The results are essentially the same regardless of which end is analyzed. The meridional bending strain was used for this analysis because it is the largest strain and also the most sensitive to differences in convolute shape. This means that the strain patterns and levels of the center convolution duplicated those in a multiple convolute bellows.

The three convolution bellows specimens are ideal for the vibration tests because of the degree of control possible with just one convolute impacting and abrading on the tank shell segment. In a typical positive expulsion tank, the bellows profile is not perfectly uniform, with some convolutions protruding several thousandths of an inch beyond others. These "proud" convolutions result in a non-uniform loading pattern since they assume the majority of the load and are most severely worn. By applying the load to just the center convolution, the profile variation of a typical multi-convolution bellows is not a factor and need not be considered in data evaluation.

The operating range of the bellows configuration shown in Figure 1 is based upon maximizing the extension ratio of operating pitch to nested pitch. The nested pitch is controlled to prevent material "folding" in the compressive surfaces (inside radius) of a safe margin below the experimentally determined buckling modes. The analysis of this configuration, verified by empirical results, shows that the minimum allowable bend radii for this material is 1.2 times the material thickness, .007 inch (.01778 cm) x 1.2 = .0084 inch (.0233 cm). It also shows that the incipient buckling pitch at room temperature is 0.62 inch (1.5748 cm) resulting in the selection of .39 inch (.9906 cm) as the maximum extended pitch and .37 inch (.9398 cm) as the nominal operating pitch. These pitches were selected for a span of 0.53 inch (1.3462 cm).

Test Specimen Fabrication

The bellows cores were fabricated from seamless tubes. The seamless tubes were cold-roll extruded from type 347 SST forgings to a 12.5 inch (31.75 cm) diameter and 0.007 inch (0.178 mm) thickness. The cores were fabricated in accordance with existing production bellows forming techniques and tooling. The convolutions were individually formed by expanding the tube outward into the forming dies with internal pressure. The dies were then closed providing the basic convolution shape and size. The cores were formed in

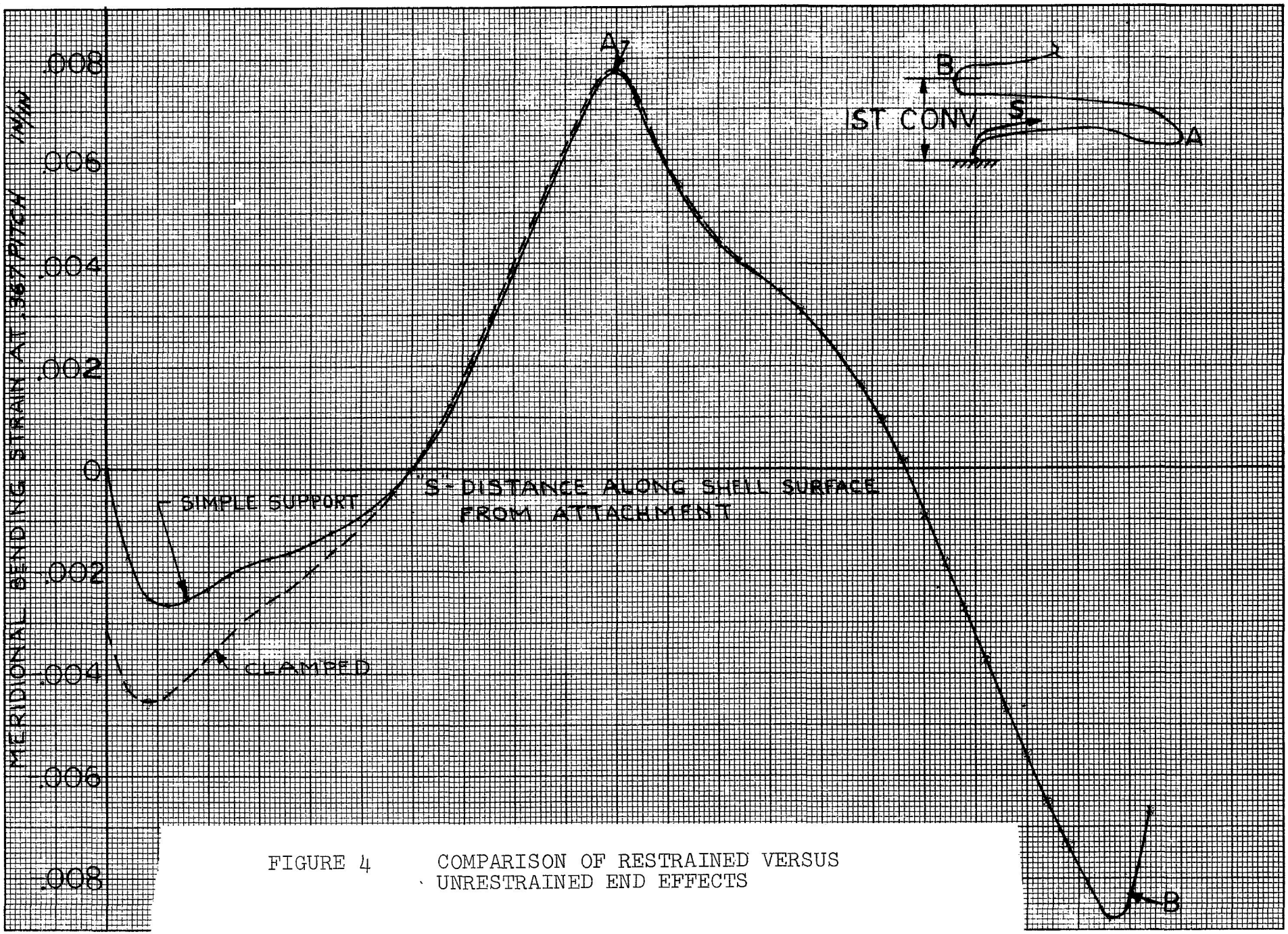

FIGURE 4 COMPARISON OF RESTRAINED VERSUS UNRESTRAINED END EFFECTS

groups of 3 convolutions with a space between them to facilitate trimming and separation for welding. After forming the final convolution shape is achieved by the close pitch operation which compresses each convolution between two dies forming the root and crest bend radii and sidewall shape. The bellows core is then cleaned and packaged to prevent contamination.

The bellows test specimen end plates were fabricated from 347 SST sheet material by simultaneously piercing the holes and shearing the profile. The end plates were then straightened, machined and cleaned in preparation for welding. After the trunnions fittings, and studs were welded to the end plates, the end plate assemblies were straightened and final trimmed in preparation for the bellows to end plate weld.

It is impossible to separate the design of the bellows from that of the shell since it is the shell that transmits the dynamic loads and provides the mating surfaces for bellows motion. The tank shell used in the dynamic fixture simulated that for the Minuteman tank assembly. It was "shear-formed" from an A-286 stainless steel forging. After final machining, the shell segment is 13.605 inch (34.556 cm) inside diameter, .025 inch (.0635 cm) thick, .375 inch (.9525 cm) wide and with an inside surface finish of 16 RMS. The clearance between the bellows and shell is approximately .07 inch (.1778 cm).

A very precise final trim on the bellows cores was required to maintain a very closely controlled amount of metal in the bellows to end plate weld joint. This trimming was accomplished by assembling the core in trimming rings which act as guides for the final trim operation. This operation is depicted photographically in Figure 5. After final trimming the bellows core neck diameter is carefully measured and trimmed prior to assembly into the weld fixtures. Each end plate is also trimmed to the same diameter and matched as sets, prior to assembly.

The clearance between the final trimmed end plate and bellows assembly was controlled to a tolerance of +.000 and -.002 inches. This close tolerance fitup provided a uniform heat sink and consequently uniform weld bead. The bellows and end plate was then tack welded to provide positive location of mating parts and finally the closure weld was made. During welding the weld area was purged with Argon to prevent oxidation. The weld apparatus is shown in Figure 6. A cross-section metallurgical sample of the final assembly including the closure weld is shown in Figure 7. The port side of a completed bellows test specimen is shown in Figure 2 and the closed side of the specimen is shown in Figure 3.

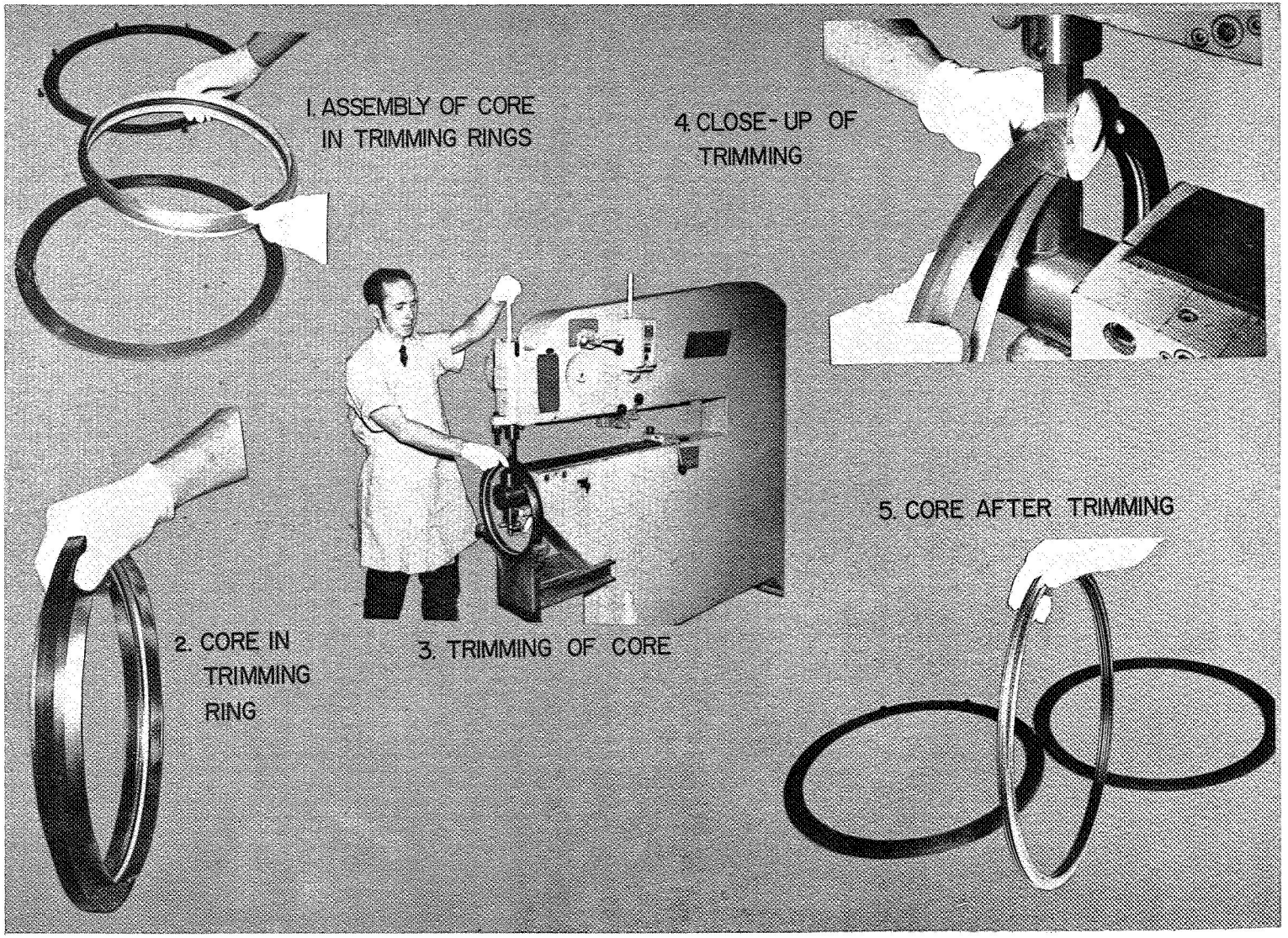

FIGURE 5. TRIMMING OF CRYOGENIC BELLOWS

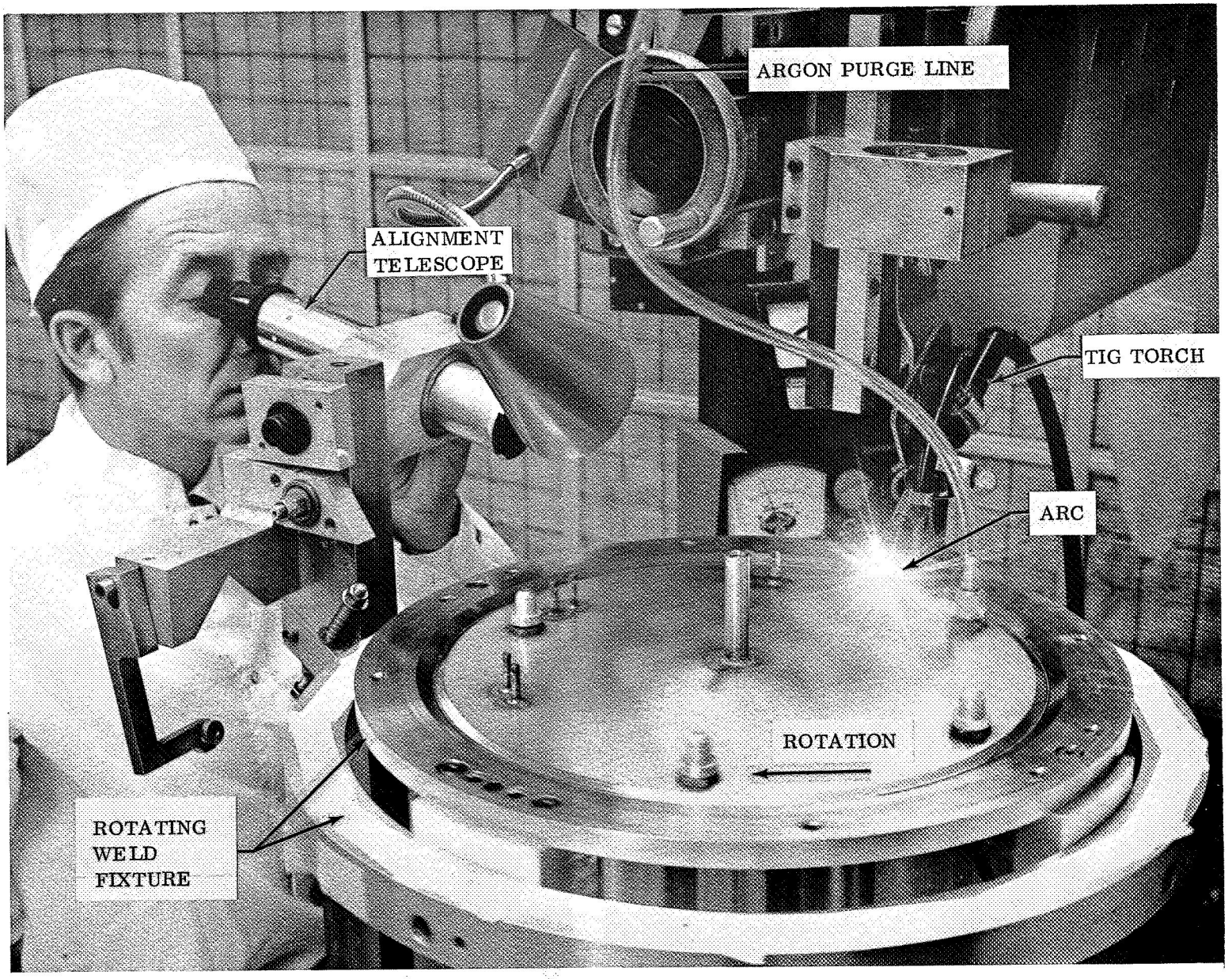

FIGURE 6. BELLOWS CORE TO END PLATE WELD APPARATUS

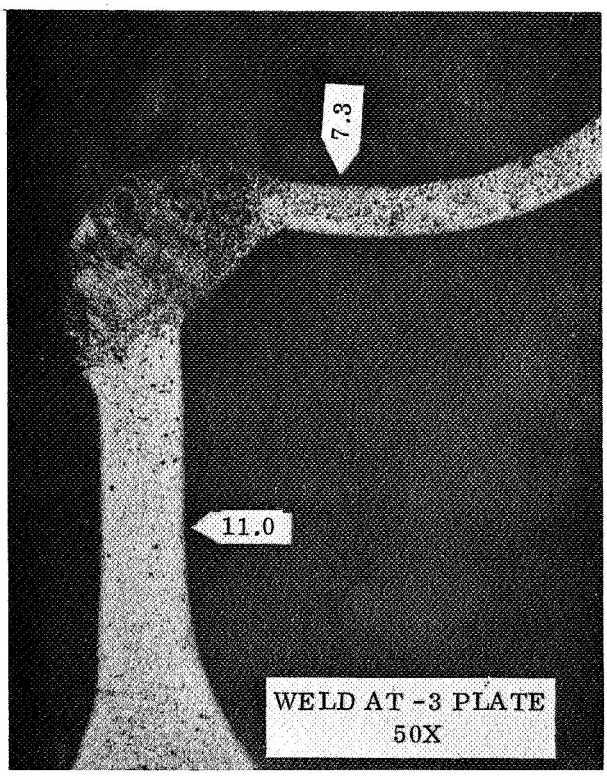

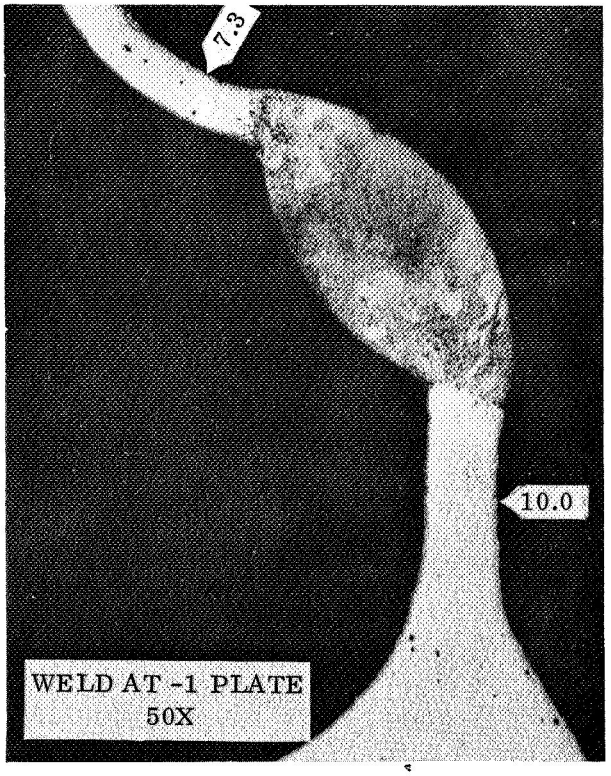

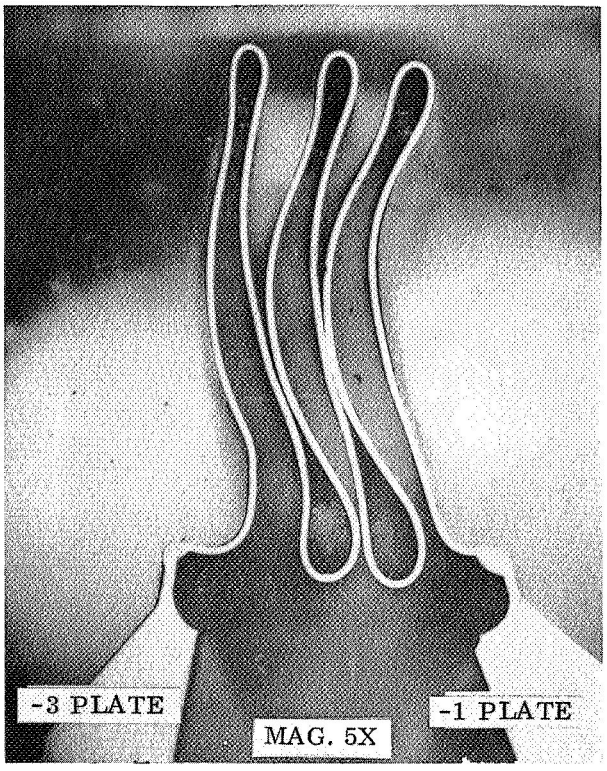

THE WELDS ARE OF SATISFACTORY CONTOUR AND ARE FREE OF DEFECTS.

METAL THICKNESS, IN MILS, WAS DETERMINED AT 200X WITH FILAR EYEPIECE.

BELLOWS WAS DISTORTED SOMEWHAT DURING MOUNTING.

PART NO. 8606-471001

ETCHANT: MIXED ACID.

FIGURE 7. SECTION THRU BELLOWS AND WELDS OF S/N 1 CRYOGENIC TEST BELLOWS

TEST PROGRAM

The test program was designed to impose particular damage mechanisms, to predetermined levels and durations on the bellows after which they were carefully examined metallurgically to determine the degree of damage incurred. This degree of damage was then compared to the damage incurred during similar testing at the various temperatures as well as to that predicted analytically. The baseline for the imposed test levels and durations were derived from the Minuteman Mission Duty Cycle. A typical Minuteman Mission Duty Cycle (MDC) would include 5 complete expulsion cycles to simulate bellows fabrication, cleaning and loading, exposure to transportation and handling vibration, flight dynamics and one complete expulsion. The test program not only imposed the damage mechanisms singly at various temperatures, but also in combinations, with the sequence of these combinations varied to determine if sequence had any effect on the degree of damage incurred.

A total of 22 bellows specimens were tested in the program, 14 were tested in liquid hydrogen (LH_2), 7 in liquid oxygen (LO_2) and 1 at room temperature (RT). The greater emphasis was placed on the LH_2 tests because of the extreme environment associated with LH_2 and the lack of available data for 347 SS at these temperatures. In order to make maximum use of the specimens, each vibration specimen was used in three modes (impact alone, abrasion alone and combined impact and abrasion) by rotating the specimen to an undamaged area for each test. The LH_2 test program was as follows:

Specimen No's.	Test Sequence
1,2	a) Pretest expulsion cycling b) 45 Day Storage c) Vibration d) Leak Test e) Metallurgical Evaluation

Specimen No's.	Test Sequence
3,4	a) 45 Day Storage b) Leak test c) Metallurgical Evaluation
5,6	a) 45 Day Storage b) Vibration c) Leak Test d) Metallurgical Evaluation
7,8	a) Vibration b) Leak Test c) 45 Day Storage d) Leak Test e) Metallurgical Evaluation
9,10	a) Vibration b) Leak Test c) Metallurgical Evaluation
11,12	a) 45 Day Storage b) Incipient Buckling c) Leak Test d) Metallurgical Evaluation
13	a) 200 Expulsion Cycles b) Leak test c) Expansion Cycling to Failure d) Metallurgical Evaluation
14	a) 200 Expulsion Cycles b) Leak Test c) Metallurgical Evaluation

The LO_2 Program was as follows:

15,16,17	a) Pretest Expulsion Cycling b) Vibration c) Leak Test d) Metallurgical Evaluation
18,19	a) Vibration b) Leak Test c) Metallurgical Evaluation
20,21	a) Expulsion Cycling to Failure b) Metallurgical Evaluation

One bellows specimen, an unused spare, was expulsion cycled to failure at room temperature for comparison purposes.

This report discusses each of the damage mechanisms individually to facilitate comparisons at various temperatures and with analytically derived predictions. Any variation in damage due to sequence is also discussed in the individual sections.

EXPULSION CYCLING

Expulsion cycle life is an important feature for positive expulsion devices. With the advent of multi-mission concepts, this capability takes on additional importance to insure that the reliability of the device is maintained during reuse. The cycle life of a metallic bellows is limited by the fatigue life of the material for the particular strain pattern imposed by the design and operating conditions. In most cases the bellows is designed to operate in the plastic region of the material property curve. Since it is deliberately yielded during cycling, work hardening results, and coupled with operation at cryogenic temperatures the question of multiple cycle operation at these temperatures was raised. These tests were conducted to determine if cryogenic operation would result in any unexpected life limiting damage mechanism.

Expulsion cycling can be divided into cycling for pretest conditioning and expulsion cycle life test. The test results were compared to the cycle life predictions from the analytical strain determination derived from the elastic deformation computer program described in Reference 5. The sequence of test and summary of results is presented in Figure 8.

Bellows Pretest Conditioning

These bellows test specimens were conditioned for future testing such as storage or vibration by conducting five expulsion cycles. This was done to expose the specimens to plastic deformation, simulating the stressed condition associated with the cleaning and loading of a tank assembly. The purpose of this conditioning was to assess the effect of testing the specimen in varying sequences.

Expulsion Cycle Life Test

This test was designed as a verification test to demonstrate a 200 expulsion cycle cability sufficient to complete the expulsion cycle portion of 20 to 40 typical mission duty cycles without failure while submerged in cryogen. After confirming this capability additional cycle testing was conducted on a cycle to failure basis to establish design margins.

These tests must not be construed as material fatigue data, but as a gross comparison of bellows cycle life capability at various temperatures to indicate temperature effects and associated cycle life limiting damage mechanisms, if any. The cycle to failure test was conducted with one specimen in liquid hydrogen, two with liquid oxygen and one at room temperature.

Test Spec.	Spec. Ser.#	LH_2 Test Sequence					Results
1 2	2 4	(5) Pre-test cycling	45-day LH_2 Storage	Vibration Testing	Leak Test	Metall. Eval.	Any damage seen was attributed to the vibration test, no evidence of corrosion, did not leak after test, hardness levels typical
3 4	8 11	45-day LH_2 Storage	Leak Test	Metall. Eval.			No evidence of any type of corrosion or attack, did not leak.
5 6	19 33	45-day LH_2 Stor.	Vibr. Test	Leak Test	Metall. Eval.		Any damage seen was attrib. to the vibr. test, no evidence of corrosion, did not leak after test, hardness levels typical.
7 8	15 13	Vibr. Test	Leak Test	45-day LH_2 Stor.	Leak Test	Metall. Eval.	Any damage seen was attrib. to the vibr. test, no evidence of corrosion, did not leak, hardness levels typical.
9 10	20 14	Vibr. Test.	Leak Test	Metall. Eval.			The damage was identical to specimens with other test sequences. Hardness levels typ.
11 12	7 32	45-day LH_2 Stor.	Incipient Buckling	Leak Test	Metall. Eval.		Any damage was attributed to the buckling test, did not leak, no evid. of corrosion.
13	31	(200) Expulsion Cycling	Leak Test	Expul. cycle to Failure	Metall. Eval.		The test was terminated at 2601 cycles when the weld failed, fatigue cracks were evident in structure.
14	29	(200) Expulsion Cycling	Leak Test	Metall. Eval.			Did not leak, no fatigue cracks, typical hardness levels.
LO_2 Test Sequences							
15 16 17	17 21 22	(5) Pretest Cycling	Vibr. Testing	Leak Test	Metall. Eval.		Any damage seen was attrib. to the vibr. test, did not leak, hardness levels typical no evidence of corrosion.
18 19	23 24	Vibr. Testing	Leak Test	Metall. Eval.			The damage was identical to specimens with other test sequences, hardness levels typ.
20 21	25 26	Expulsion Cycling to Failure		Metallurgical Evaluation			#20 failed at 1935 cycles, #21 at 5350 cycles both failures occurred at crest of first convolute.
Room Temp Test Sequence							
	28	Unused Spare	Expulsion cycled to failure				Failed at 856 cycles in the root of second convolute.

FIGURE 8. TEST MATRIX

Test Equipment

The multi-purpose storage test apparatus included the necessary equipment to perform the pre-storage or pre-vibration cycling, storage, expulsion cycling and incipient buckling tests. (See Figure 9).

Cycle Test Dewar

The cycle test Dewar was cylindrically shaped and constructed of stainless steel with an inside diameter of 17 inches (43.18 cm) and 42 inches (106.68 cm) in length. It was vacuum jacketed on all surfaces except the top. The Dewar was constructed by the Minnesota Valley Engineering Company, New Prague, Minnesota.

Expulsion Cycling Test Fixture

The expulsion cycling/buckling fixture provides a stable surface for measuring bellows movement, refer to Figure 9. The test specimen is attached to the fixture bottom plate. The bottom plate is attached to the Dewar cover by four "hold down" rods. The fixture fits inside the Dewar when it is bolted in place, refer to Figure 10). Displacement of the cycle or buckling test specimen was measured by a movable rod which extended through the Dewar cover. (Refer to Figure 11).

Instrumentation

The instrumentation for the expulsion cycling test monitored the bellows movement while maintaining an adequate liquid level.

Liquid Level Instrumentation

A germanium resistance thermometer in a specially designed case was used to detect the level of cryogen by measuring the change in temperature from liquid to gas phase. An electronic impulse was used to excite the probe and the output signal was conditioned to control a cryogenic flow valve. The operator had a choice of manual or automatic operation of this valve. In the automatic mode, the cryogenic fill valve was controlled by the liquid level probes. In the manual mode, the cryogenic fill valve was controlled by an ON/OFF switch independent of the output of the liquid level probes.

Bellows Motion Monitor

A linear potentiometer was connected to the movable end plate of the bellows by means of a rod extending through the cover plate of the storage Dewar. The potentiometer output was recorded on a speed-o-max strip graph recorder calibrated directly in inches. A typical cycle test record is shown in Figure 12. Adjustable limit switches were incorporated in the recorder so that the operator had the choice of manual or automatic operation. In the automatic operating mode the limit switches, which were triggered by the recorder arm movement, provided the alternate application of helium pressure or vacuum at the proper stroke location. See Figure 9 for schematic of apparatus.

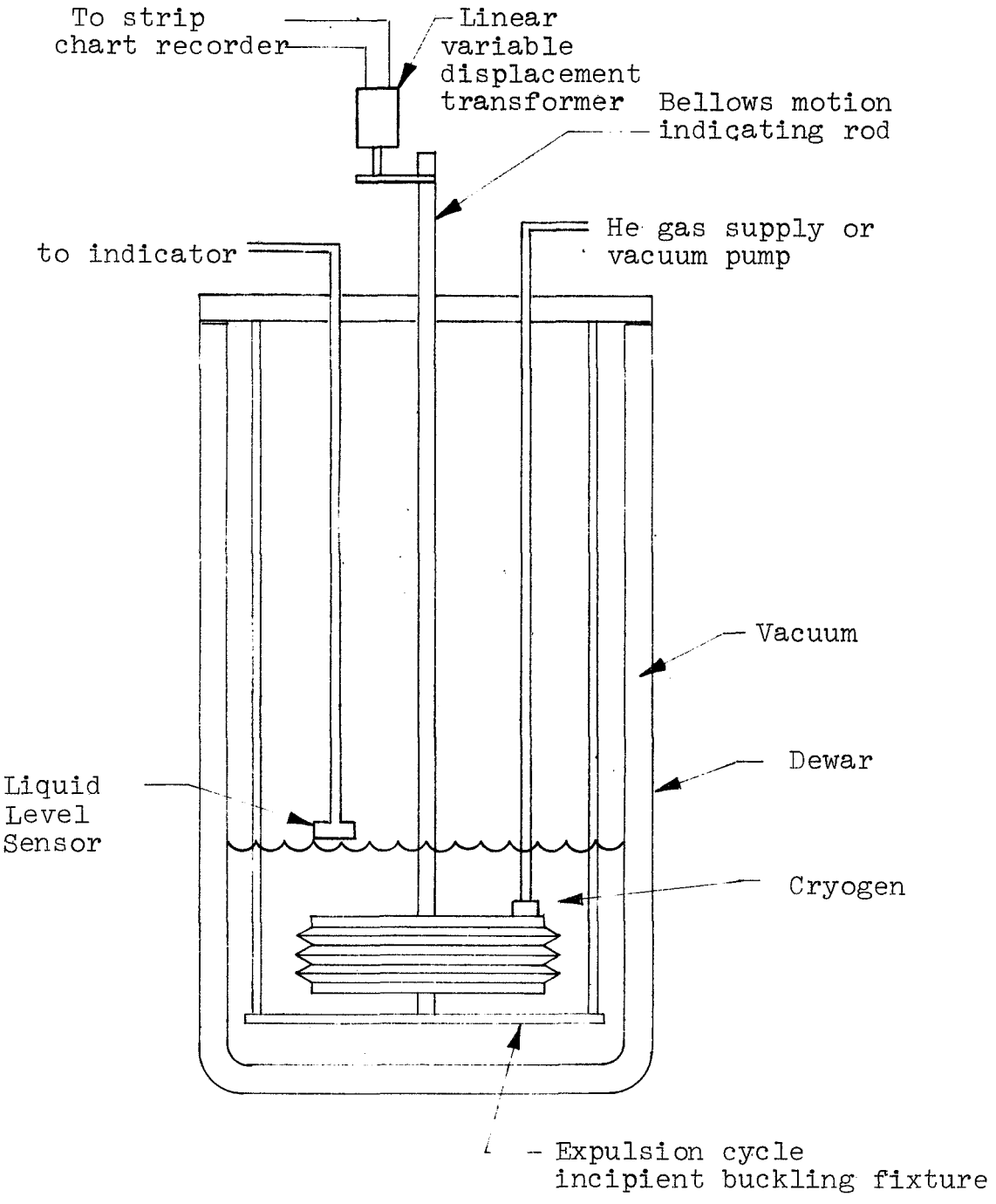

FIGURE 9. MULTI-PURPOSE EXPULSION CYCLING/INCIPIENT BUCKLING APPARATUS

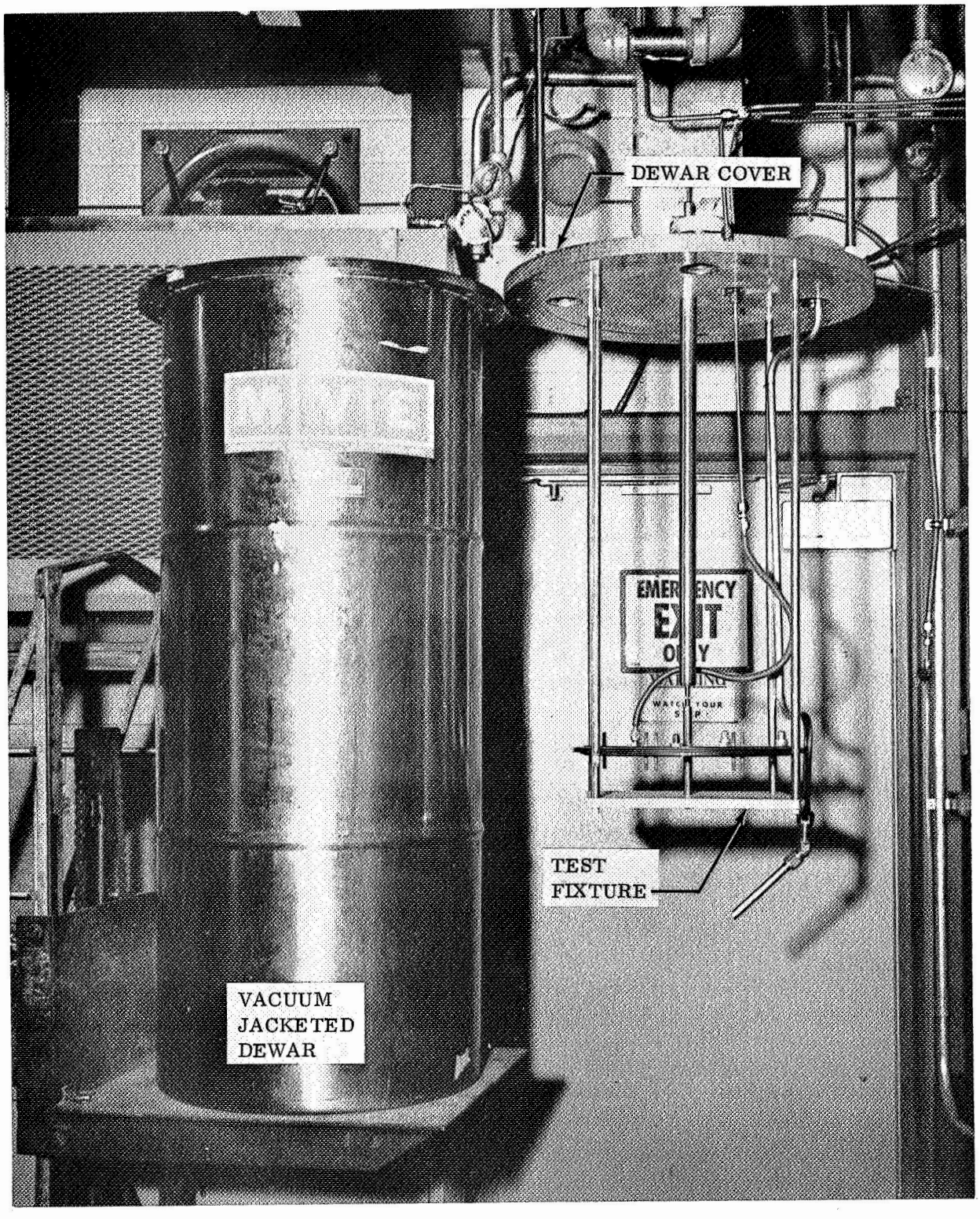

FIGURE 10. EXPULSION CYCLING INCIPIENT BUCKLING TEST APPARATUS DISASSEMBLED

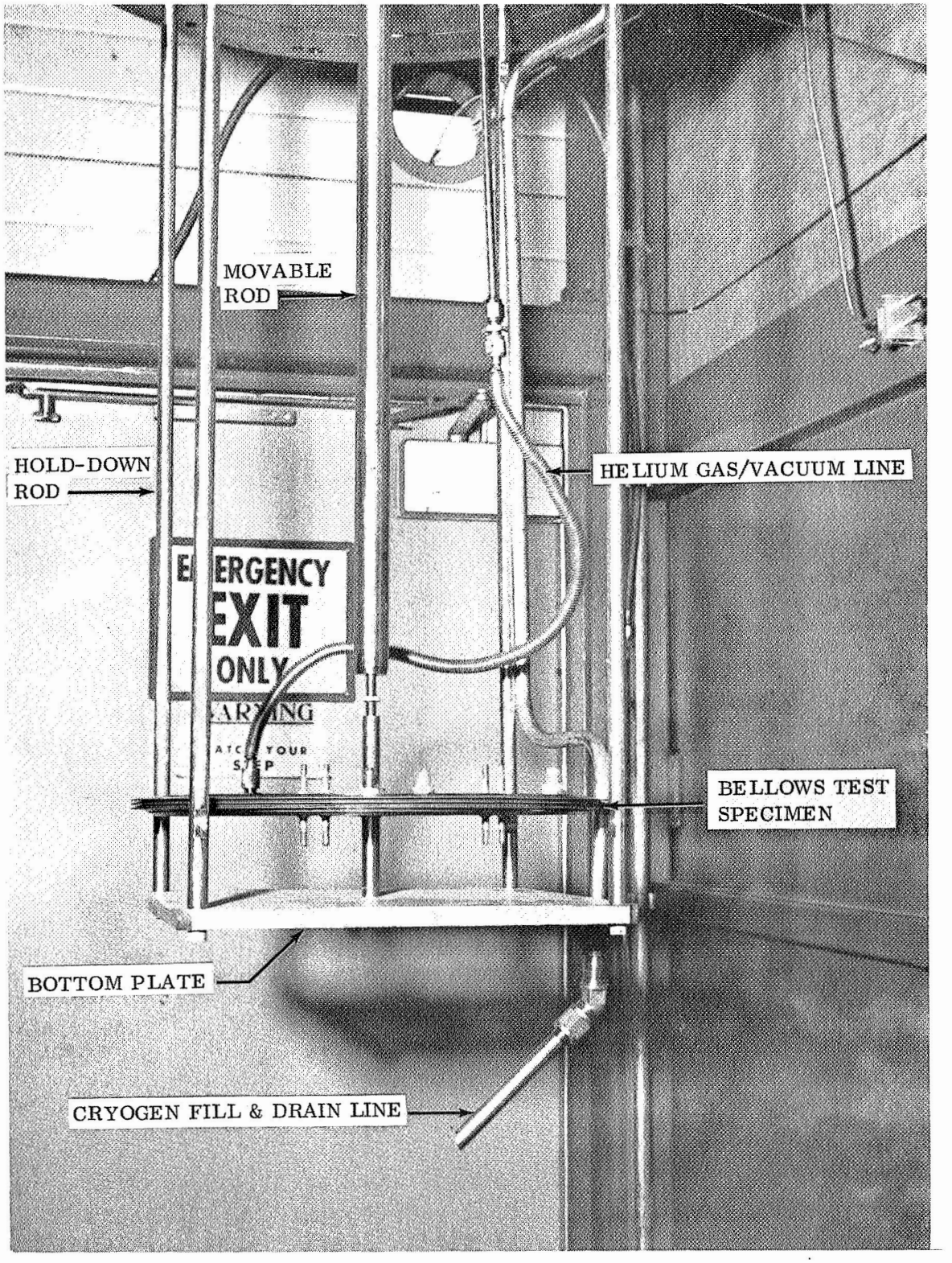

FIGURE 11. EXPULSION CYCLING INCIPIENT BUCKLING TEST FIXTURE WITH BELLOWS INSTALLED

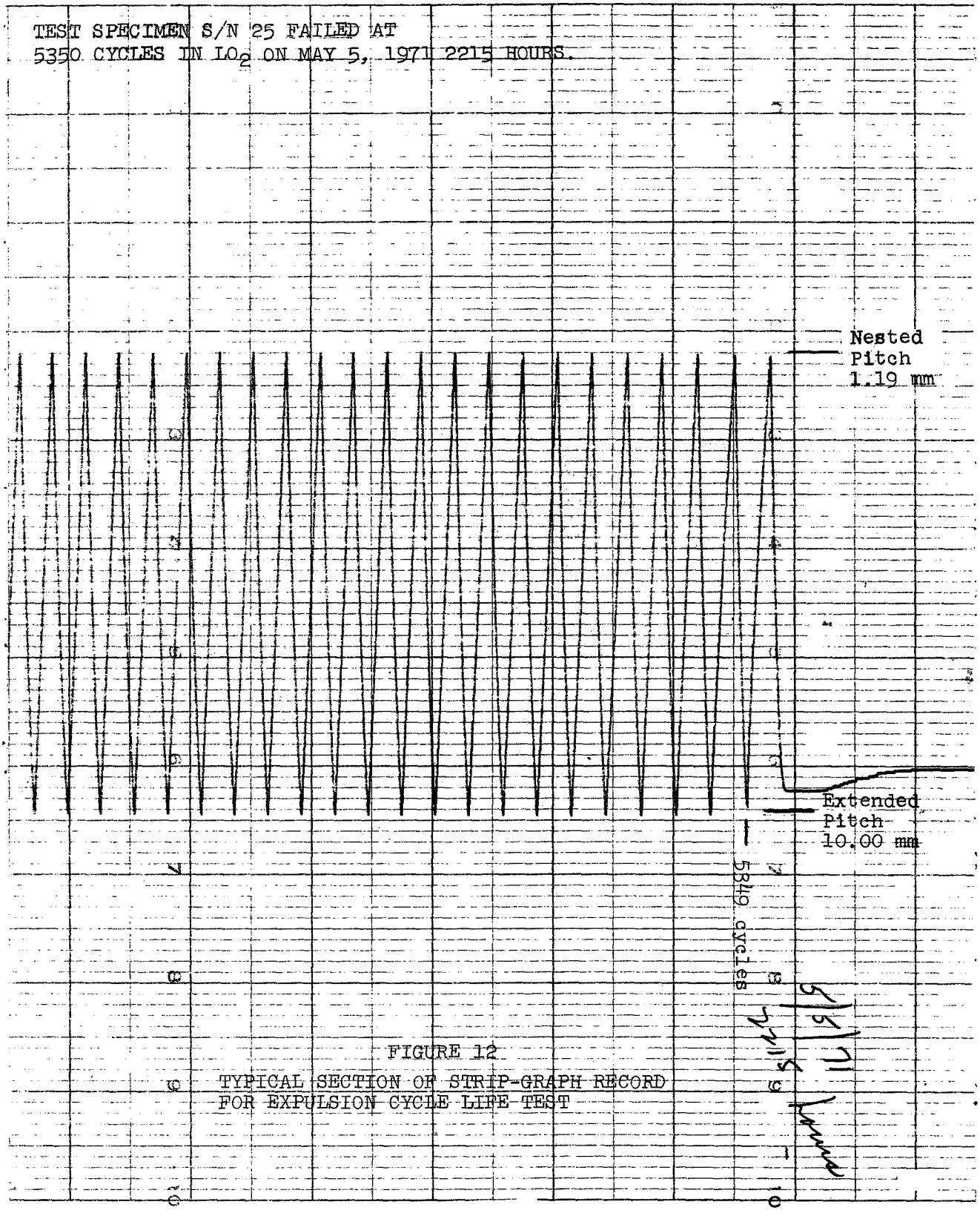

FIGURE 12

TYPICAL SECTION OF STRIP-GRAPH RECORD
FOR EXPULSION CYCLE LIFE TEST

Expulsion Cycling Procedure

When the test specimen was installed in the test fixture, pitch measurement were taken at free and nested length and noted on the strip graph record. The bellows was then extended to the proper operating pitch (0.394 in. - 1.0 cm) and renested to coordinate the proper pitch change with the measurements on the strip graph recorder. Once the measurement correlation was verified between the strip graph recorder and the actual pitch measurements taken at room temperature, the Dewar was raised and bolted into place. Prior to cryogen flow, the entire test system, including the transfer line was purged with helium gas for 15 minutes (900 sec.), then evacuated and purged again with helium.

During the second purge, gas samples were periodically taken at the end of the purge system and analyzed on a gas chromatograph. When the analysis indicated that all combustible and/or solid particles were removed, the cryogen was admitted into the Dewar. A thermocouple located at the bottom of the Dewar indicated when the environment was capable of maintaining liquid cryogen. Located approximately four inches above the bellows top end plate was the liquid level sensor. The cryogen was allowed to flow until the sensor indicated that the level of the liquid was at the level of the sensor. At this point in the test, the bellows position was again noted on the strip graph recorder and compared to the position at room temperature. The change in position was due to contraction of the rod attached to the linear potentiometer and taken into consideration to assure that the bellows was cycled at a correct operating pitch. Bellows cycling was accomplished by helium pressurization until the correct maximum operating pitch was reached, at which time the limit switch provided for application of vacuum and returned the bellows to the nested position. At this end of the cycle, the opposing limit switch provided for application of pressure and completed the cycle. This cyclic action was repeated until the required number of cycles was obtained or failure occurred.

Expulsion Cycling Results

Life Cycle Test Results

Four specimens were subjected to a cycle to failure test; one on liquid hydrogen, two in liquid oxygen, and one at room temperature. Failure was defined as a leak in a convolute. Any other leak, such as attachment weld failure would be repaired, if possible, and cycling continued until bellows convolute failure occurred since the attachment weld does not represent a flight configuration.

Liquid Hydrogen Test Results

The only liquid hydrogen specimen subjected to this test was serial number 31. This specimen was previously subjected to 200 expulsion cycles and a leak test and then selected as the cycle to failure specimen when the program plan was changed to add this test. (See test matrix Figure 8). During this portion of the test an additional 2401 cycles were completed, at which time the test was terminated due to an unrepairable attachment weld failure. The subsequent metallurgical evaluation detected fatigue type micro-cracks, however similar to those shown in Figure 13. (the diamond shaped indication on the photograph is the hardness test impression). It is impossible to predict how many more cycles it could have sustained before failure. The only conclusion available from this test is that it demonstrated a cycling capability of 2601 cycles. In comparison the metallurgical examination of specimen S/N 29, which was subjected to only 200 expulsion cycles in liquid hydrogen revealed no detectable fatigue type microcracks. The typical hardness measurements for both S/N 31 and S/N 29 are comparable indicating that the increased cycling did not result in significantly increased hardness (See Table I). However, the cycled bellows were somewhat (Knoop 300) harder as compared to the, as formed condition (Knoop 280).

Liquid Oxygen Test Results

Two specimens were subjected to life cycling tests in liquid oxygen. Specimen S/N 26 failed in crest Number 3 (See Figure 14) after 5350 cycles. Specimen S/N 25 failed in the same location, crest Number 3 (Figure 14) after 1935 cycles. Both failures were fatigue type cracks along crest Number 3 (See Figure 15) These bellows specimens were not subjected to any previous testing and the testing was continuous until crest failure occurred. The typical hardness measurements for both S/N 25 and S/N 26 do not vary significantly indicating that the increased cycling does not result in additional work hardening (See Table I). Cycling caused work hardening of the material in a range similar to the liquid hydrogen test results when compared to the " as-formed" condition. S/N 26 had many fatigue type micro-cracks throughout all three convolutes which are shown typically by Figure 13. No cracks were detected in S/N 25.

Room Temperature Test Results

Specimen S/N-28 was cycled to failure at room temperature. It failed at root number 3 (See Figure 14) in a typical fatigue type crack after 856 cycles. The attachment weld failed after 780 cycles and was repaired with epoxy before continuing the test. The hardness levels after cycling were again similar to those reported in the liquid hydrogen test results.

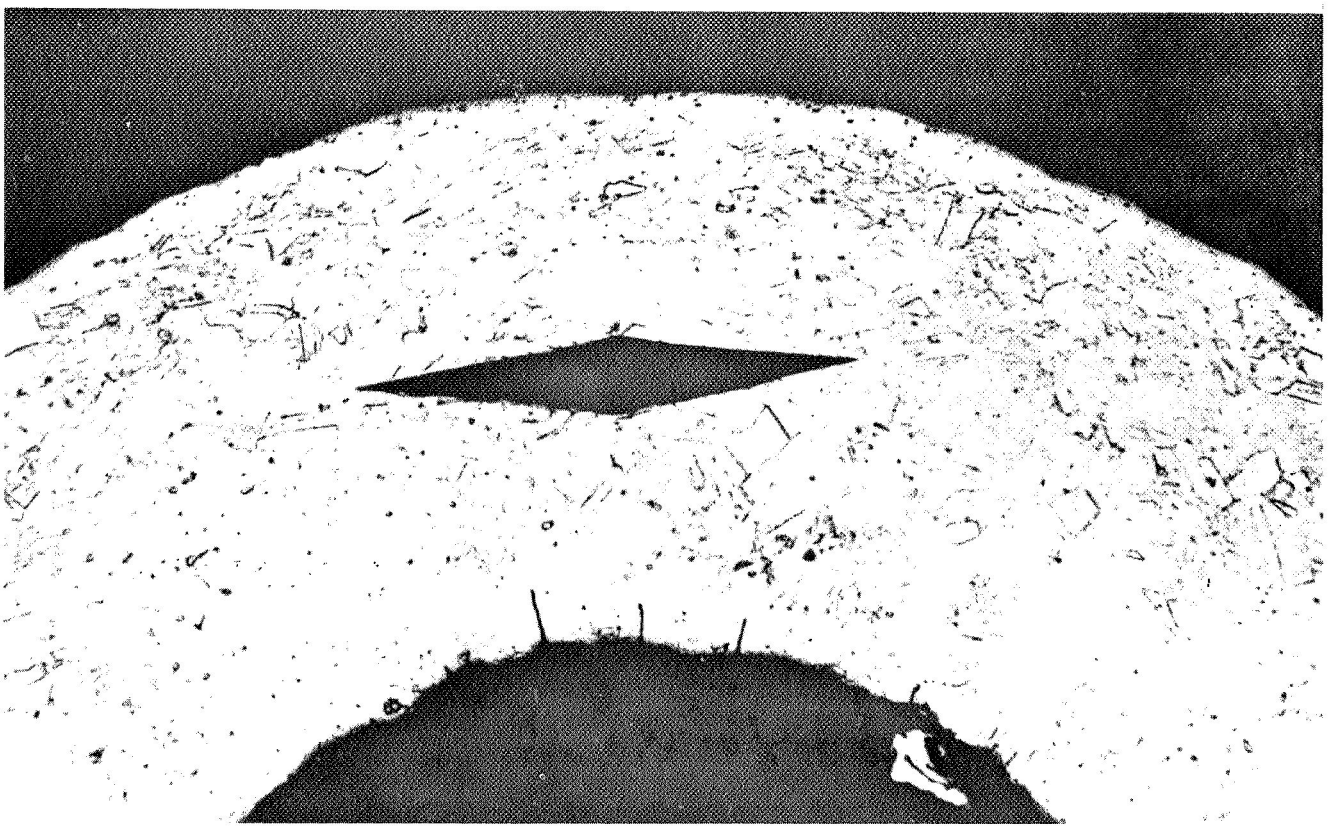

FIGURE 13.

START OF FATIGUE CRACKS AT CREST BEND I.D. OF BELLOWS S/N 26, LIFE CYCLED TO FAILURE IN LIQUID OXYGEN

ETCHANT: OXALIC ACID
MAG: 200X

TABLE I

COMPARISON OF HARDNESS VS TEST SEQUENCE
(KNOOP 500 GRAMS)

	TEST CONDITION	S/N	CREST	ROOT	LEAF	REMARKS
LH_2	Storage & Buckling	6	292	191	177	In buckle area
	Storage & Buckling	7	329	267	217	In buckle area
	45 day storage	8	274	240	177	
	45 day storage	11	285	193	185	
	Expulsion Cycled (200 cycles)	29	296	338	224	
	Expulsion Cycled (2601 cycles)	31	304	316	205	
	Buckled	32	374	205	187	In buckle area
	Vibration	2	316	281	249	
		4	312	277	227	
		13	296	277	219	
		14	267	222	187	
		15	300	274	219	
		19	316	249	187	
		20	308	214	191	
		33	358	232	195	
LO_2	Expulsion Cycled (1935 cycles)	25	296	255	207	Failed in Crest
	Expulsion Cycled (5350 Cycles)	26	297	277	235	Failed in Crest
	Vibration Test	17	348	255	201	
		21	316	258	219	
		22	308	232	217	
		23	320	240	232	
		24	308	237	224	

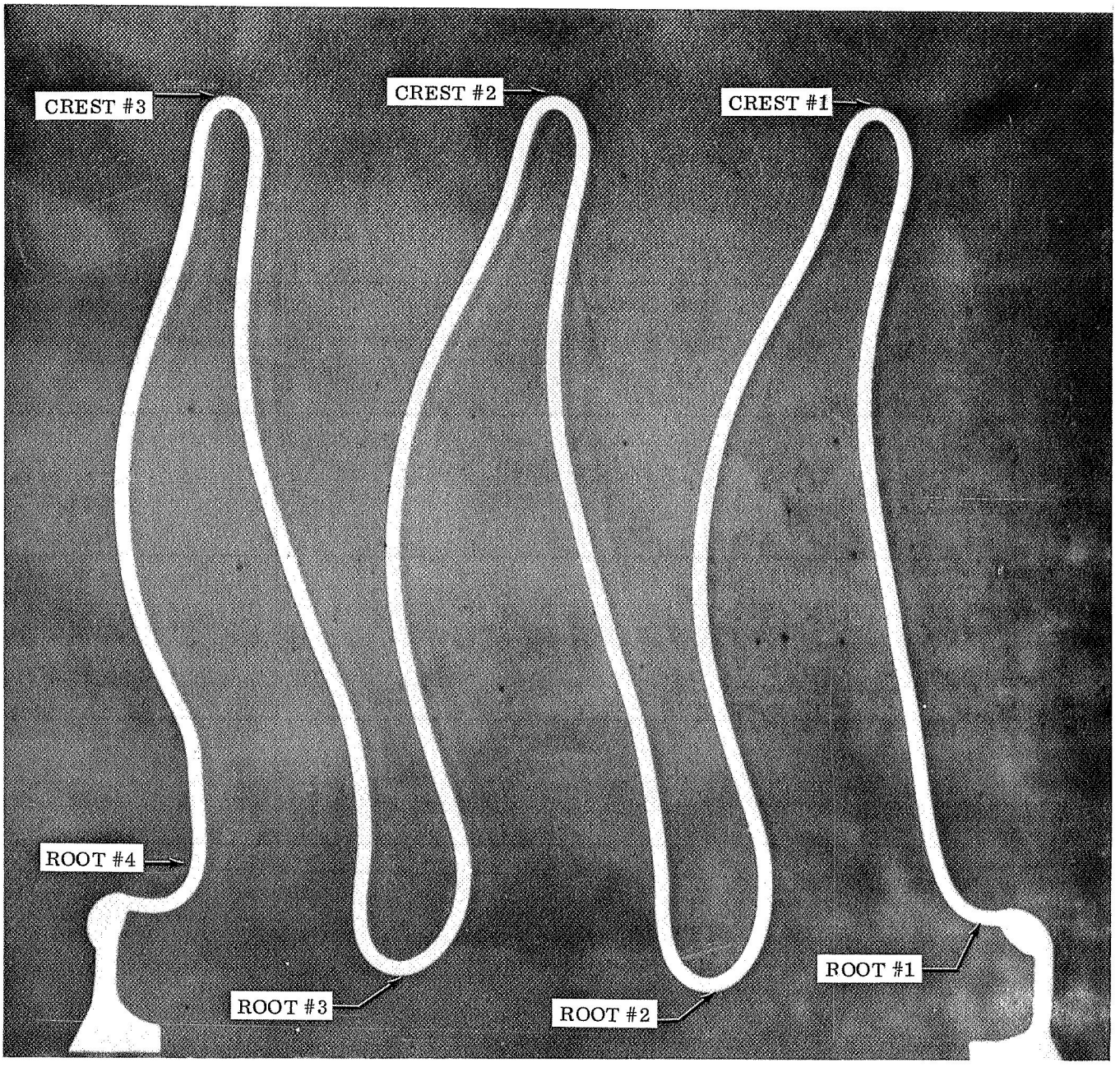

FIGURE 14. 10X PHOTOGRAPH OF TYPICAL BELLOWS CONVOLUTION SHAPE

FIGURE 15

FATIGUE CRACK TYPICAL OF FAILURE
PRODUCED BY LIFE CYCLING TESTS

Discussion of Results

The metallurgical comparison of the life cycled test specimens indicate that cycling causes the material to go from approximately 1/8 hard as formed to approximately 1/4 hard due to cold working or work hardening. This is not associated, however, with a basic crystalline change or cryoforming, but only the metallurgical mechanisms associated with any type of plastic deformation. A comparison of fatigue indications shows the presence of micro-cracks in S/N 31 (2601 cycles in LH_2) and S/N 25 (5350 cycles in LO_2), but none in S/N 26 (1935 cycles in LO_2) or S/N 28 (856 cycles at room temperature). It thus appears that work hardening occurs very rapidly within the first 200 cycles and then does not continue, but levels off and maintains that level while the fatigue type micro-cracks do not appear until approximately 2000 cycles. The hardness of the life cycled bellows specimens increased fairly uniformly in the crest, root and convolute leaf as a result of work hardening induced by plastic deformation at all three temperatures room, liquid oxygen and liquid hydrogen.

In a comparison of analytical life cycle prediction to test results it is important to note that the fatigue prediction does not predict the failure point, rather, it predicts the number of cycles expected without failure. A particular specimen may exceed this minimum expected cycle life by a large margin depending upon many individual variations, such as: material quality, thickness, shape, etc. Material fatigue property data is presented as a single curve without showing the scatter of results from which it was obtained.

In each bellows life cycle (fatigue) test the bellows was extended to an average pitch of 0.394 inches (1.0 cm) and compressed to an average pitch of 0.047 inches (.119 cm). Average pitch values for the three convolute specimen was required because of the necessity of monitoring end plate motion. Examination of Figure 14 reveals that no two convolutions have exactly the same pitch. Since the mathematical model used by the computer program is exactly like Figure 14, the strains were computed for the same total bellows travel used in the tests.

The objective in these tests was to study the gross effects of fatigue on the center convolute which represents a typical convolute of any operational expulsion bellows. The two end convolutions may vary considerably from one design to another in the type of end restraint employed. Failures within the end convolutions are of value to the degree that the analytical techniques used are capable of predicting them. However, the actual number at which they fail are of secondary importance, unless they fail prematurely, since they do not represent the typical bellows convolute as the center convolution does.

Analytical Strain Determination

In order to correlate the test results, an accurate assessment of the strains produced was required to determine the expected fatigue life. The analytical stress-strain-deflection data was obtained using the digital computer program developed under Contract NAS 7-149. Details of the program including accuracy verification are provided in Reference 5. This program computes the nonlinear deformation of axisymmetric thin shells of revolution with a complete distribution of the bi-axial bending and membrane strains.

The geometric configuration used in this analysis is shown in Figure 14. The cross section was obtained from test bellows Number 25 in a region moved from any detectable fatigue failure.

The state of strain in the bellows is biaxial while the fatigue data available is uniaxial. The computed biaxial strains, therefore, were converted to an equivalent uniaxial strain. This was accomplished using the shear-distortion or shear-energy theory of Hencky-Von Mises which provides the formula:

$$e_{EQUIV} = \sqrt{e_1^2 + e_2^2 - e_1 e_2}$$

The bending strains provided by the computer program do not contain strain distortions from curved beam effects which become significant in the sharp curvature regions of the roots and crests of the bellows convolutions. These convolution corrections were applied at each convolution root and crest and the resulting strain added to the membrane strains and converted to a uniaxial equivalent. Only the roots and crests are included because the largest strains occur at these points. These calculations are shown in Table II. The curvature correction factors, "K", applied to the bending strains were obtained from curves of K vs r/c in Reference 6. Roots number 1 and 4 are not included in Table II because the fully clamped boundary assumed for the mathematical model does not exactly represent the actual support condition. The fully clamped strains computed tend to be conservatively high, but still less than the total strain at other locations indicating that failure at the attachment weld would not be expected during cycling unless the welds were substandard.

The total strain range at each point is the sum of the values in the last column of Table II. With these strains and the fatigue properties of Figure 16, the predicted room temperature cycle life range is shown in Table III.

FREE TO EXTENDED LENGTH

LOCATION	μ/K	K	BENDING STRAIN x 10^{-3}		K x BEND. STRAIN x 10^{-3}		MEMBRANE STRAIN x 10^{-6}		TOTAL STRAIN		EQUIL. STRAIN
			MERID.	HOOP	MERID.	HOOP	MERID.	HOOP	MERID	HOOP	
Crest #1	1.80	1.26	9.375	3.094	11.812	3.898	.0634	-2.391	11.876	1.507	11.199
Root #2	3.17	1.14	-10.031	-3.311	-11.435	-3.774	.0602	1.988	-11.375	-1.786	10.596
Crest #2	1.91	1.24	9.621	3.188	11.930	3.953	.0634	-2.252	11.993	1.701	11.239
Root #3	3.32	1.13	-9.924	-3.276	-11.214	-3.702	.0602	1.836	-11.154	-1.866	10.348
Crest #3	2.14	1.21	10.034	3.310	12.141	4.005	.0633	-1.990	12.204	2.015	11.332
FREE TO NESTED LENGTH											
Crest #1		1.26	-5.166	-1.704	-6.509	-2.147	-.0253	.3583	-6.534	-1.789	5.848
Root 2		1.14	5.096	1.682	5.809	1.917	-.0232	-.2301	5.786	1.687	5.154
Crest 2		1.24	-5.393	-1.781	-6.687	-2.208	-.0253	.3352	-6.713	-1.873	6.00
Root 3		1.13	4.914	1.621	5.553	1.832	-.0233	-.1350	5.530	1.697	4.907
Crest 3		1.21	-5.100	-1.634	-6.171	2.038	-.0254	.0638	-6.196	-2.044	5.468

TABLE II
ANALYTICAL STRAIN PATTERN

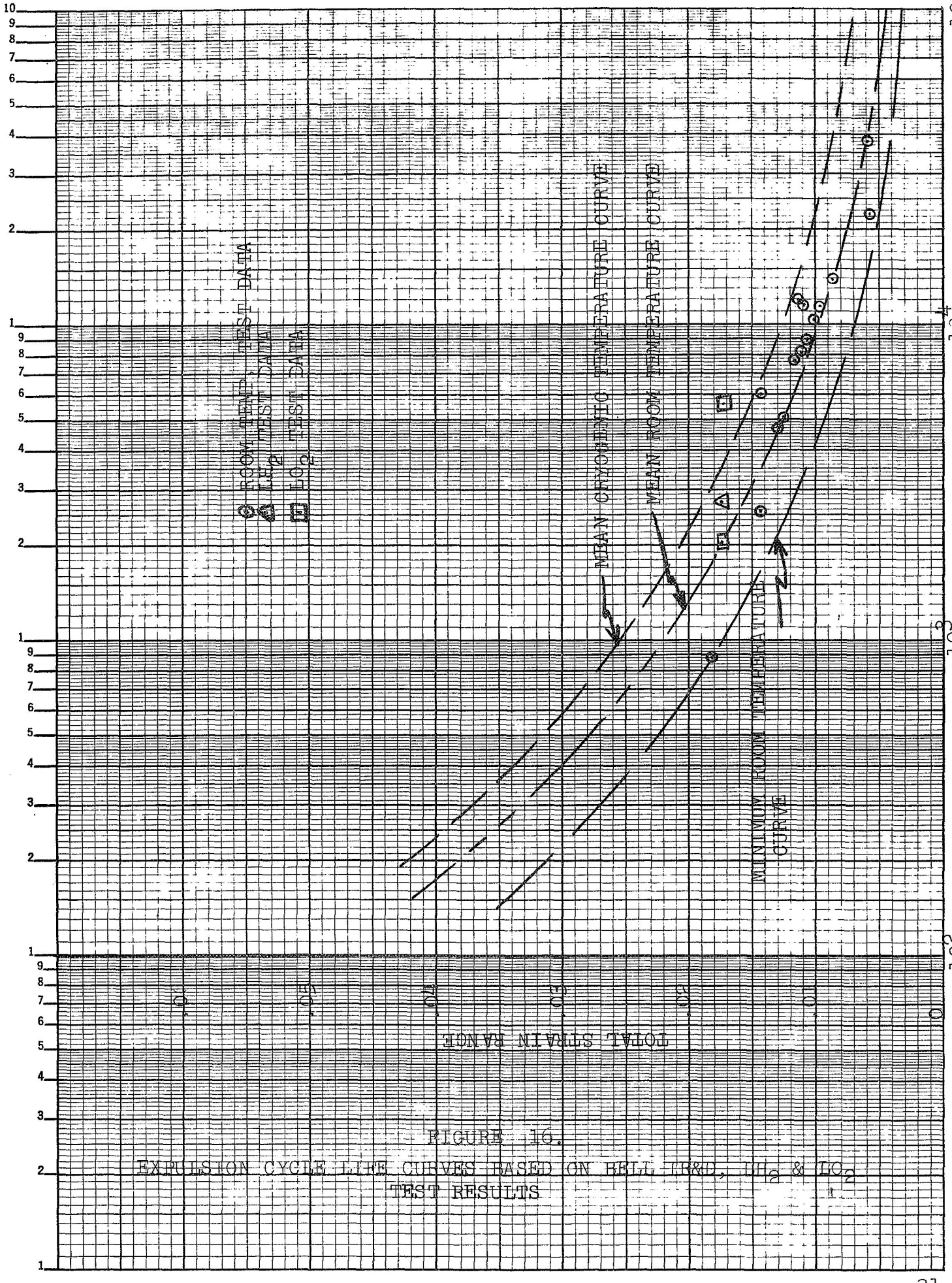

FIGURE 16.

EXPULSION CYCLE LIFE CURVES BASED ON BELL IR&D, UH_2 & LC_2 TEST RESULTS

Location	Predicted			Actual Cycles to Failure			
	Total Strain Range	Mean Strain	Range of Cycles to Failure at Room Temp.	S/N 31 LH_2	S/N 25 LO_2	S/N 26 LO_2	S/N 28 Amb. Temp.
Crest 1	.01705	.00267	1050 - 3600	2601 cycles-failed in weld-test terminated			
Root 2	.01575	.00272	1230 - 4400				
Crest 2	.01723	.00262	1020 - 3400				
Root 3	.01626	.00322	1140 - 3900				856 cycles failed in root #3
Crest 3	.01680	.00293	1100 - 3700		1935 cycles-failed in crest 3	5350 cycles failed in crest 3	

TABLE III. COMPARISON OF CYCLE LIFE
(Predicted Vs. Actual)

The available fatigue data at cryogenic temperatures, Figure 17, does not extend into the high strain - low cycle range required by the results in Table III. However, Figure 17 does show considerable improvement of smaller strain fatigue properties at cryogenic temperatures compared with those at room temperature. It seems reasonable to expect some degree of improvement will exist in the high strain range as well, and this trend is indicated by the cycle life test results indicated in Figure 16. In all cases at cryogenic temperatures the actual cycle life exceeded the predicted room temperature cycle life and as previously stated the cycle life variation is assumed due to fatigue data spread. It is interesting to note that in all cases where the bellows failed within the convolute, it failed in an area of high predicted strains indicating good correlation between analytical and empirical results. The range of predicted cycles to failure in Table III indicate that failure is most probable at any one of the points shown in Table III since the strains are nearly equal at these points.

In the process of this analysis it was discovered that contact between neighboring convolutions occurs before the 0.047 inch nesting pitch is achieved. Since the computer solution allows points to deform through each other, the effect of contact forces is unknown. A solution of the strain state in two thin, non-linear shells forced into contact is a formidable problem beyond the scope of this program. Speculation on the effect of the contact is that the strains can be expected to magnify slightly with the largest effect in the root and only a minor effect on the crest strains which may explain the low cycle life of S/N 28 which failed at 856 cycles in Root No. 3 at ambient temperature. Any evaluation of the contact force has been neglected in Table III.

200 Expulsion Cycle Test Results

The only bellows subjected to the 200 cycle verification test was Serial Number 29. The test was conducted in liquid hydrogen, prior to the program change which substituted the cycle to failure test for this test. A metallurgical evaluation of S/N 29 revealed that the hardness levels were approximately the same as S/N 31 which performed 2601 cycles indicating that work hardening is not linear. It appears that the bellows behaves the same at cryogenic temperature as it does at ambient temperature in that the majority of the work hardening occurs within the first 10 cycles as indicated by the fact that the specimen hardness is approximately the same for the bellows subjected to only pre-storage cycling as for those cycled to failure. There were no indications of fatigue type micro-cracks nor any other type of damage as a result of the 200 cycles.

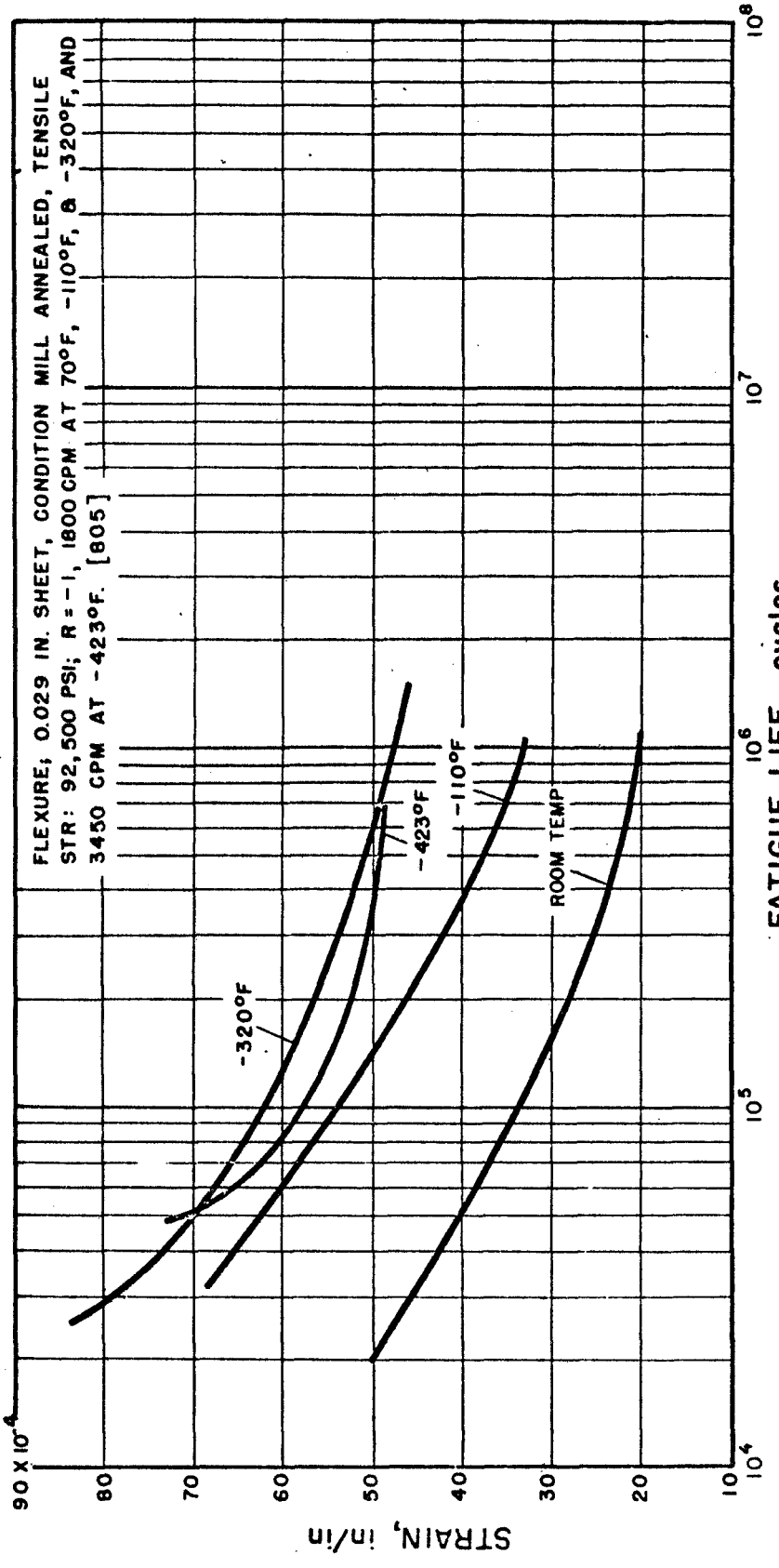

FATIGUE BEHAVIOR OF AISI 347 STAINLESS STEEL

FIGURE 17

VIBRATION TESTS

Of importance to reliable cryogenic bellows design is the knowledge of the effects that launch dynamic-environments will have on their integrity. If severe damage or material structural changes result from vibratory exposure, the bellows required cycle life may be seriously compromised. The primary damage mechanisms from such exposure are wear of bellows crest material caused by abrasion on the tank shell during bellows motion parallel to its axis and the impact of the bellows crest on the tank shell from lateral motion perpendicular to its axis. The tests were designed to simulate these types of motion while maintaining a cryogenic environment. The vibration inputs specified for the cryogenic tests are the same as those used for previously conducted room temperature tests of three convolute bellows specimens of similar configuration. The abrasion input levels were based on Minuteman III tank responses measured photographically (Reference 8) during sinusoidal and random vibration tests simulating transportation, handling and flight environments. The impact input was selected to simulate the MM III impact frequency range. Moderate buckling on some of the room temperature specimens, which does not occur on the MM III bellows, indicated that the actual impact test levels were more severe than the MM III test environments.

For the vibration tests the bellows specimens were installed in a test fixture which contained a section of tank shell (ring) to provide an impact and abrasion surface. The fixture was mounted on a vertical shaker which was used to apply radial impact vibration inputs (See Figure 18). A second shaker mounted normal to the impact shaker was used to apply axial abrasion vibration inputs. In order to maintain a cryogenic environment the entire fixture was thermally insulated by using a double-walled cryostat, capable of effecting a complete vacuum between the inner and outer walls. The inner chamber maintained a pressurized gaseous helium environment (See Figure 19).

The impact and abrasion tests were performed in a hazardous duty test cell in the Chemistry Laboratory of the Bell Aerospace Company. All controls were remotely located to provide safe operation with the cryogenic propellants.

Test Equipment

The test setup comprised the following major sub-system as depicted in Figure 20.

Cryostat

The cryostat consisted of an inner chamber which contained the test fixture and was complete with access ports, door and seals to prevent the escape of any environmental gases or liquids, and an outer chamber which completely encapsulated the inner chamber. The

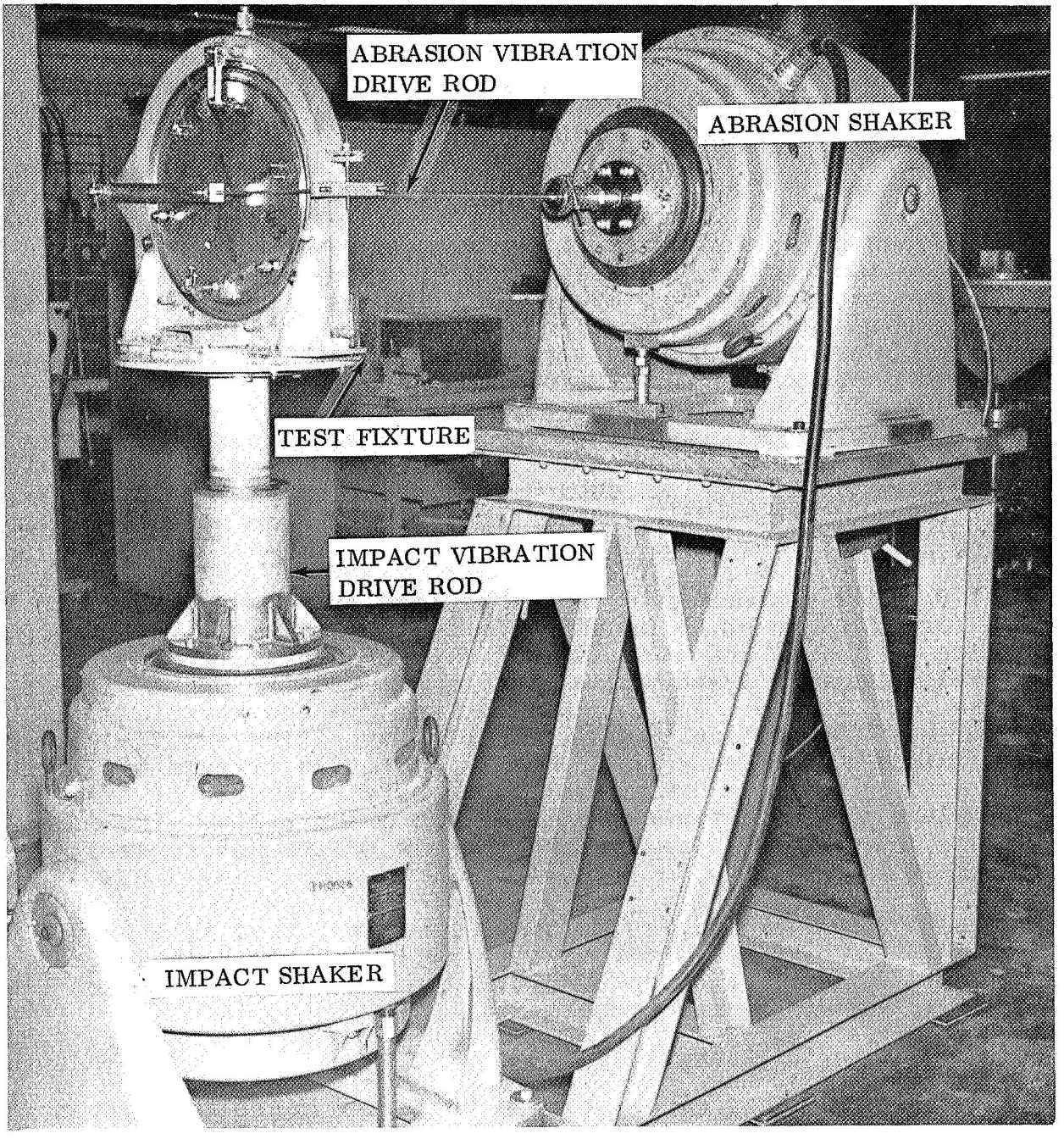

FIGURE 18. VIBRATION TEST APPARATUS WITHOUT CRYOSTAT

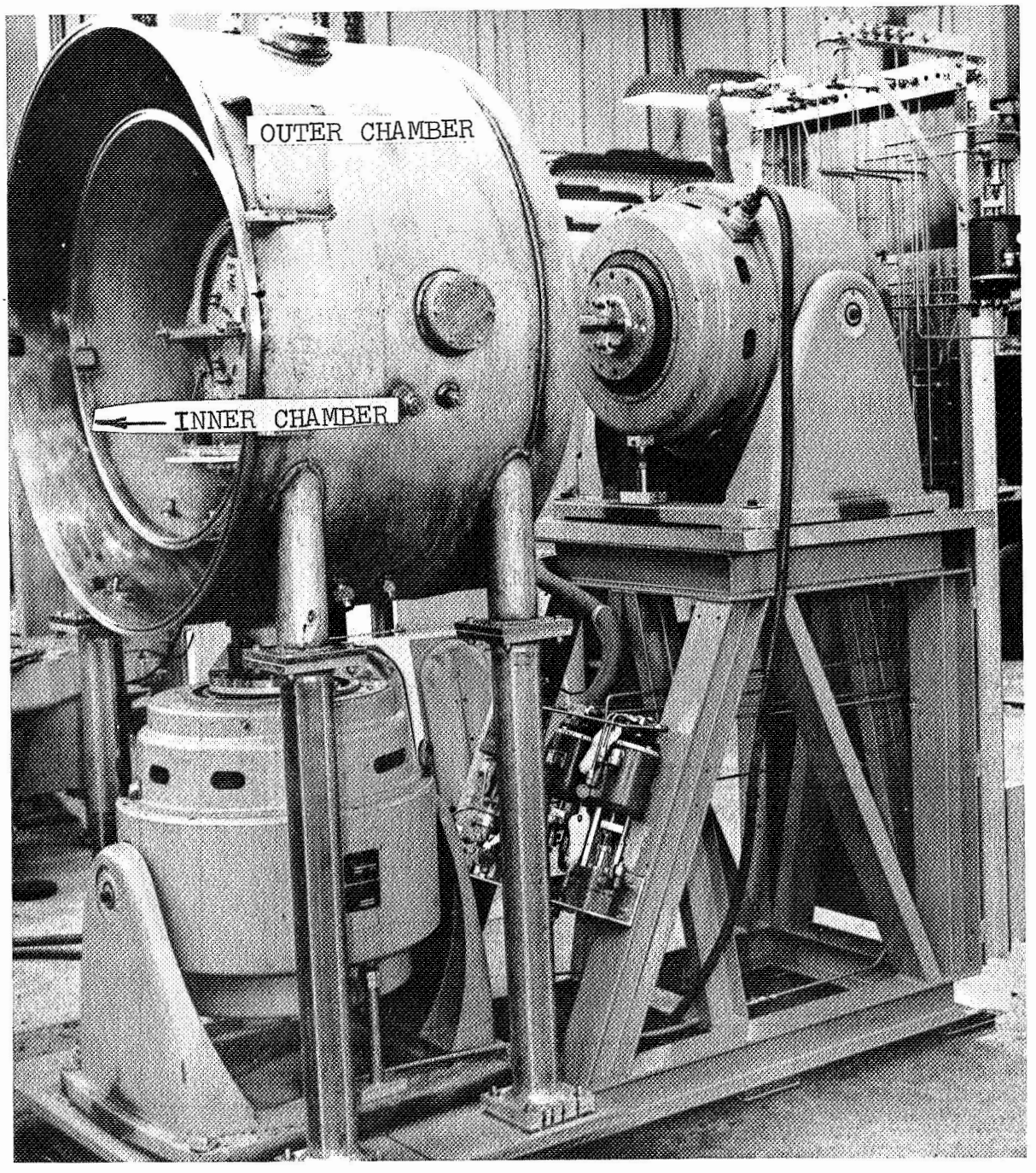

FIGURE 19
VIBRATION TEST APPARATUS WITHOUT INNER
AND OUTER CHAMBER DOORS

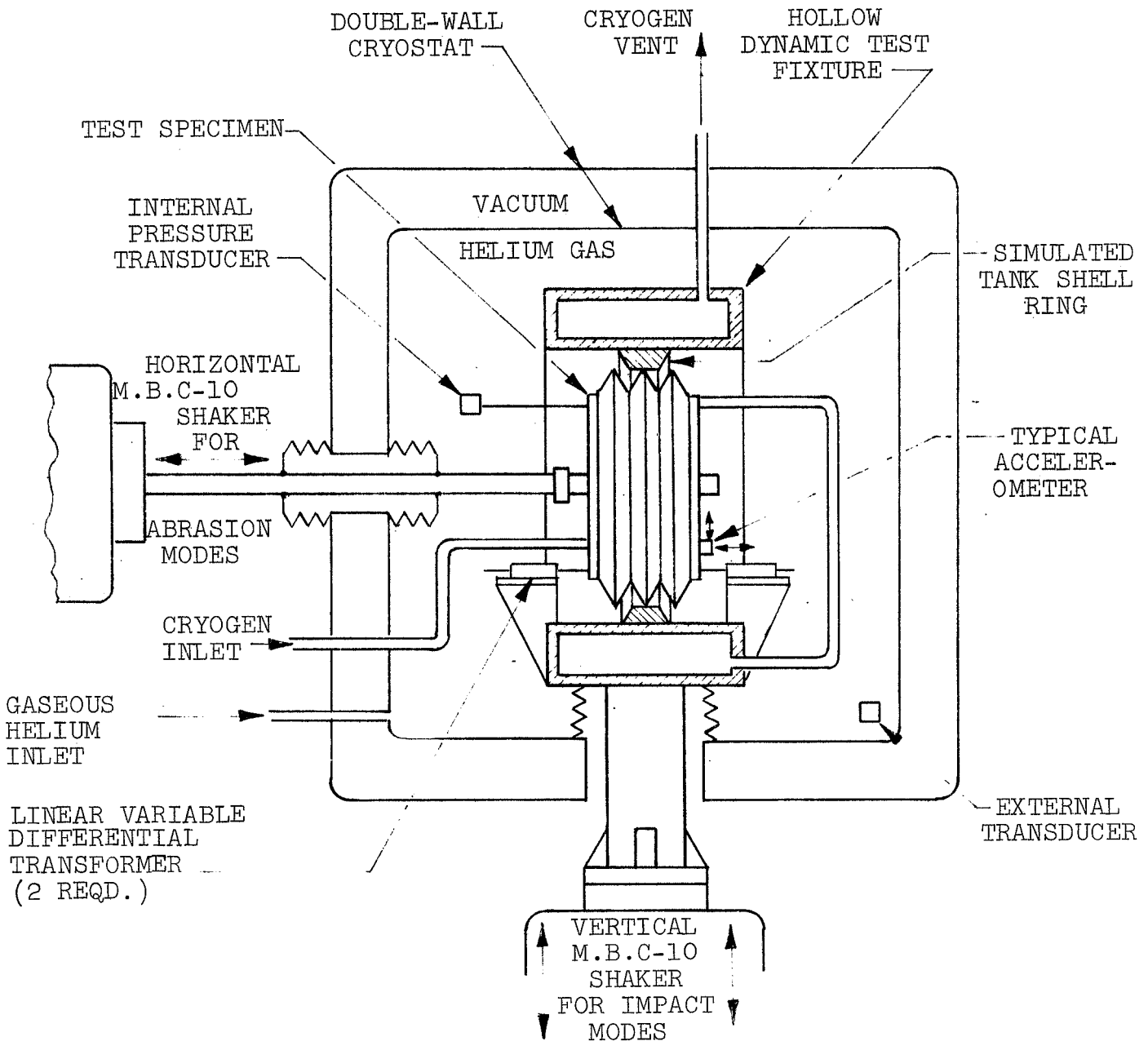

FIGURE 20. VIBRATION TEST APPARATUS

outer chamber was complete with an access door and seal to prevent any ambient gases from entering the space between the two chambers. The space between the two chambers was connected to a heavy duty vacuum pump for maintaining a high vacuum during the tests. The entire cryostat has access ports for vents, cryogen input, instrumentation "feed-throughs" and atmosphere control tubes. See Figure 21 for a photograph of the vibration test apparatus completely assembled.

Bi-Axial Vibration System

The impact and abrasion excitation was provided by two M.B. Model C10 electrodynamic vibrators arranged as shown by the photograph in Figure 18. The vertical exciter provided impact vibration to the test specimen through the dynamic fixture. Abrasion was obtained by longitudinal vibration through a horizontal drive rod connected to one side of the end plate trunnion of the bellows specimen.

The vibrators were programmed to produce random vibration inputs of specified bandwidths and level. Impact and abrasion vibration inputs were capable of being applied either individually or combined as required.

Dynamic Fixture

The dynamic fixture consisted of a hollow ring supported by a vertical post attached to the head of the impact exciter. The hollow fixture was designed so that the cryogen flowed through the fixture to aid in maintaining a cryogenic environment similar to that expected for a typical bellows using cryogenic propellants. The replaceable tank shell ring was completely enclosed and retained on the inside of the fixture and duplicated the material, surface finish, heat treatment and thickness of a typical production tank shell. This provided the specimen impact and abrasion interface surface. A photograph of a test specimen installed in the dynamic fixture is shown in Figure 21.

The test bellows is supported at the center of each end plate by trunnions and trunnion guide arms. These arms allowed vertical motion for impact and longitudinal motion for abrasion. Lateral adjustment of the specimen was provided by a lockable eccentric under the guide arms. This ensured that the test bellows was centered within the tank shell ring. An adjustable flexure on each guide arm provided the required specimen-to-ring contact load.

The cryogen flow path, as shown in Figure 20, was through the test specimen then through the fixture and out the fixture vent. Connections were made with flexible metal bellows interconnect tubing, which provided cryogen cooling of the structure adjacent to the test bellows.

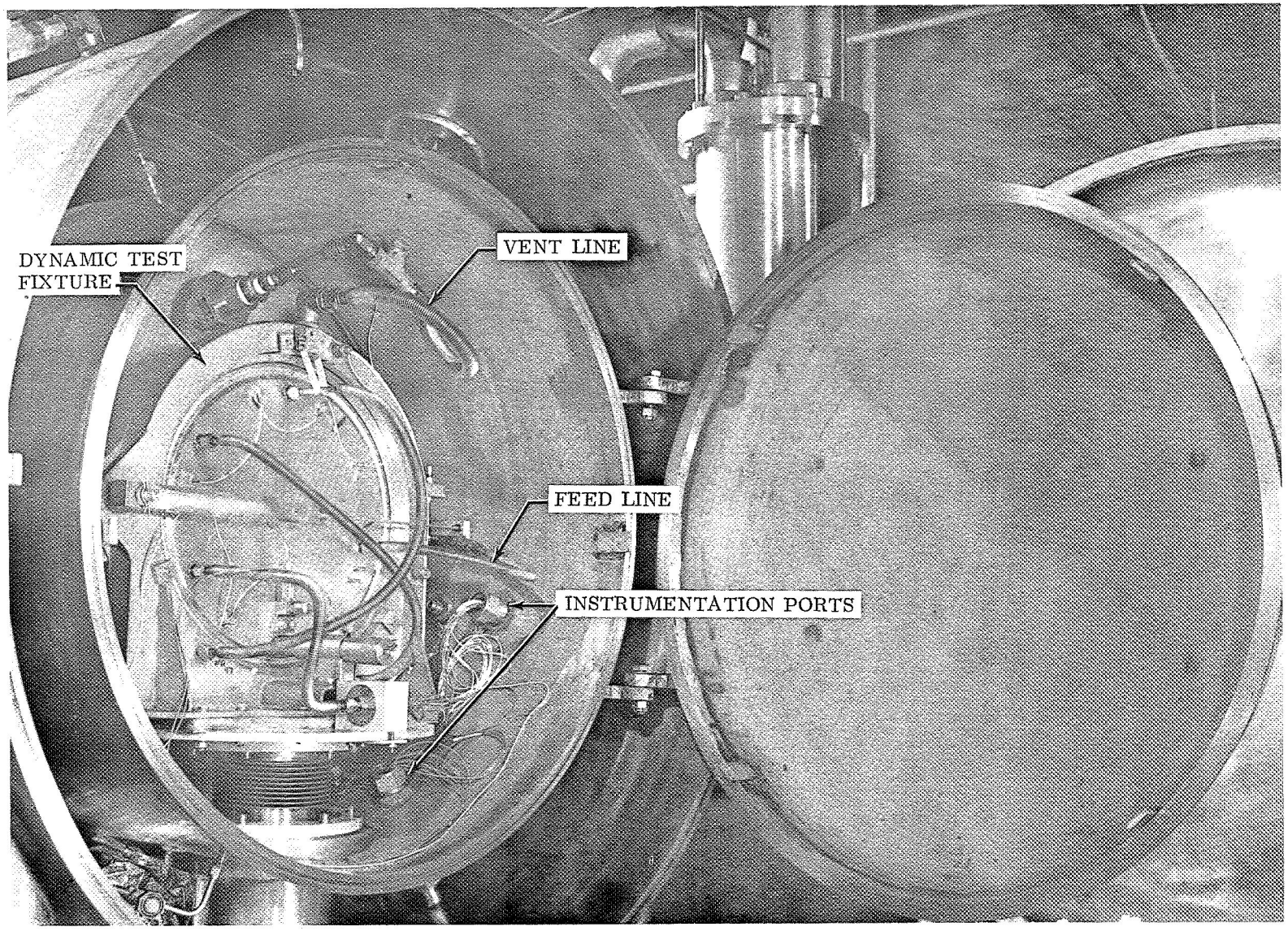

FIGURE 21. VIBRATION TEST APPARATUS COMPLETELY ASSEMBLED WITH TEST SPECIMEN, FEED, DISTRIBUTION, AND INSTRUMENTATION LINES INSTALLED

Prior to cryogenic testing the fixture and shakers were setup and operated at room temperature to check on fixture/bellows behavior and to identify resonances. The resonances found are described in Figure 22. Also, an abrasion axis sine vibration test was performed to obtain fixture-bellows relative displacement for a constant shaker input acceleration. No detrimental modes were encountered in the 20 to 50 Hz test frequency bandwith, thus ensuring that the desired abrasion vibration spectrum could be applied to the bellows.

Instrumentation

Measurements for Impact and Abrasion Testing were divided into five categories; acceleration, displacement, temperature, pressure and liquid level, (See Figure 23.) All acceleration, displacement and pressure signals were recorded on a FM tape recorder utilizing one inch 14-channel magnetic tape. Ten recorder channels having a frequency response of 1.25 KC constantly recorded the above parameters. During vibration, the reproduced output was monitored on an oscilloscope for proper recording and detection of anomalies.

Pre- and post- calibration signals for LH_2 and LO_2 sensitivities were used to range the instrumentation. For calibration accuracy, the sensitivity of the accelerometers, displacement transducers, and temperature sensors were checked at room temperature and at liquid nitrogen and liquid neon temperatures. Sensitivities were also checked after a soak period. See Appendix A for instrumentation calibration report.

Post test data reduction for all vibration consisted of oscillograms. Power spectral density and probability density plots were made of selected responses.

Acceleration

Kistler quartz accelerometers, Model 808H, were used for measurement of acceleration at the cryogenic temperatures. The unit is heli-arc welded, hermetically sealed, and ceramic insulated.

Blocks containing 2 stud-mounted accelerometers were bolted to the welded studs provided in the bellows end-plates. Two additional accelerometers were stud mounted to a welded block on the fixture near the impact and abrasion point. Accelerometer locations are illustrated in Figure 24.

Accelerometers mounted directly on the shaker head were monitored on a meter/scope and connected to safety circuits to prevent serious over-test conditions.

Displacements

A specially designed cryogenic Linear Variable Differential Transformer (LVDT) (See Figure 23) incorporating a spring loaded tip was manufactured at Schaevitz Engineering Company. The tip was

FIGURE 22.

SUMMARY OF RESONANT VIBRATION MODES OF CRYO-IMPACT AND ABRASION WEAR FIXTURE

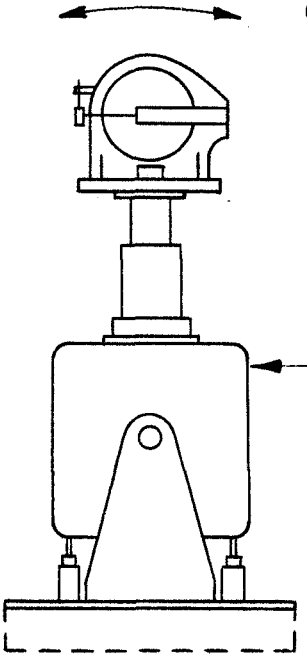

6 HZ:

Rocking Mode of whole (rigid) fixture on impact shaker head suspension stiffness (motion is perpendicular to abrasion and impact axes)

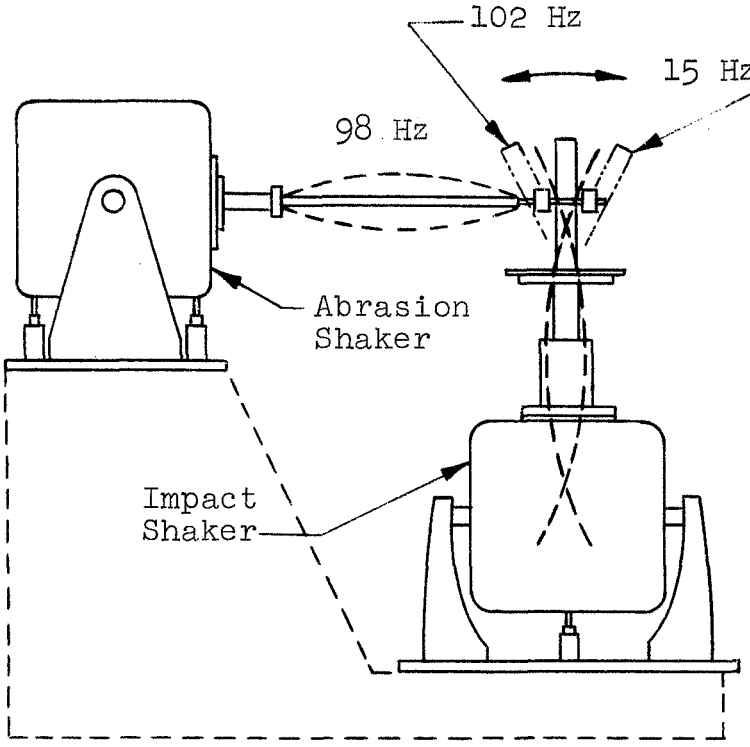

98 HZ:

Lateral Bending mode of abrasion drive rod

15 HZ:

Rocking mode of rigid fixture, in abrasion direction, due to impact shaker head suspension stiffness.

102 HZ:

Quasi-Free-Free bending mode of fixture and pedestal, and impact shaker head in abrasion direction. Excited by abrasion shaker at 34 HZ fundamental input freq.

FIGURE 22. (Continued)

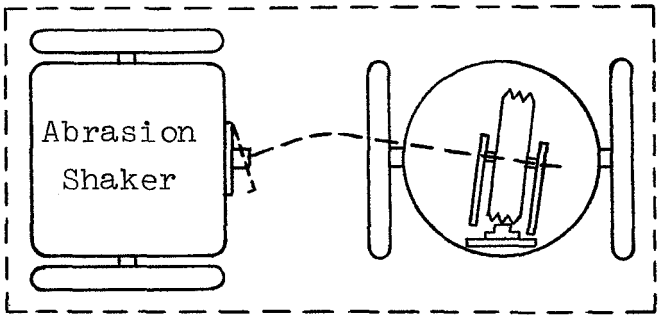

Top View

45 Hz: Bellows pivoting mode about a vertical axis thru arm support shaft. Abrasion drive rod also deflecting laterally

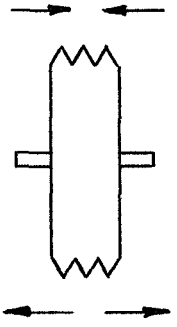

195 Hz: Bellows side plate wobble. Also excited by impacting.

180 Hz: Pre-load flexure Lateral bending mode

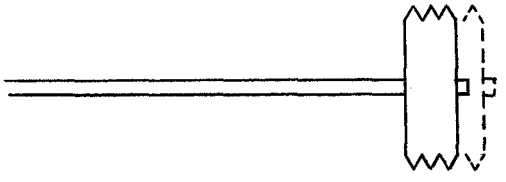

60-65 Hz: Pumping mode of bellows (gas filled)

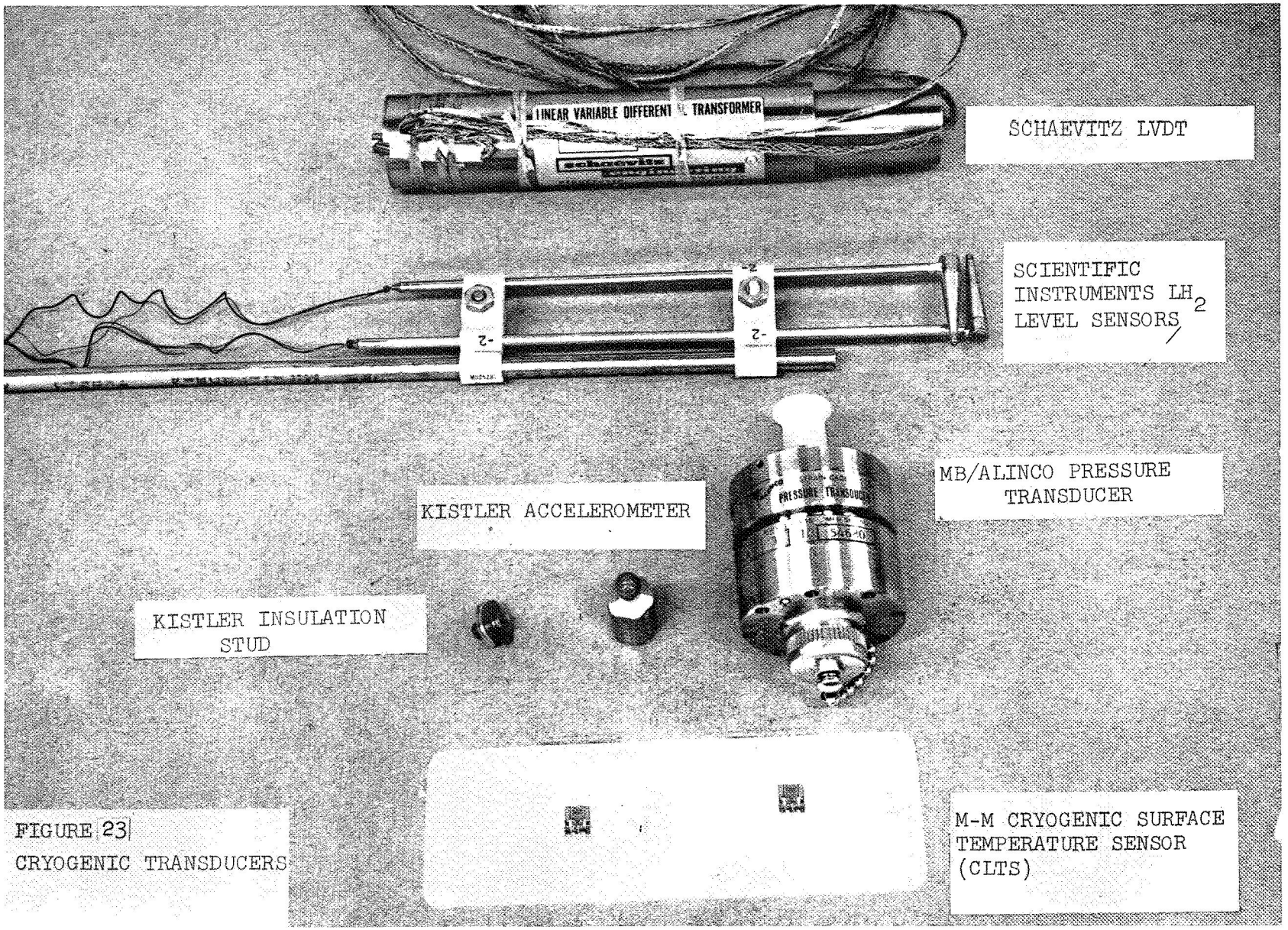

FIGURE 23
CRYOGENIC TRANSDUCERS

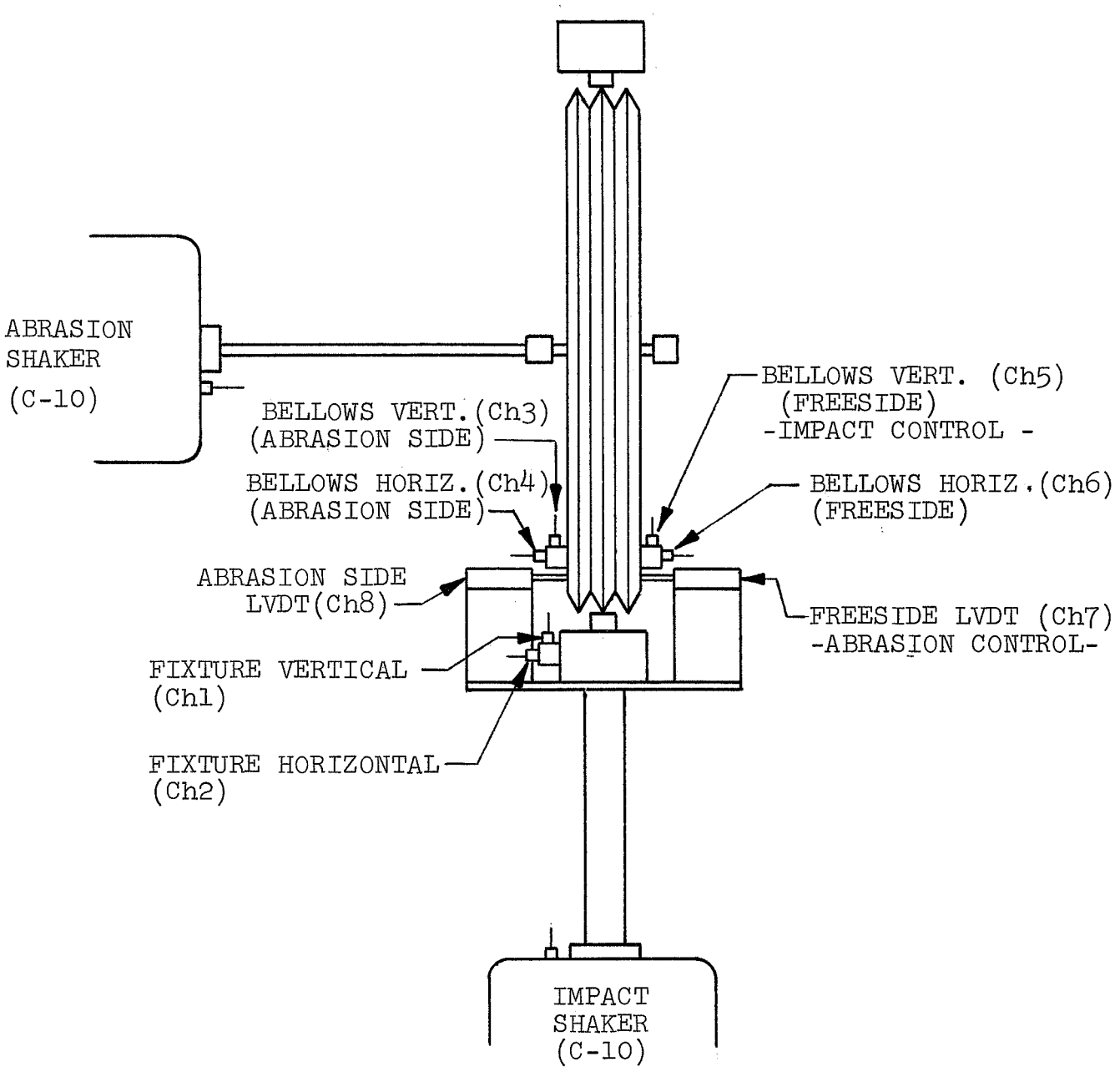

FIGURE 24.
IMPACT AND ABRASION INSTRUMENTATION

preloaded to follow vibration up to 20g's at 100 Hz while being vibrated in a cross-axis. Two LVDT's were clamped to the fixture to sense movement in the abrasion axis of the bellows sample. The difference in transducer readings provided the operator with the correct pitch prior to vibration testing.

During abrasion testing the output of one LVDT was used to set the correct level of displacement in the abrasion axis. This was monitored on the control console with an RMS meter.

Temperature

The Cryogenic Linear Temperature Sensor (CLTS) is a small (.430 inch (1.092 cm) long x .310 inch (.787 cm) wide x .004 inch (.010 cm thick) Surface Thermometer Gage consisting of 3 thin foil sensing grids laminated in an epoxy resin matrix (See Figure 23). Two alloys of special grades of nickel and manganese were processed for equal and opposite non-linearities in Resistance vs. Temperature characteristics. As a result, the composite sensor has an essentially linear change of resistance with temperature.

Six CLTS were installed to monitor the following temperature locations.

Bellows	Top
Bellows	Bottom
Fixture	Top
Fixture	Bottom
Door (inner chamber)	Bottom
Dewar	Bottom

These temperature points were constantly monitored on a readout device to insure temperature equilibrium of the fixture and bellows specimen prior to and during vibration tests.

Pressure

Model 172DBA-1 MB/Alinco Bonded Strain Gage Pressure Transducers were designed for measurements of pressure at cryogenic temperatures. (See Figure 23). The body and diaphragm are integral, machined from a solid body of 17-4 PH stainless steel. These units were disassembled and cleaned for LOX usage.

The pressure differential between the inside and outside of the bellows sample were monitored by two separate pressure sensors. The inside pressure of the bellows was sensed at one of the unused vent ports by means of a flexible coupling to the transducer. The outside pressure of the bellows was obtained by placing the pressure transducer in the inner chamber and leaving the port open to the helium atmosphere.

The pressure transducers were fixed to the base of the bellows fixture. The static output of the transducer was read on D.C. voltmeters during the fill procedure.

Liquid Level

A germanium resistance thermometer in a specially designed case was used to detect the level of liquid hydrogen and LOX by measuring the change in temperature from liquid to gas (See Figure 23).

An electronic control designed and built at Bell, was used to excite the probe and condition the output signal to control a cryogenic fill valve. The operator had the choice of manual or automatic operation of this valve. In the automatic mode, the cryogenic fill valve was controlled by the liquid level probes. In the manual mode, the cryogenic fill valve was controlled by an on-off switch "over-riding" the control of the liquid level probes.

Test Procedure

Specimen Installation

Prior to installation, the tank shell ring and the test specimen were inspected and cleaned to ensure freedom from defects and contaminants.

The tank shell ring segment was installed in the fixture oriented so that an undamaged surface was presented to the test specimen. The bellows specimen was then installed and centered laterally by adjustment of the eccentric on the trunnion guide arms and the trunnions of the specimen were checked for unrestricted longitudinal motion in the guide arm bushing (See Figure 21).

After the specimen to fixture interconnection tubing was installed, the horizontal drive rod was adjusted to position the center convolute of the specimen at mid-position along the tank shell ring segment. Since the width of the ring is 0.375 inch (0.952 cm) the center convolute only was in contact with the ring when the bellows pitch was set at 0.375 inch (.952 cm). The drive rod was adjusted to compensate for shrinkage due to temperature change and offset resulting from inner-chamber pressure. The convolute to ring contact loading mechanism on the trunnion guide arms was adjusted to obtain the required contact force. When all instrumentation was attached and calibrated the access doors to the cryostat were closed and sealed.

Pre-Test System Purge

Prior to introduction of cryogen into the test specimen, the inner-chamber and the dynamic fixture/specimen were evacuated by a high-capacity vacuum pump and then purged with dry helium gas. A gas sample from these systems was analyzed prior to proceeding to ensure that conditions were compatible with the test cryogen.

Cryogen Fill and Drain

To prevent damage by over-extension during the cryogen fill operation, the test bellows internal pressure was maintained at a lower pressure than the chamber pressure. This was monitored by pressure transducer readings from the specimen and inner chamber. The test bellows pitch was also monitored by two linear variable differential transformers located on each side of the test specimen to monitor the end plate movement.

The cryogen was slowly fed into the system to pre-cool the specimen and dynamic fixture. When the temperature sensors indicated liquid was maintained within the specimen, the cryogen flow was increased and maintained for the duration of the test. The test bellows pitch was set at 0.375 inch (.952 cm) by adjustment of bellows internal pressure and inner-chamber pressure and cryogen flow. When the bellows pitch was stabilized and maintained, the vibration test was performed.

After each vibration test, the cryogen in the bellows and fixture was allowed to boil off. The system was purged with helium gas, the interchamber vacuum was released, and the system allowed to warm up.

Dynamic Test

Each test specimen was vibrated for ten minutes in each of three different modes: Impact only, abrasion only, and combined impact and abrasion. After each test mode, the bellows specimen was rotated 60° to a new test point to avoid overlapping of wear areas.

Impact Vibration

The impact exciter was programmed to produce random vibration of bandwidth 15 to 25 Hz. The band pass filter was adjusted to minus 3 db at the high and low end frequencies. An acceleration of 3.0 ±0.3g was maintained for 10 minutes. This was monitored by the bellows freeside impact accelerometer (Ch5 in Figure 24) mounted on the specimen adjacent to the impact contact point.

Abrasion Vibration

The abrasion exciter was programmed to produce random vibration of bandwidth 20 to 50 Hz. The band pass filter was adjusted to minus 3 db at the high and low end frequencies. The exciter output was adjusted to obtain a 0.035 ±0.003 inch rms (0.89 ±0.08 mm rms) bellows displacement as monitored by the freeside LVDT (CH7 in Figure 24, which sensed longitudinal movement of the bellows end plate near the contact point.

Impact and Abrasion Vibration

The impact and abrasion tests of the above paragraphs were performed simultaneously. Shaker control settings obtained from the individual tests were used. The combined impact and abrasion vibration was maintained for a period of ten minutes.

Test Results and Discussion

The impact and abrasion vibration test program was successful in producing various amounts of bellows wear. The results presented in this section include the tape-recorded vibration inputs and bellows response data, and the metallurgical evaluation of the worn areas of the bellows convolutes.

A chronological test summary is presented in Table IV, including bellows tests prior to vibration, bellows-to-ring contact force, overall RMS levels, and general comments.

The vibration input levels, as determined from root-mean-square (RMS) meter readings during the test, oscillogram records from all tests, and power spectral density (PSD) plots of a few representative tests, showed that satisfactory test inputs were achieved for 38 of the 39 vibration tests performed. One (S/N 17) combined I and A test with LO_2 was higher than specified and resulted in excessive specimen damage.

Analysis of the bellows response records was similar to that for the input records. Overall RMS meter readings and oscillogram records were reviewed on a quick-look basis for all tests and subsequently, PSD and peak probability density analyses were produced for 14 of the tests.

Typical PSD plots are presented in Figures 25 to 30. Figure 25 presents a typical impact test input with energy concentrated between 12 and 25 Hz. Figure 26 presents a typical displacement spectrum for an impact test showing the concentration of vibration energy between 9 and 15 Hz. Figure 27 presents a typical displacement spectrum for an abrasion test showing a higher frequency content, most of the energy being between 20 and 40 Hertz. Figure 28 presents the displacement spectral density from a combined impact and abrasion test distinctly showing the two previously mentioned frequency bands superimposed. Figures 29 and 30 are the impact axis and abrasion axis responses, respectively, of the bellows side plate showing the two primary input frequency bands, and several additional higher frequency bellows responses during a combined test. The review of the overall RMS response levels (Table IV) indicates that the response levels are generally consistent among the test specimens and support the indicated input levels.

TABLE IV. SUMMARY OF CRYOGENIC BELLOWS VIBRATION TEST DATA

BELLOWS S/N	TESTS, Previous	TESTS, Vibration	VIBRATION TEST DATE	NET CONTACT FORCE, NEWTONS	FIXTURE IMPACT AXIS grms	FIXTURE ABRASION AXIS g rms	BELLOWS ABR. SHAKER SIDE IMPACT g rms	BELLOWS ABR. SHAKER SIDE ABRASION g rms	BELLOWS FREE SIDE IMPACT g rms	BELLOWS FREE SIDE ABRASION g rms	BELLOWS SKR SIDE LVDT MM rms	FREESIDE LVDT MM rms	REMARKS
LH_2:													
15		IMPACT(I)	12-11-70	5.58	.77	.26	.93	.86	.85	.72	.135	.18	Low input inner door leak 10cpm pitch oscilln.
		ABRASION(A)	12-12-70	4.45	.26	.44	.85	2.6	1.2	3.6	.60	.525	Door leak
		COMBINED(C)	12-14-70	Var.	3.08	1.76	13.5	10.4	13.5	16.0	.45	1.335	Door leak feed line failed LVDT Chatter
13		I	12-18-70	37.8	1.02	.44	3.45	3.52	3.45	3.13	.325	.350	
		A	12-19-70	24.5	1.17	1.06	12.7	18.6	8.7	15.6	.98	.70	LVDT Chatter
		C	12-21-70	6.67	1.57	1.64	4.6	5.6	3.78	4.86	.50	-	Loss of Bellows pitch control (9.5mm) Part of Test
19	STORAGE	I	3-5-71	4.45	1.77	1.42	2.21	2.83	3.19	3.54	.625	.525	Long LVDT Mark, ramp impact damage on center convolute.
		A	3-8-71	- 6.67	.35	.27	3.01	6.2	3.01	6.73	.88	.852	
		C	3-9-71	0.00	1.38	.90	3.5	4.8	3.5	5.7	.88	.726	
33	STORAGE	I	3-10-71	6.67	1.77	.80	3.01	3.10	3.89	3.89	.625	.65	Long LVDT mark ramp mark on center convolute
		A	3-11-71	4.45	.35	.89	3.89	4.43	2.61	4.87	1.030	.955	Fill problems, wear on top of bellows
		C	3-12-71	0.00	2.12	1.42	5.31	7.43	5.66	7.08	.98	1.03	Cryogen feed line failed.
2	PRE-TEST	I	3-15-71	0.00	1.95	.53	3.01	1.59	3.10	1.68	.25	.30	Long LVDT Mark
	CYCLING	A	3-16-71	- 0.44	.34	.80	2.12	4.60	2.83	5.31	.88	.955	Fill problems bellows stuck at start of test
	STORAGE	C	3-18-71	0.00	1.12	1.10	3.54	4.43	3.89	2.10	.575	.675	
4	PRE-TEST	I	3-19-71	6.67	1.42	.97	3.54	2.92	3.54	3.36	.35	.374	
	CYCLING	A	3-22-71	6.67	.39	.89	1.77	3.72	2.66	5.13	.852	.778	
	STORAGE	C	3-23-71	6.67	1.59	1.59	3.36	4.96	4.43	6.37	.852	.955	Slow oscillations in bellows pitch
20		I	3-24-71	0.00	2.12	1.15	3.54	1.95	3.01	2.57	.225	.175	
		A	3-25-71	- 4.45	.35	.80	2.66	5.31	3.54	5.31	.70	.827	
		C	3-26-71	0.00	.62	.88	2.66	4.07	2.76	4.43	.98	.827	Long LVDT Mark
14		I	3-29-71	8.90	1.28	.69	1.82	2.08	2.05	2.68	.30	.225	Slow oscillations in bellows pitch
		A	3-30-71	6.67	.68	.95	1.86	4.4	2.6	4.7	.803	.88	
		C	3-31-71	6.67	.52	.82	1.77	3.84	2.39	5.14	.78	.78	
LO_2:													
17	PRE-TEST	I	5-20-71	37.8	2.09	.95	3.64	2.71	3.77	2.98	1.03	.524	Interrupt test twice to refill cryogen Dewar
	CYCLING	A	5-21-71	4.45	.50	.97	1.52	3.12	1.35	1.21	1.206	1.255	Poor Pitch Control marks
		C	5-24-71		1.14	.97	2.46	2.94	2.51	3.9	-	.88	Overtest: Long LVDT Mark wear on top. ramp /
21	PRE-TEST	I	5-26-71	44.5	1.85	1.07	3.06	1.91	2.95	1.72	.675	.35	
	CYCLING	A	5-27-71	40.0	.56	.97	2.08	4.08	1.80	4.13	.98	1.205	
		C	5-28-71	40.0	1.69	1.54	3.42	4.78	3.44	4.78	1.205	1.41	
22	PRE TEST	I	6-1-71	17.8	1.90	.97	2.65	1.57	2.5	1.15	.55	.35	
	CYCLING	A	6-2-71	20.0	.38	.97	.95	2.55	1.16	2.48	1.02	.955	
		C	6-3-71	22.24	1.77	1.94	3.06	3.34	3.28	3.88	1.08	1.02	
23		I	6-4-71	22.24	2.01	1.24	2.64	1.75	2.87	2.23	.625	-	
		A	6-7-71	20.0	.40	1.41	1.49	3.98	1.31	3.31	1.03	1.03	
		C	6-8-71	26.7	2.01	1.57	2.98	3.10	3.19	3.80	.905	.778	
24		I	6-9-71	42.26	1.61	1.0	2.07	1.19	1.88	1.16	.525	.225	
		A	6-10-71	42.26	.32	1.12	1.16	3.18	.90	2.89	1.155	.827	
		C	6-11-71	44.5	1.93	1.85	2.89	3.66	3.44	4.79	1.08	1.03	

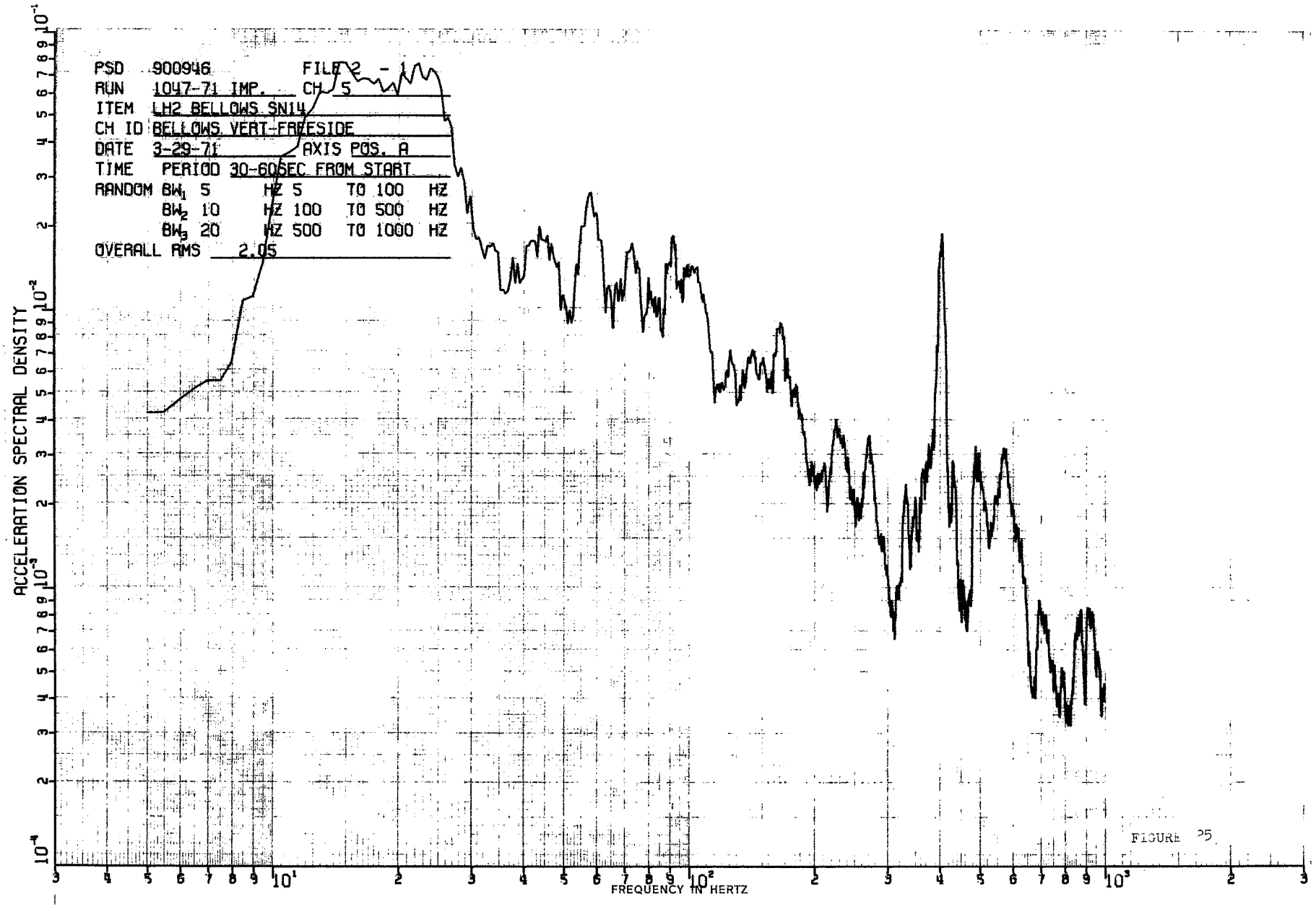
PSD 900946 FILE 2 - 1
RUN 1047-71 IMP. CH 5
ITEM LH2 BELLOWS SN14
CH ID BELLOWS VERT-FREESIDE
DATE 3-29-71 AXIS POS. A
TIME PERIOD 30-60SEC FROM START
RANDOM BW1 5 HZ 5 TO 100 HZ
BW2 10 HZ 100 TO 500 HZ
BW3 20 HZ 500 TO 1000 HZ
OVERALL RMS 2.05
ACCELERATION SPECTRAL DENSITY
FREQUENCY IN HERTZ

FIGURE 25

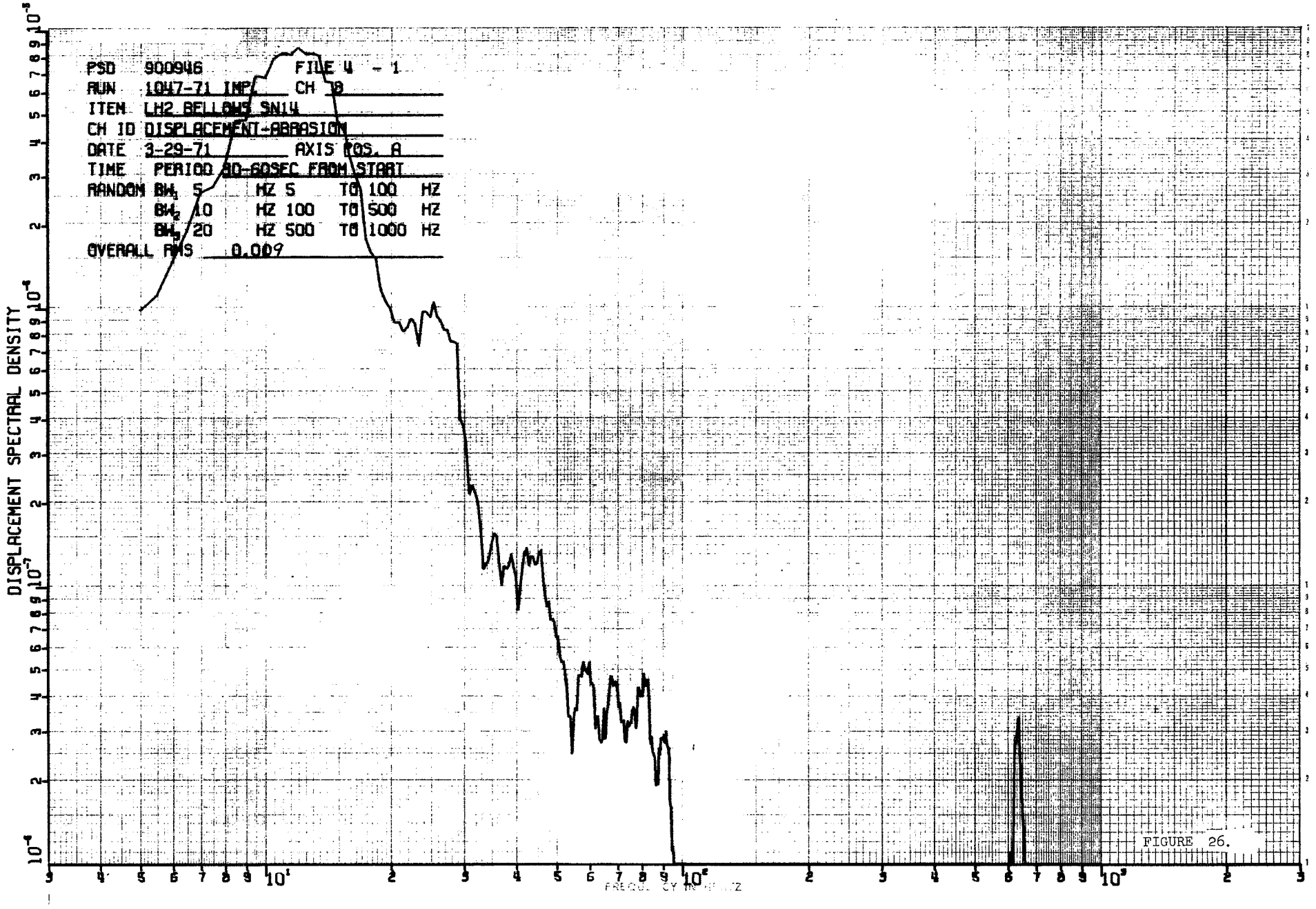
PSD 900946 FILE 4 - 1
RUN 1047-71 IMPL CH 10
ITEM LH2 BELLOWS SN14
CH ID DISPLACEMENT-ABRASION
DATE 3-29-71 AXIS POS. A
TIME PERIOD 30-60SEC FROM START
RANDOM BW1 5 HZ 5 TO 100 HZ
BW2 10 HZ 100 TO 500 HZ
BW3 20 HZ 500 TO 1000 HZ
OVERALL RMS 0.009
DISPLACEMENT SPECTRAL DENSITY
FREQUENCY IN HERTZ

FIGURE 26.

PSD S00SW6 FILE 7 - 1
RUN LOW-71 888 CH 7
ITEM LH2 BELLOWS SN11
CH ID DISPLACEMENT-FREESIDE
DATE 3-30-71 AXIS POS.B
TIME PERIOD 30-60SEC FROM START
RANDOM BW1 10 HZ 5 TO 100 HZ
BW2 20 HZ 100 TO 500 HZ
BW3 20 HZ 500 TO 1000 HZ
OVERALL RMS 0.033
DISPLACEMENT SPECTRAL DENSITY
FREQUENCY IN HERTZ
FIGURE 27.

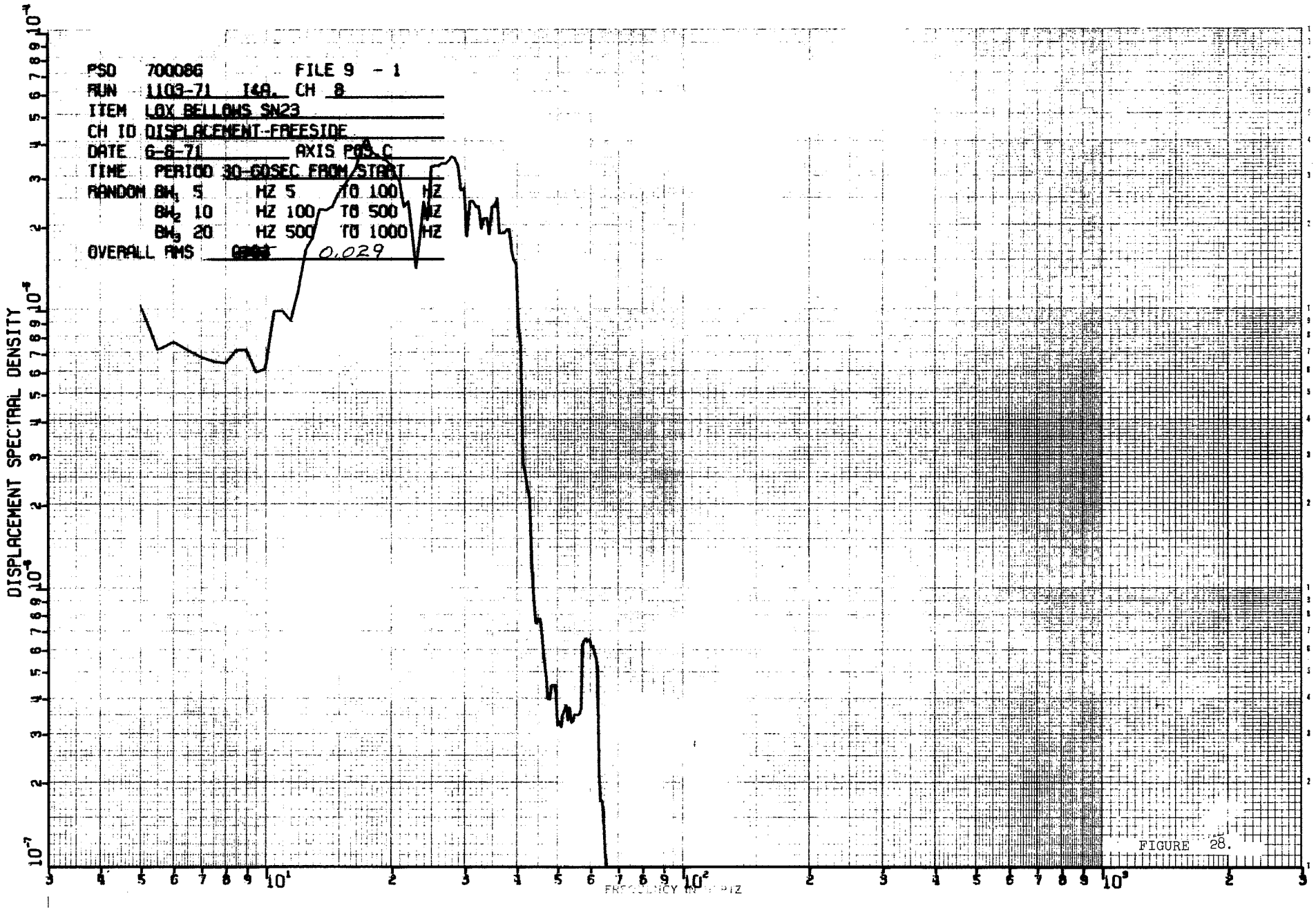
PSD 700086 FILE 9 - 1
RUN 1103-71 I4A CH 8
ITEM LOX BELLOWS SN23
CH ID DISPLACEMENT-FREESIDE
DATE 6-6-71 AXIS P&S C
TIME PERIOD 30-60SEC FROM START
RANDOM BW1 5 HZ 5 TO 100 HZ
BW2 10 HZ 100 TO 500 HZ
BW3 20 HZ 500 TO 1000 HZ
OVERALL RMS 0.029
DISPLACEMENT SPECTRAL DENSITY
FREQUENCY IN HERTZ

FIGURE 28.

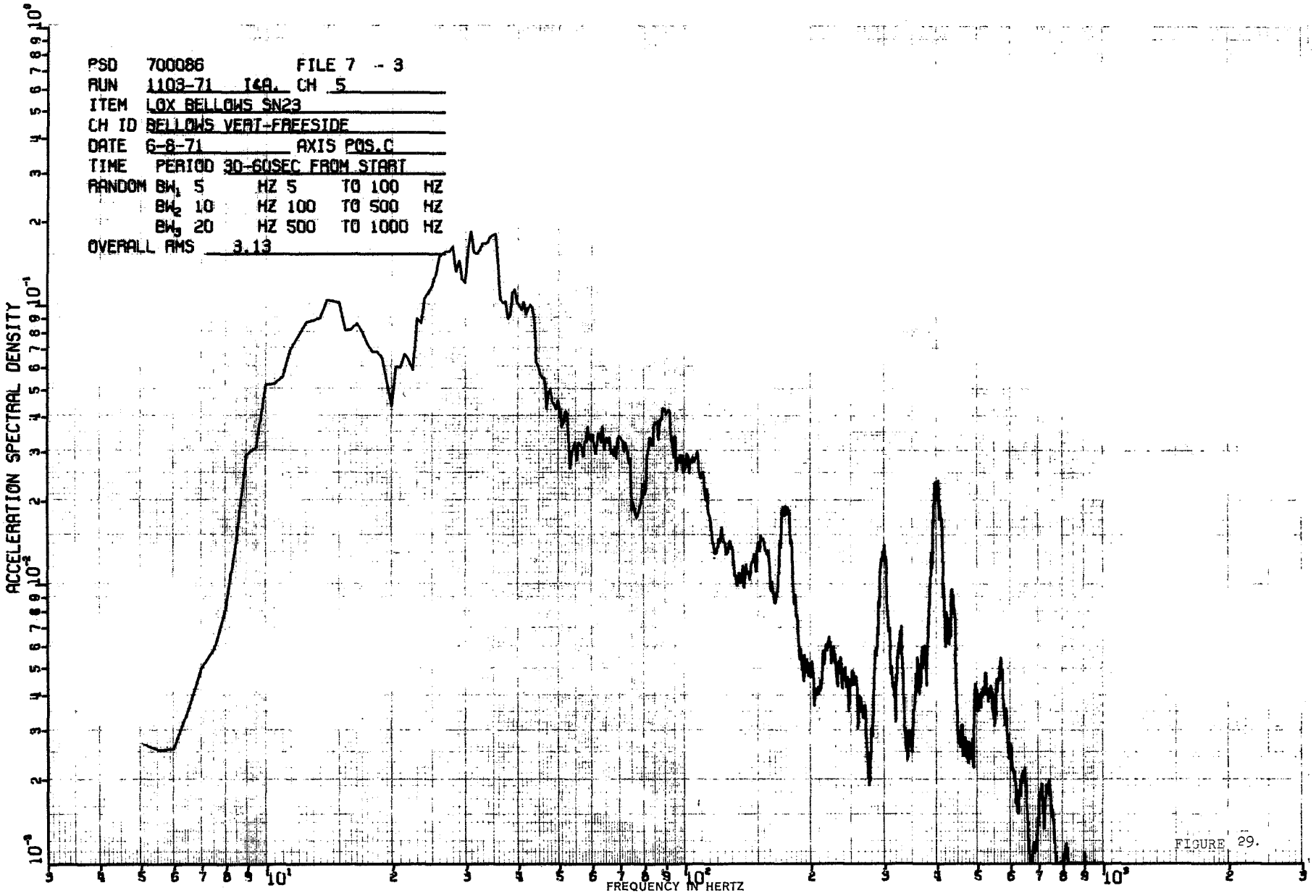
PSD 700086 FILE 7 - 3
RUN 1103-71 I&A. CH 5
ITEM LOX BELLOWS SN23
CH ID BELLOWS VERT-FREESIDE
DATE 6-8-71 AXIS POS.C
TIME PERIOD 30-60SEC FROM START
RANDOM BW1 5 HZ 5 TO 100 HZ
BW2 10 HZ 100 TO 500 HZ
BW3 20 HZ 500 TO 1000 HZ
OVERALL RMS 3.13
ACCELERATION SPECTRAL DENSITY
FREQUENCY IN HERTZ

FIGURE 29.

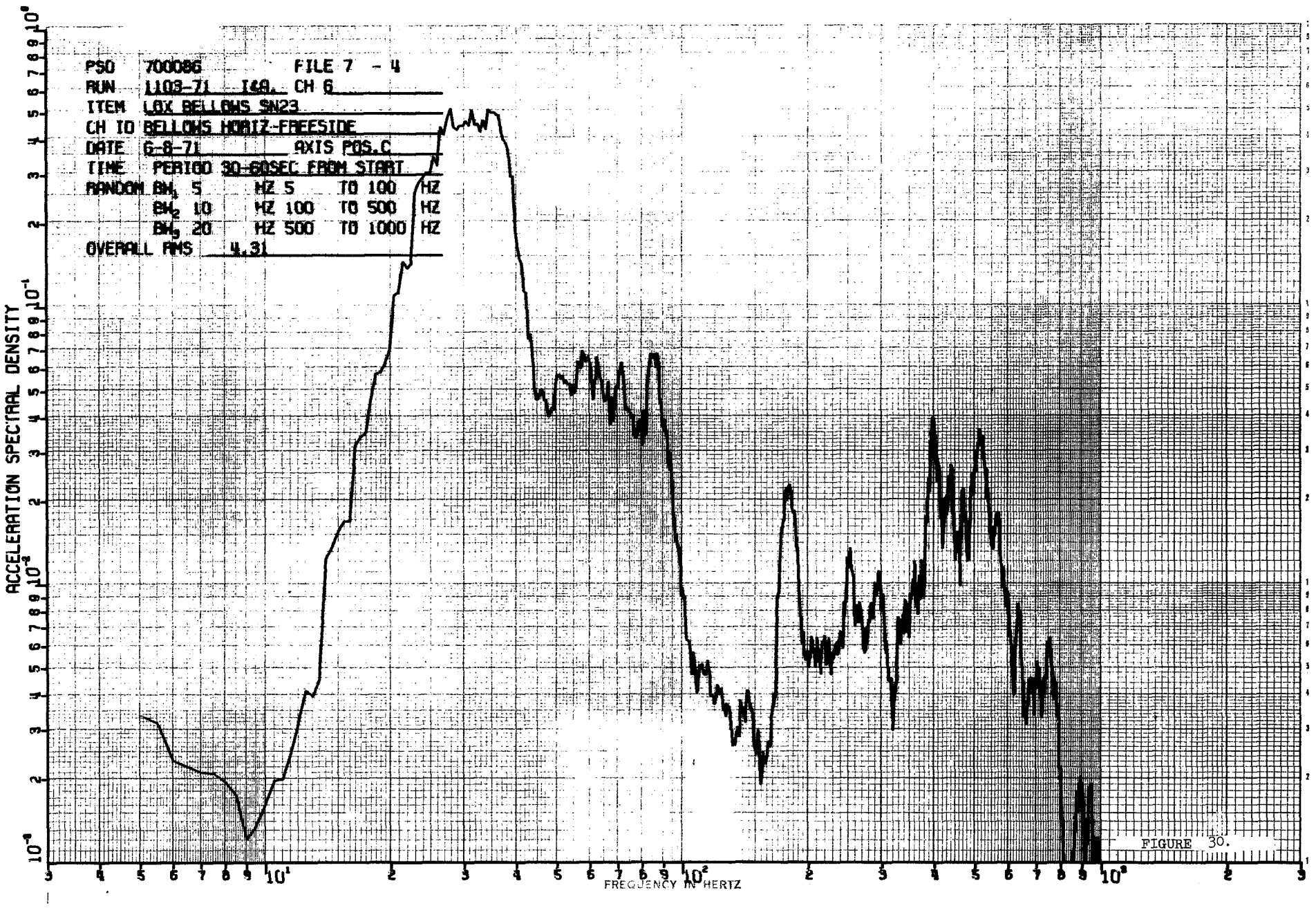
PSD 700086 FILE 7 - 4
RUN L103-71 I&R. CH 6
ITEM LOX BELLOWS SN23
CH ID BELLOWS HORIZ-FREESIDE
DATE 6-8-71 AXIS POS.C
TIME PERIOD 30-60SEC FROM START
RANDOM BH1 5 HZ 5 TO 100 HZ
BH2 10 HZ 100 TO 500 HZ
BH3 20 HZ 500 TO 1000 HZ
OVERALL RMS 4.31
ACCELERATION SPECTRAL DENSITY
FREQUENCY IN HERTZ

FIGURE 30.

There is reasonable agreement between the bellows freeside and abrasion side response indicating that no significant pitch change (except as noted below) or end plate oscillation took place during the tests. This is confirmed by the oscillogram traces of the LVDT's.

Three tests show unusual response levels, these are LH_2 specimen S/N 15 abrasion only and combined impact and abrasion, and LH_2 specimen S/N 13 abrasion only. The S/N 15 abrasion test shows generally low response levels which were attributed to a low input level. The primary control (the freeside LVDT) was lost near the beginning of the test, but control was maintained at a set shaker input. The other two tests showed higher than usual accelerometer responses, which are attributed to chattering of the LVDT's due to insufficient pre-load against the bellows side plates.

The cryogenic propellant handling requirements requires that the bellows be extended and filled remotely after the cryostat has been closed and temperature conditioned. Bellows pitch was controlled by maintaining pressure across the bellows. The LVDT's monitored the pitch while the pressure was maintained by manually controlled valves. In general, loss of pitch or pitch control oscillations are not detrimental to the test specimen although they were factors in the ramp impact damage on the center convolute and possibly contributed to unusually long LVDT marks.

During vibration testing the LVDT's made marks on the bellows end plates. After several impact and combined impact and abrasion tests unusually long marks were noted. They were .3 to .4 inches (.75 to 1.0 cm) long and indicated that the bellows vertical motion exceeded the clearance between the bellows and the shell. Although not definitely explained, the probable cause is lack of sufficient clearance between the LVDT and the bellows accelerometer mounting block. During some impact vibration the block may have deflected the LVDT causing the indication of excessive vertical motion. After the clearance was increased (Specimen S/N 21 and subsequent) there was no further occurrence of long marks. If the long marks were caused by this lack of clearance, all test results remain valid. Antoher possible cause of the long LVDT marks is loss of or decrease in bellows pitch which allows the bellows to draw back and oscillate outside the confines of the ring. The effect on impact damage if this occurred is unknown. Thus, the application of these test results must be restricted. Specimens affected are S/N 19, S/N 33 and S/N 2 impact only and S/N 20 and S/N 17 combined impact and abrasion.

A ramp was required on the test fixture to permit the bellows, when being loaded, to enter the ring without catching. Loss of or decrease in bellows pitch allows the center and freeside convolutes to draw back and impact on the ramp. The ramp was not a normal type of contact point and such specimens had somewhat distorted wear and impact damage areas. Specimens affected were S/N 19 and 33 impact only and S/N 17 combined impact and abrasion.

The bellows to shell normal force was specified in the test plan to be either 4.0 or 8.5 lb (17.8 or 37.8 newtons). However, after completion of tests on bellows S/N 17, it was found that pressurization of the inner chamber above atmospheric caused the fixture to deflect downward. Due to the vertical stiffness of the abrasion axis drive rod, the net force on the bellows/shell interface was less than desired. The actual forces were computed from a pressure, force, deflection analysis of the fixture and shaker supports to obtain the actual contact forces.

The last four LO_2 bellows had approximately the desired 4 or 8.5 lb loads by increasing the pre-test load settings to compensate for the inner chamber pressurization effect.

Another condition which was noted but did not affect the test results was a jamming of the freeside LVDT particularly at the beginning of the run and failure of the LVDT's to follow the bellows motion at all times. These effects occurred during some of the tests and are apparent in the LVDT response data.

Table V is a summary of large and small buckles noted in the bellows center convolute following impact tests.

Post vibration metallurgical evaluation consisted of visual and microscopic evaluations. A detailed microscopic examination was made of each area damaged by impact, abrasion and combined impact and abrasion. Cross sections of these areas were mounted for metallographic examination and physical measurement of wear patterns. The samples were examined for evidence of cold working, fatigue cracks, corrosion, micro structural changes or other defects and/or damage. The measurements included wear width and wear depth. Microhardness measurements were made at the crest, root and leaf of the cross section samples from the wear area. Wear dimensions and microhardness values are listed in Table VI. Figure 31 shows the bellows angular orientation for the metallurgical evaluation. Figure 32 shows typical results of vibration testing in each of the three-dynamic modes tested.

The range of hardness values recorded for bellows abrasion-impact tested in liquid hydrogen was greater than that observed for the room temperature tested bellows. Maximum crest bend hardness levels were also higher for the liquid hydrogen test bellows. The maximum hardness values and the range of values for the liquid oxygen bellows were about the same as those measured on the bellows tested

TABLE V SUMMARY OF BELLOWS CENTER CONVOLUTE

IMPACT DAMAGE - CRYOGEN TESTS

SPECIMENS	TEST	VERTICAL (LOAD (NEWTONS)	IMPACT INPUT-Ch5 (g rms)	DESCRIPTION (L.P. = Load Point)
S/N 19	IMPACT	4.45	3.19	Buckle 5 cm from L.P. Small sharp buckle 3.7 cm from L.P.
S/N 33	I & A	0.00	5.66	Slight buckle 1.9 cm from L.P.
S/N 20	IMPACT	0.00	3.01	Buckle & dents 3.4 cm and 5.3 cm from L.P.
	I & A	0.00	2.76	Severe buckling 1.25 to 3.1 cm from L.P.
S/N 21	IMPACT	44.5	2.95	Small sharp buckles
S/N 22	IMPACT	17.8	2.5	5 wrinkles 1.85 cm apart
S/N 23	IMPACT	22.24	2.87	Small sharp buckle near L.P.
	I & A	26.7	3.19	Small buckles near L.P.

TABLE VI METALLURGICAL EVALUATION OF CRYOGENIC BELLOWS WEAR

BELLOWS S/N	TEST	LOCATION (SEE FIGURE 24)	+CREST MICRO-HARDNESS Kg/mm^2	+ROOT MICRO-HARDNESS Kg/mm^2	+LEAF MICRO-HARDNESS Kg/mm^2	WEAR* DEPTH mm	WEAR AREA MAXIMUM WIDTH, mm.	WEAR AREA LENGTH, cm.
15	I	315°	300	261	177	0.0	0.0	
	A	0°	296	267	177	.0147	.0833	1.27
13	I	310°	384	219	219	.0110	.295	
	A	15°	296	229	191	.0185	.325	
	I+A	60°	271	277	207	.0046	.0874	1.9
19	I	300°	421	246	183	0	0	.95
	A top	180°	271	225	187	.0122	.112	.64
	I+A	60°	316	249	179	.0099	.084	
33	I	300°	296	246	197	.0086	.0625	3.3
	A	0°	350	255	191	.0109	.108	1.27
	I+A	60°	300	232	187	.0094	.079	.95
	A top	220°	353	255	191	.025	.302	
2	I	300°	343	274	210	.0135	.142	4.5
	A	0°	264	277	207	.0094	.080	
	I+A	60°	264	277	203	.00685	.0915	
	A top	150°	316	249	214	.0261	.411	
4	I	60°	312	277	203	.0101	.075	3.2
	A top	180°	312	232	227	.0094	.0875	1.6
	I+A	300°	277	271	222	.0046	.1270	1.8
20	I	300°	310	181	191	.014	.0833	
	A	0°	308	183	189	.0094	.159	
	I+A	60°	310	214	177	.014	.0625	
14	I	300°	255	189	183	.0134	.0833	1.9
	A	0°	264	222	181	0.0	0.0	1.6
	I+A	60°	267	189	187	.0203	.166	1.8
17	I	280°	348	201	217	0.0	.166	
	A	0°	285	189	255	.0046	.100	
21	I	285°	296	229	258	.0046	.175	
	A	20°	274	224	281	.00254	.150	
	I+A	55°	277	212	258	.00915	.133	
22	I	300°	296	232	246	.0046	.150	
	A	0°	264	205	232	.0046	.089	
	I+A	60°	288	217	224	.0046	.099	
23	I							
	A	0°	363	203	227	.0025	.183	
	I+A	75°	408	229	258	-.0025	.212	
24	I	270°	264	217	224	.0053	.158	
	A	340°	288	217	217	.0094	.175	
	I+A	65°	329	243	271	.0053	.176	

* Based on nominal thickness of 0.168 mm

\+ Measured at room temp. after testing.

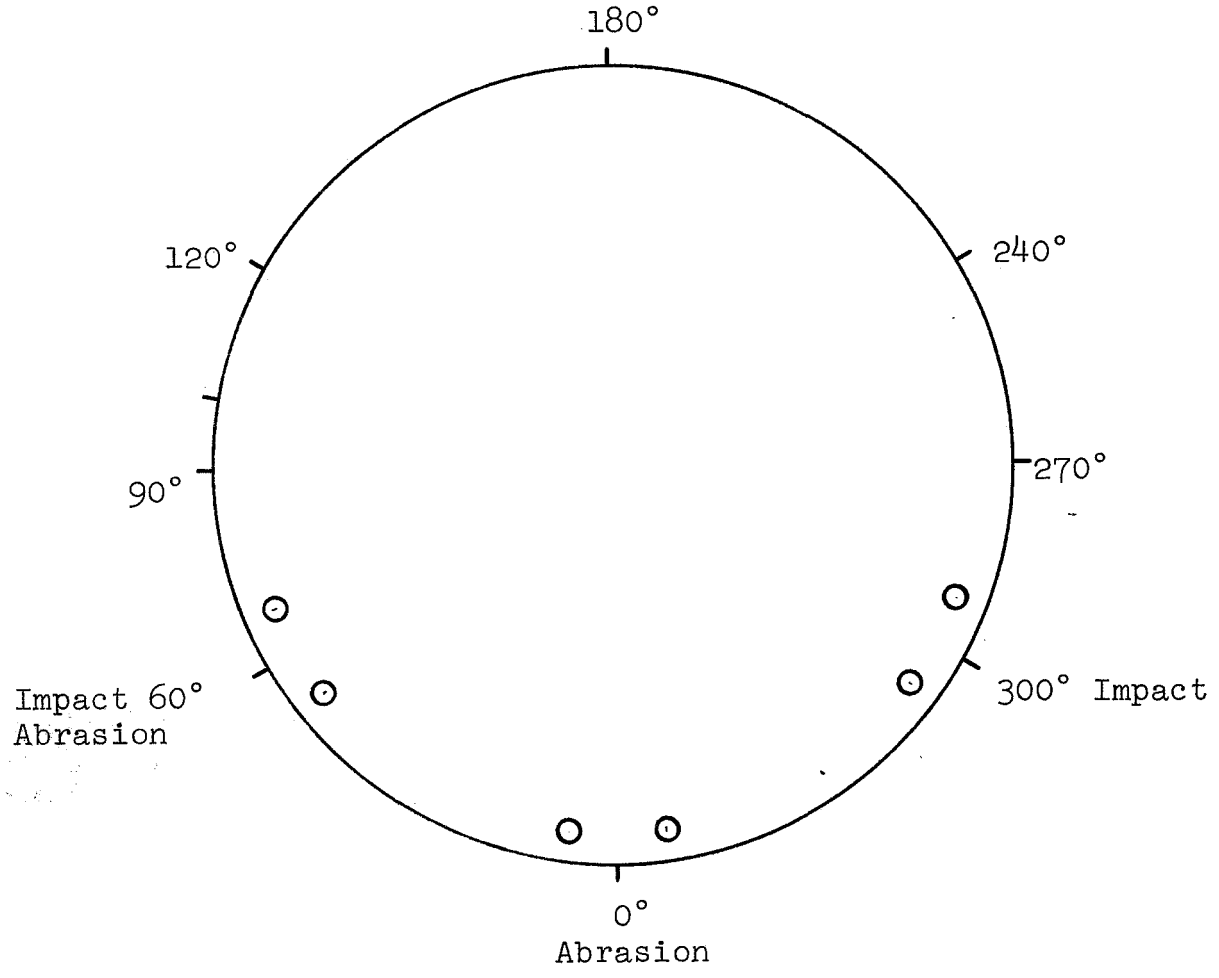

View Looking at Back Plate Of
Bellows - No Ports

FIGURE 31 TEST ORIENTATION DIAGRAM
OF CRYOGENIC BELLOWS

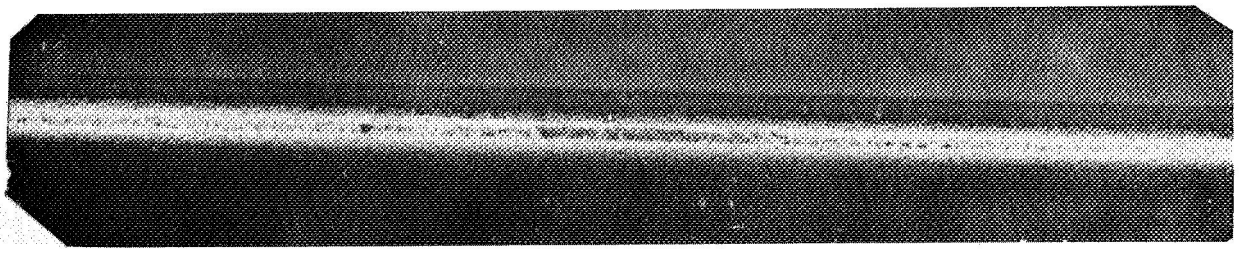

RESULTS OF IMPACT VIBRATION, SPECIMEN S/N 2

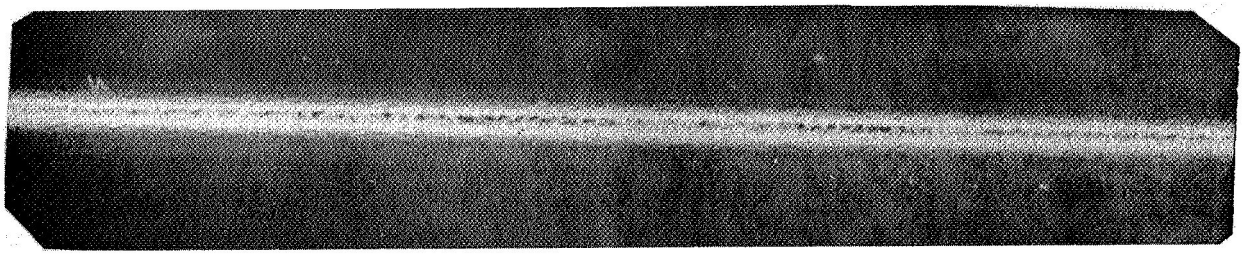

RESULTS OF ABRASION VIBRATION, SPECIMEN S/N 2

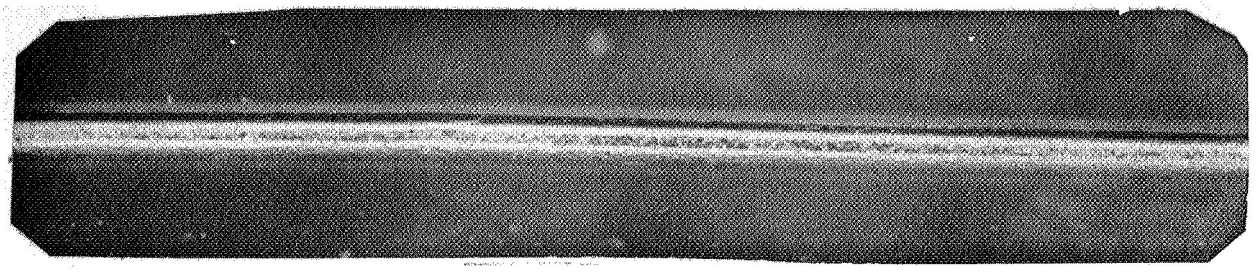

RESULTS OF COMBINED IMPACT & ABRASION, SPECIMEN S/N 19

FIGURE 32

"STRAIGHT-ON" VIEW OF THE CENTER CONVOLUTION CRESTS AFTER VIBRATION TESTING IN LIQUID HYDROGEN

in LH_2. Regardless of test temperature, crest and root bend hardnesses were generally higher than the convolute hardness, reflecting the effect of work hardening induced during the bellows forming operation.

The somewhat greater hardening observed at the liquid hydrogen and liquid oxygen test temperatures is attributed to a greater propensity for work hardening of face centered cubic alloy at cryogenic temperatures. Examination of microstructures provides additional verification of this observation. Note strain lines in Figures 33 through 40 (the diamond shaped impressions in the photographs are caused by the hardness tests).

Cross section microphotographs of typical LH_2 abrasion load points and impact load points are presented in Figures 33 to 36. Figure 35 shows the maximum abrasion wear of a LH_2 specimen. Figures 37 and 38 present a typical LO_2 abrasion load point and impact load point. Figure 39 shows an undamaged section taken between impact and abrasion load points. Figure 40 shows the start of a small fatigue crack in LO_2 specimen S/N 23 at the combined impact and abrasion load point.

Correlation of Analytical Results to Empirical Results

The wear of materials in sliding contact has been the subject of much testing and literature. Most analyses of wear are partly empirical due to the complicated and incompletely understood mechanisms involved. A common wear equation has been adapted for use in correlating the bellows wear due to impact and abrasion vibration tests at cryogenic temperatures.

Factors affecting wear include normal load and apparent contact stress, relative sliding distance, material hardness, material modulus of elasticity crystal orientation with respect to the direction of sliding, lubrication, and surface finish, (Ref. 1). When the apparent contact stress is less than 1/3 the hardness of the softer material, the volumetric wear is directly proportional to the normal load and distance traveled, and inversely proportional to three times the microhardness (Ref. 2). Thus, the volume of softer material lost due to sliding is:

$$V = \frac{k\ P\ D}{3.0\ Hm\ g}$$

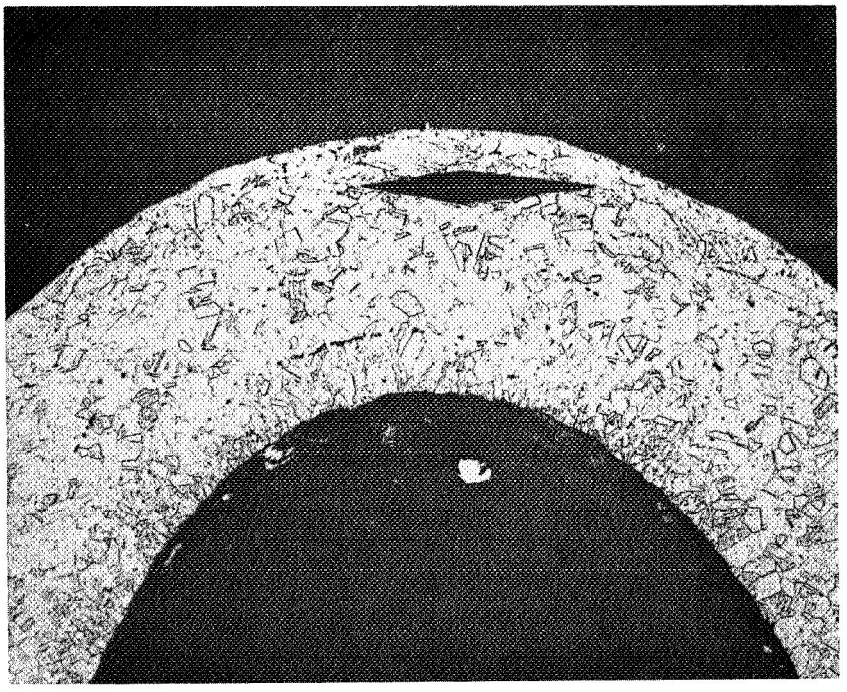

FIGURE 33
CROSS SECTION OF ABRASION LOAD POINT OF BELLOWS
SERIAL NUMBER 4, TESTED IN LIQUID HYDROGEN

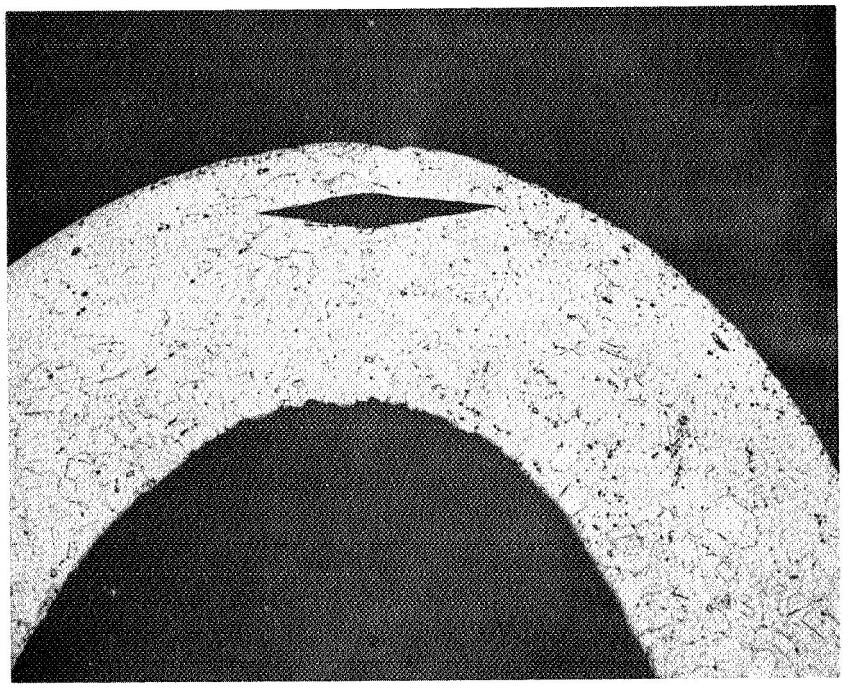

FIGURE 34
CROSS SECTION OF IMPACT LOAD POINT OF BELLOWS
SERIAL NUMBER 20, TESTED IN LIQUID HYDROGEN

FIGURE 35

CROSS SECTION OF MAXIMUM WEAR OCCURRING NEAR ABRASION LOAD POINT OF BELLOWS SERIAL NUMBER 13, TESTED IN LIQUID HYDROGEN. (ETCHANT: OXALIC ACID, MAG: 300X)

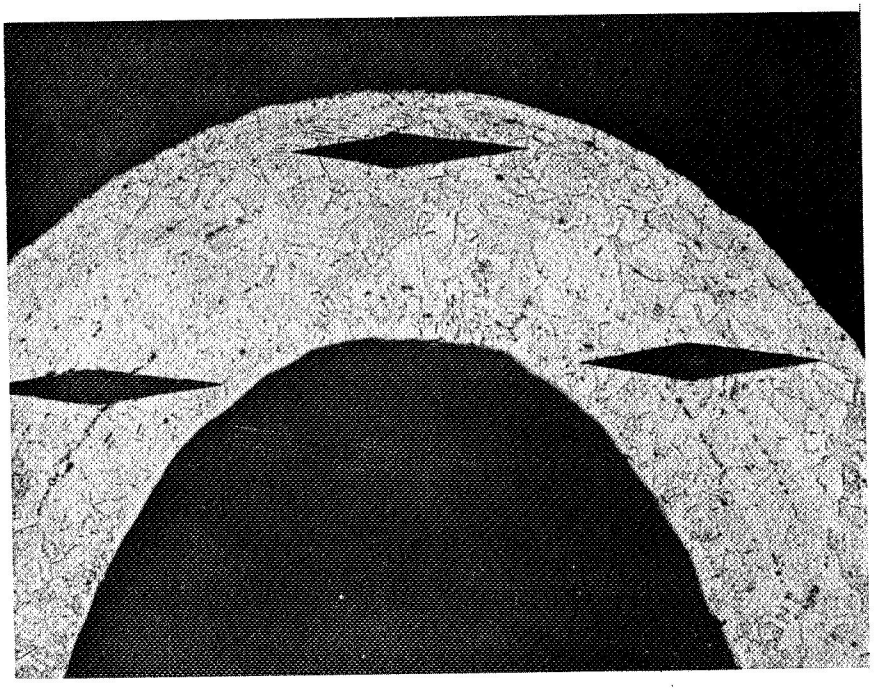

FIGURE 36

SLIGHT WEAR FLAT NOTED NEAR ABRASION POINT OF BELLOWS SERIAL NUMBER 21, TESTED IN LIQUID HYDROGEN. NOTE STRAIN LINES.

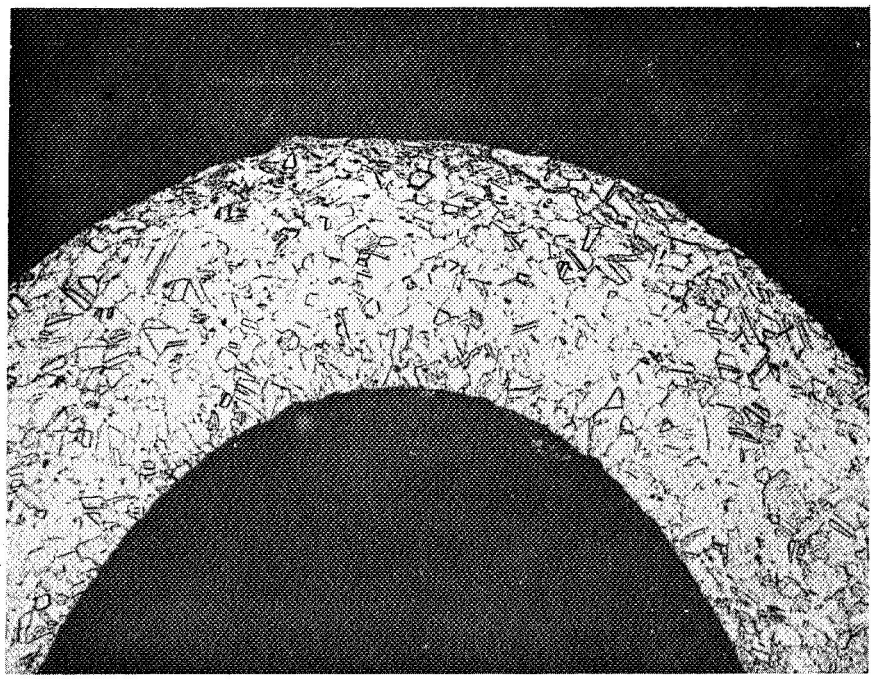

FIGURE 37

SLIGHT WEAR FLAT NOTED NEAR IMPACT POINT OF BELLOWS S/N 24, TESTED IN LIQUID OXYGEN. NOTE STRAIN LINES IN STRUCTURE.

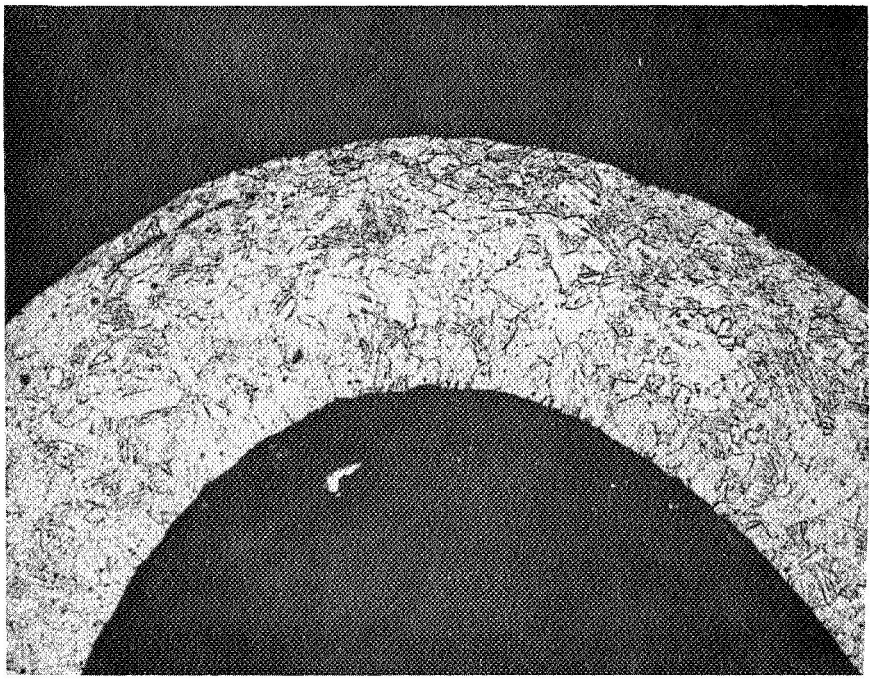

FIGURE 38

NO MEASURABLE WEAR FLAT IN BELLOWS S/N 23, BETWEEN IMPACT AND ABRASION POINTS. NOTE PRESENCE OF STRAIN LINES IN STRUCTURE. (ETCHANT: OXALIC ACID, MAG: 200X)

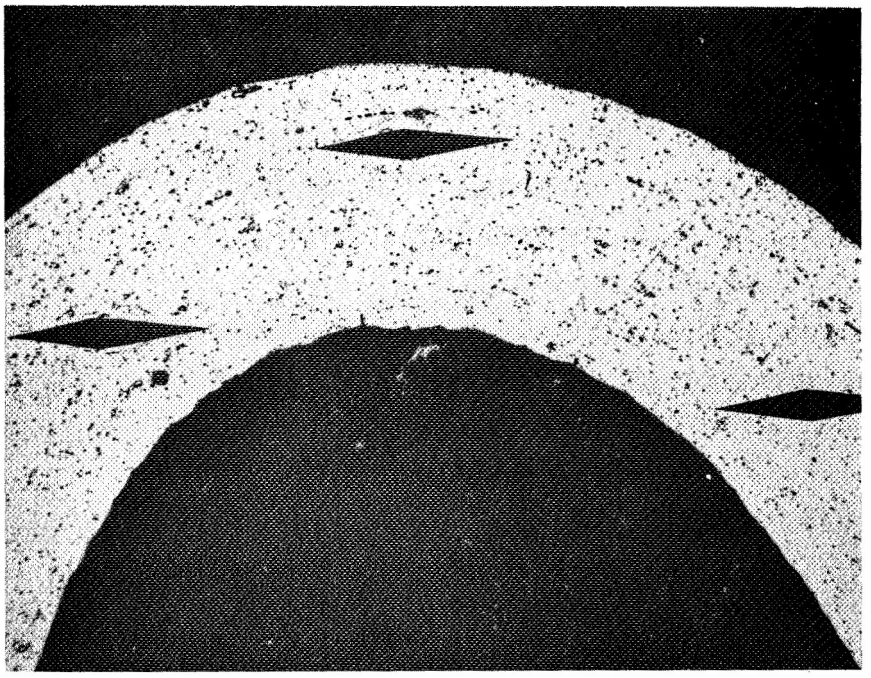

AFTER
HARDNESS
MEASUREMENTS

FIGURE 39

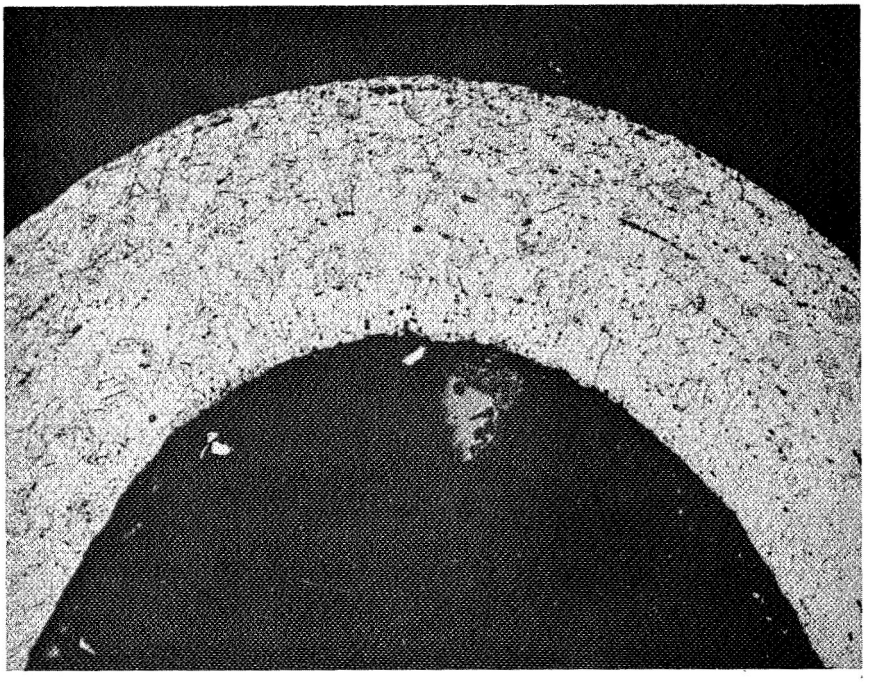

AFTER
REPOLISHING
AND
ETCHING.
NOTE STRAIN
LINES IN
STRUCTURE

FIGURE 40

START OF SMALL FATIGUE CRACK AT CREST BEND I.D. OF BELLOW S/N 23 AT IMPACT. - ABRASION LOAD POINT. TESTED IN LIQUID OXYGEN

where

V = volume of softer material lost in mm^3

k = wear coefficient for material pair

P = normal load in Newtons

D = relative sliding distance in millimeters

Hm = microhardness of softer material (Vickers, Knoop, or Brinell tester) in Kg/mm^2

g = acceleration of gravity = 9.807 $meter/sec^2$ (Reference 3).

The wear coefficient "k" can be physically interpreted as the probability of a high spot breaking off to form a wear particle, Reference 4. For example, a coefficient of 0.001 means that for every one-thousand contacts of the microscopic surface irregularities, one wear particle will be formed. A particle may break off the first time a particularly high spot contacts the opposing surface by gross shearing of the peak, or the spot may make contact several times elastically before fatiguing.

A computer program existed based on the above wear volume equation in support of previous Bell IR&D room temperature bellows wear tests. A block diagram of the program is shown in Appendix B.

A few trial calculations of the bellows wear using nominal test conditions and previously used room temperature values for the wear coefficient and bellows microhardness resulted in greater predicted wear than actually occurred at cryogenic temperatures. Consequently, each input parameter was temperature corrected for variations due to cryogenic temperatures and the actual conditions for each vibration test. Cryogenic bellows wear analysis input data are listed in Table VII.

Bellows microhardness values obtained from the post-test metallurgical evaluations of the worn bellows areas are listed in Table VI. In addition, a curve of hardness vs temperature for annealed A.I.S.I. 347 stainless steel was compiled for various temperatures and used in this evaluation. See Figure 41. The bellows hardness was corrected by using the post-test room temperature value and adding temperature corrections from Figure 41 of 69 kg/mm^2 for the LO_2 tests and 89 kg/mm^2 for LH_2 tests.

TABLE VII

CRYOGENIC BELLOWS WEAR ANALYSIS INPUT DATA

BELLOWS S/N	TEST	BELLOWS TEMP. °K	BELLOWS CREST MICRO-HARDNESS Kg/mm^2	VIBRATION DISPLACEMENT, MM rms	AVERAGE FREQUENCY, Hz	EFFECTIVE TEST DURATION, Secs.	PEAK PR. DENSITY FACTOR 1.0Rayleigh 0.0=Gauss	NORMAL LOAD, NEWTONS	WEAR COEFFICIENT
15	I	36.0	389	.160	20.0	150	.25	5.78	.00064
	A	66.0	385	.572	30.0	150	.61	4.45	.00064
13	I	32.0	385	.343	20.0	93	.37	37.8	.00064
	A	30.0	385	.851	30.0	90	.61	24.5	.00064
	I+A	30.0	360	.508	28.0	87	.61	6.67	.00064
19	I	20.0	510	.584	19.0	102	.30	4.45	.0064
	A	22.0	360	.876	30.0	99	.75	6.67	.00064
	I+A	27.0	405	.813	27.8	93	.55	1.33	.00064
33	I	20.0	385	.648	18.6	93	.22	6.67	.00064
	A	20.0	444	.991	30.0	96	.61	4.45	.00064
	I+A	25.0	385	1.016	28.0	83	.579	1.33	.00064
	A top	90.0	424	1.003	30.0	500	.61	11.12	.0020
2	I	20.0	432	.305	20.0	100	.30	17.8	.00064
	A	20.0	353	.927	30.0	105	.672	0.44	.00064
	I+A	20.0	353	.635	28.2	90	.53	2.22	.00064
	A top	90.0	333	.927	30.0	450	.672	17.79	.0020
4	I	20.0	375	.368	17.5	93	.21	6.67	.00064
	A	23.0	374	.826	31.0	111	.61	6.67	.00064
	I+A	23.0	375	.914	28.5	90	.61	6.67	.00064
20	I	20.0	400	.230	22.3	96	.25	2.22	.00064
	A	20.0	385	.802	30.7	96	.762	4.45	.00064
	I+A	26.0	400	.847	28.3	102	.542	0.89	.00064
14	I	20.0	344	.257	16.9	117	.212	8.90	.00064
	A	20.0	353	.851	30.5	114	.609	6.67	.00064
	I+A	20.0	356	.814	29.6	114	.612	6.67	.00064
17	I	90.0	417	.787	20.0	90	.75	37.8	.0020
	A	90.0	354	1.245	25.0	132	.78	4.45	.0020
21	I	90.0	365	.533	20.0	99	.75	44.48	.0020
	A	90.0	344	1.105	25.0	117	.78	40.03	.0020
	I+A	95.0	389	1.321	25.0	93	.70	40.03	.0020
22	I	95.0	377	.457	20.0	105	.75	17.79	.0020
	A	95.0	346	.991	25.0	150	.78	20.02	.0020
	I+A	95.0	357	1.054	25.0	96	.70	22.24	.0020
23	I	92.0	370	.635	20.0	102	.75	22.24	.0020
	A	92.0	432	1.041	24.0	126	.78	20.02	.0020
	I+A	92.0	477	.743	28.1	99	.65	26.69	.0020
24	I	95.0	377	.381	15.5	124	.75	42.26	.0020
	A	92.0	357	1.003	26.6	150	.785	42.26	.0020
	I+A	92.0	402	1.067	25.0	96	.78	44.48	.0020

For LH_2; Bellows O.R. = 17.20 CM., Shell I.R. = 17.11 CM; Crest O.R. = .368 MM

LO_2; Bellows O.R. = 17.26 CM., Shell I.R. = 17.19 CM; Crest O.R. = .368 MM

FIGURE 41

HARDNESS Vs. TEMPERATURE

AISI 347 CRES

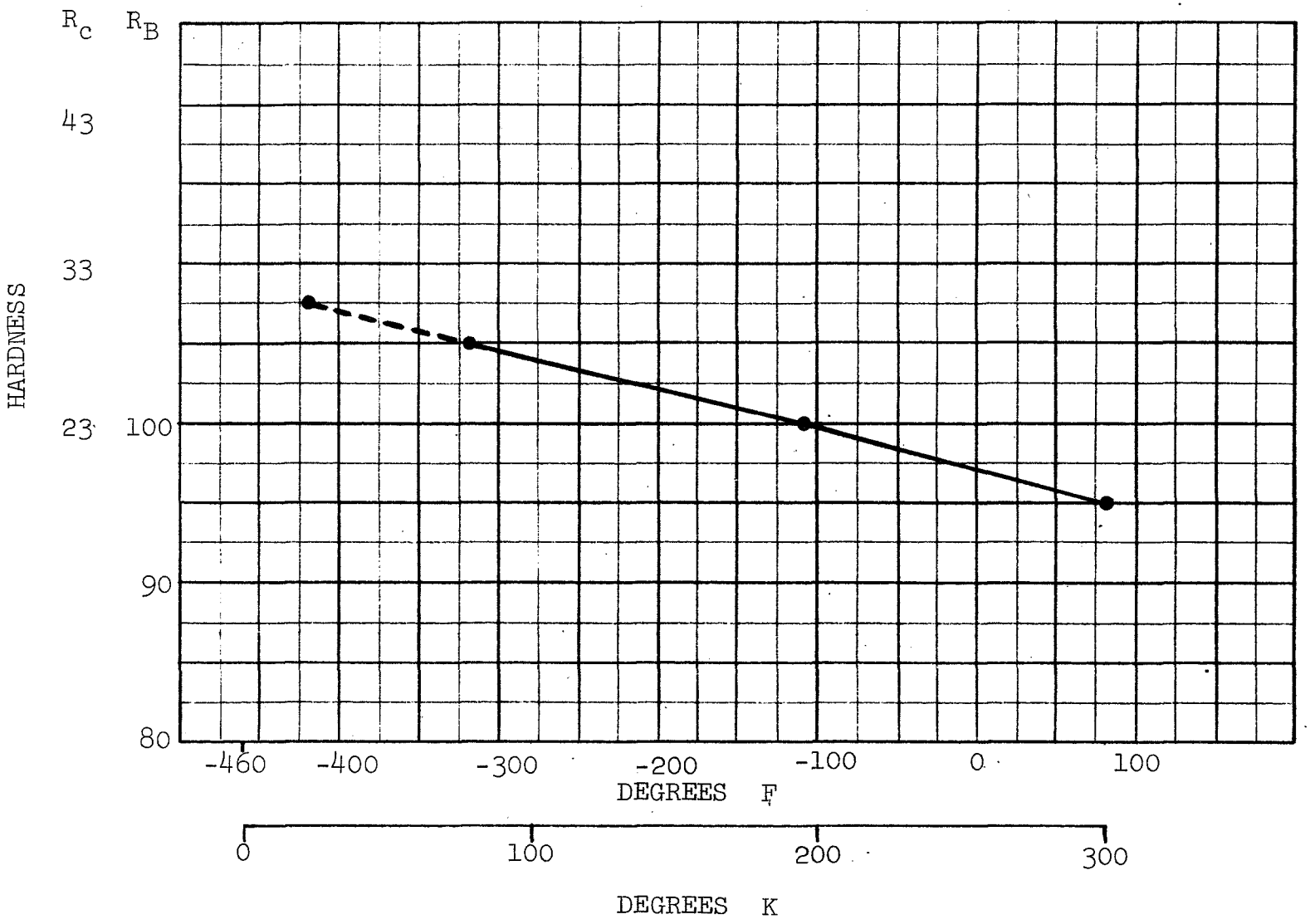

Bellows and shell geometric input data required for the analysis are bellows convolute outside radius, crest outside radius, and shell inside radius. Since these measurements were impossible to obtain during the actual cryogenic tests, room temperature measurements of several bellows and rings were averaged and then corrected to account for the contraction effect of LH_2 and LO_2 test temperatures. The normal (vertical) load condition for each test is listed in Table VII. Variations in the loads reflect difference in the cryostat inner chamber pressure, as described above.

The bellows sliding distance relative to the fixture was computed from the tape-recorded vibration response data. The bellows acceleration or displacement response power spectral densitites were analyzed to obtain average frequency, overall root-mean-square (RMS) amplitude and peak probability density as indicated in Appendix B. Each vibration test was run for 600 seconds, however, the bellows was not in contact with the ring all the time due to bouncing motion in the impact axis. Figure 42 shows the percentage of test time that the bellows actually contacts the ring versus impact axis bellows response g RMS (data from 1970 Bell IR&D bellows tests). Also, variations of cryogen feed pressure and inner chamber pressure during a few tests were noted and resulted in variations in bellows pitch causing the convolutions to slide off the ring at times, reducing the time that the bellows was actually wearing against the ring; this effect was not included in the analysis and may be a cause for some error. Estimate contact time for each test is shown in Table VII as "effective test duration."

The wear coefficient was assumed to be linearly proportional to the absolute temperature, based on the fact that 347 stainless steel exhibits a marked increase in ultimate strength which would tend to raise the resistance to wear. See Figure 43.

Bellows wear has been calculated for all the cryogenic tests except S/N 15 and S/N 17 combined impact and abrasion. The input data parameters are listed in Table VII and the analysis results are presented in Table VIII. Predicted maximum wear depth, maximum wear width, and wear length as well as volume of metal loss are tabulated.

The wear widths and depths measured on the test specimens after vibration are listed in Table VI. The wear width is considered the more reliable measurement for assessing wear damage since wear depth is based on a nominal foil thickness. Thus, to demonstrate theory to test correlation, the predicted wear width has been plotted versus measured wear width in Figure 44. Of the thirty-five data points, fourteen (40%) are within ±15% of the actual wear and twenty-nine (83%) are within ±50% of the actual wear. The average of the LH_2

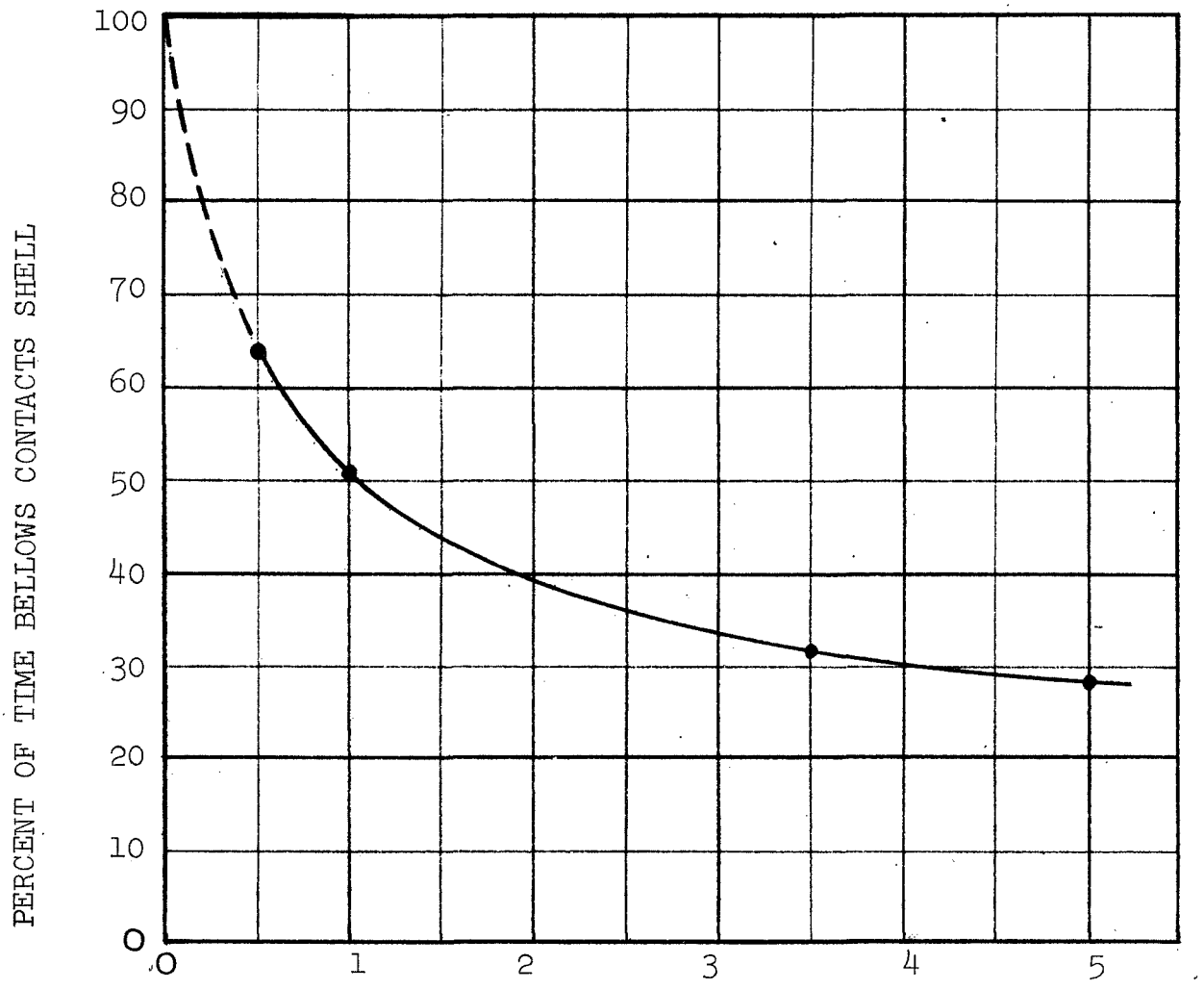

FIGURE 42

PERCENT OF TIME IN CONTACT V_S
IMPACT VIBRATION LEVEL

(Data from Test No. 2b.)

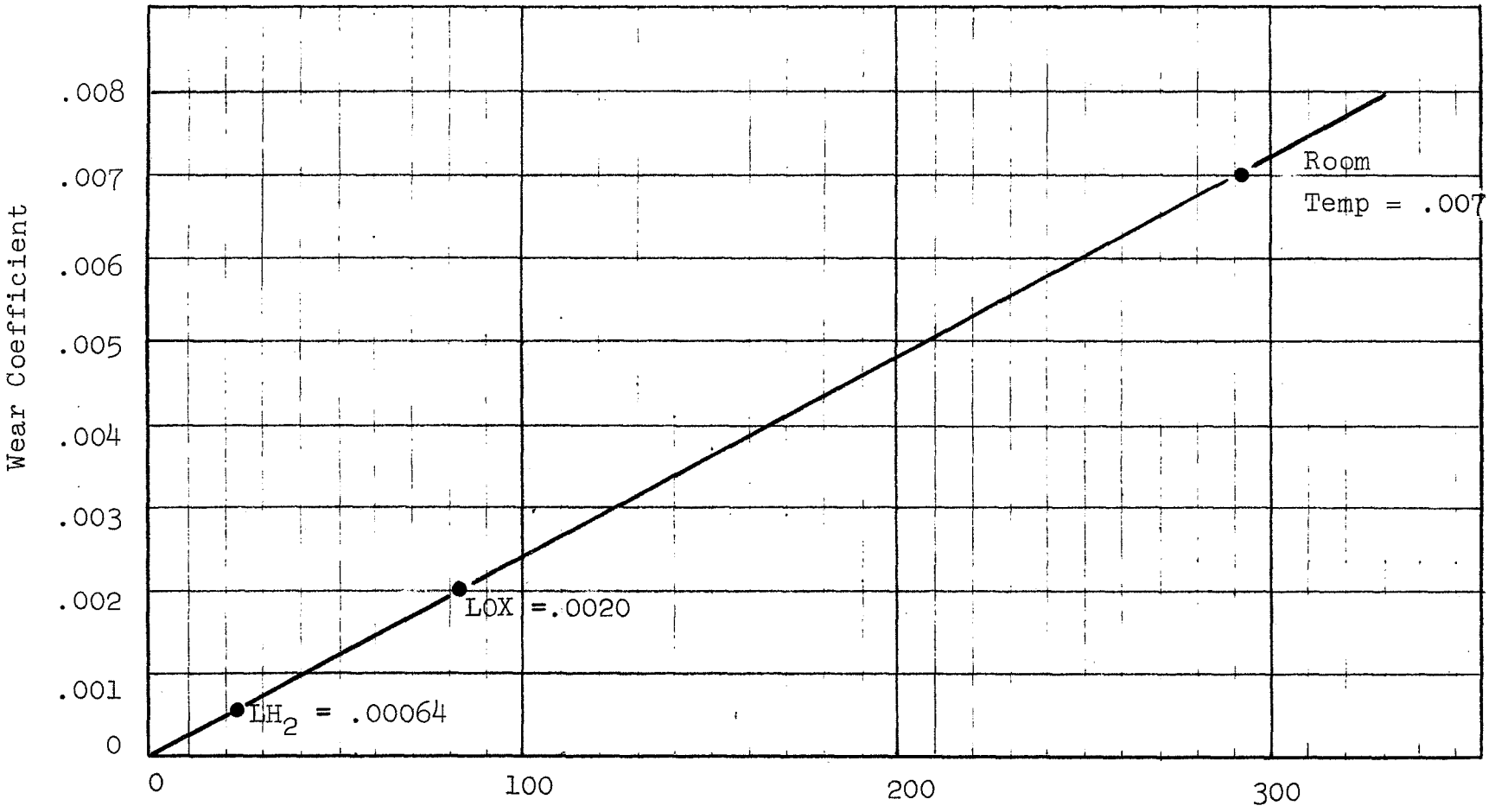

FIGURE 43

WEAR COEFFICIENT ASSUMED VARIATION WITH TEMPERATURE

TABLE VIII

CRYOGENIC BELLOWS WEAR ANALYSIS RESULTS

BELLOWS S/N	TEST	SLIDING DISTANCE, METERS	BELLOWS METAL LOSS MM3	MAXIMUM WEAR DEPTH, MM	MAXIMUM WEAR AREA WIDTH, MM.	WEAR AREA LENGTH C.M.	POINT NO. FIG 44
15	I	1.350	.0004	.00196	.0756	2.2715	
	A	9.811	.0025	.00353	.1016	3.0578	1
13	I	1.564	.0033	.00393	.1074	3.2315	2
	A	8.764	.0121	.00678	.1430	4.2309	3
	I+A	4.728	.0019	.00319	.09661	2.9067	4
19	I	3.345	.0006	.00220	.08018	2.4095	
	A	10.986	.0044	.00443	.11374	3.4242	5
	I+A	7.663	.0006	.00210	.07839	2.3553	6
33	I	3.052	.0012	.00266	.08819	2.6518	7
	A	10.88	.0024	.00349	.10091	3.0367	8
	I+A	8.801	.0007	.00225	.08106	2.4362	9
	A top	57.41	.1026	.0178	.2308	6.822	10
2	I	1.801	.0016	.00299	.09364	2.8168	11
	A	11.658	.0003	.00184	.07464	2.1950	12
	I+A	5.788	.0008	.00237	.08322	2.5016	13
	A top	49.96	.1818	.0236	.2639	7.797	14
4	I	1.611	.0006	.00220	.08018	2.4095	15
	A	10.836	.0042	.00433	.11249	3.3866	16
	I+A	8.947	.0035	.00402	.01834	3.2611	17
20	I	1.378	.0002	.00153	.06717	2.0149	18
	A	10.053	.0025	.00355	.10196	3.0683	19
	I+A	8.849	.0004	.00196	.07563	2.2715	20
14	I	1.371	.0008	.00229	.08193	2.4625	21
	A	11.278	.0046	.00447	.11436	3.4429	
	I+A	10.480	.0043	.00433	.11249	3.3866	22
17	I	5.983	.0369	.01120	.1803	5.442	23
	A	17.707	.0152	.00747	.1476	4.459	24
21	I	4.458	.0370	.01121	.1803	5.442	25
	A	13.93	.1104	.0188	.2325	7.0105	26
	I+A	12.51	.0877	.0168	.2201	6.637	27
22	I	4.053	.0130	.00701	.1430	4.3215	28
	A	16.02	.0631	.01441	.2039	6.1532	29
	I+A	10.31	.0437	.01213	.1874	5.6568	30
23	I	5.468	.0224	.00887	.1607	4.854	
	A	13.577	.0426	.01204	.1867	5.634	31
	I+A	8.125	.0310	.01029	.1728	5.218	32
24	I	3.091	.0236	.00908	.1624	4.9062	33
	A	17.32	.1396	.02105	.2454	7.396	34
	I+A	11.04	.0832	.01642	.2174	6.5575	35

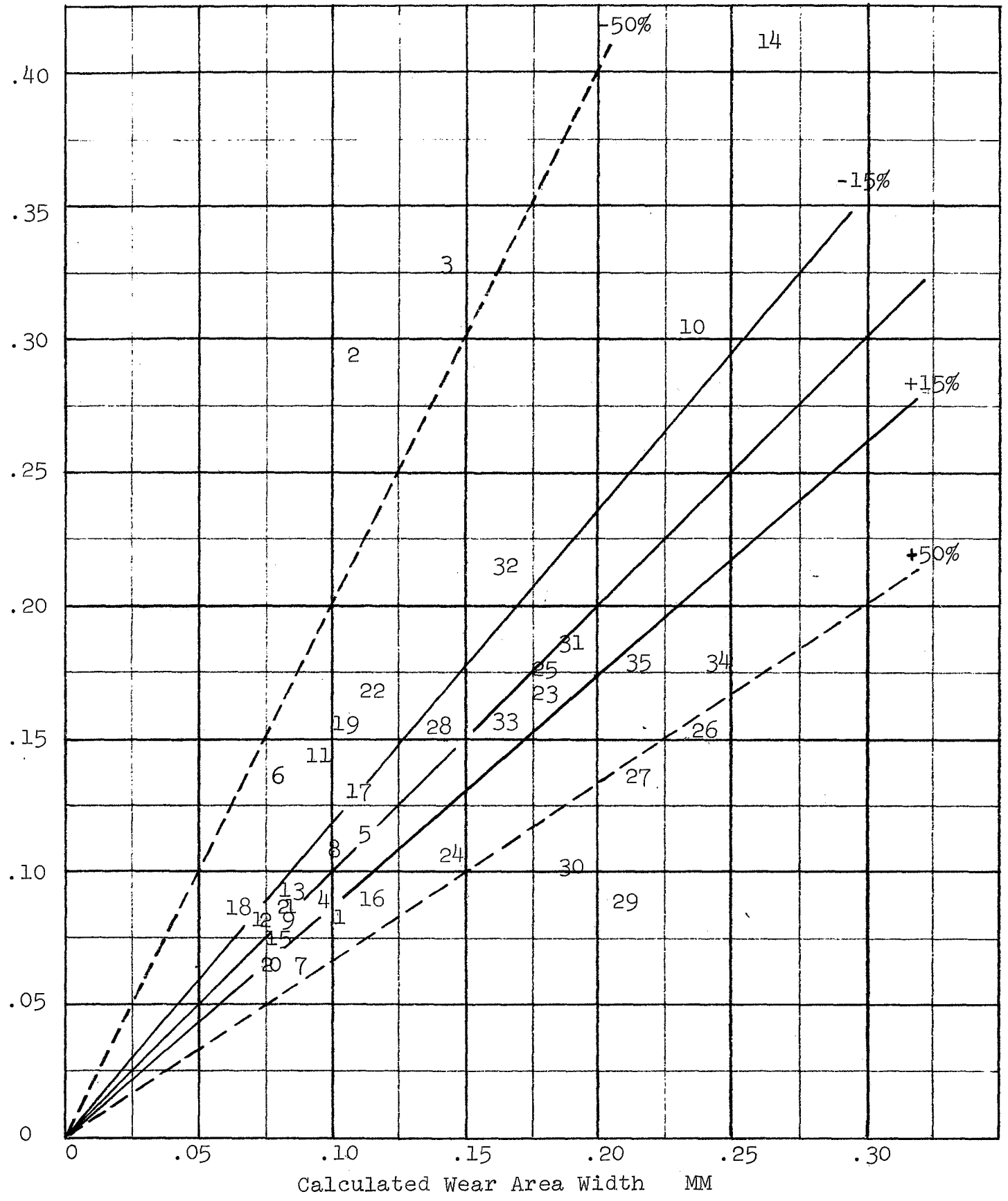

FIGURE 44. CORRELATION OF THEORY TO EXPERIMENTAL DATA

results shows that the wear was under-predicted by 10%; the LO_2 wear results average to an over-prediction of 34%. The overall average of all analytically derived values indicates a 6.6% over-estimate of the actual wear.

No attempt has been made to quantitatively assess the severity of convolution buckling due to impact vibration, because of the lack of data base and analytical techniques to make such an assessment. A qualitative comparison, however, indicates that the impact vibration levels approached the capability of the bellows to resist buckling since buckling was present on some bellows while similarly tested specimens were undamaged. The test program was unable to detect any change in the bellows resistance to impact buckling whether loaded with liquid hydrogen, liquid oxygen or water.

The bellows crests in microhardness as measured after vibration testing indicated a general increase over the baseline hardness levels, of specimens subjected to storage test only, indicating the presence of work hardening. The increase in crest hardness, however, did not vary with pre-load or input levels indicating that work hardening is not directly relatable to impact and abrasion vibration levels or pre-load.

There was no indication that pre-test cycling or storage prior to vibration had any detectable effect on vibration response or degree of wear. Neither did the pre-storage vibration test have any detectable effect on subsequent storage test results.

INCIPIENT BUCKLING TEST

As a bellows is extended, the convolution crests are drawn inward producing hoop compression strains. If the bellows is over-extended these compressive strains will cause the crests to buckle. This is characterized as an unsymmetrical buckling mode where circumferential waves are permanently formed in the convolution. Theoretical treatment of buckling generally is concerned with a mathematical definition of the load point where buckling begins. Buckling can be caused by shock and/or other dynamic motion, causing excessive pitch change. The incipient buckling pitch must be determined so that a safety factor can be incorporated in the design to ensure definition of a safe operating pitch.

The purpose of the buckling test in this program was to detect any unusual or unexpected effects as a result of operation with cryogenic propellants. This test was conducted at liquid hydrogen, liquid nitrogen and ambient temperatures. The liquid nitrogen data was obtained from a Bell sponsored IR&D program.

Test Equipment

The multi-purpose test apparatus and instrumentation used includes the necessary equipment to perform expulsion cycling and incipient buckling tests and was previously described in the expulsion cycling test equipment section.

Incipient Buckling Test Procedure

The test specimen was installed in the test fixture as shown in Figure 9, and pitch measurements at nested lengths were recorded on the stripgraph recorder. The bellows was then extended to free length and renested to correlate the proper pitch change with the measurements on the recorder. Once the measurement correlation was verified between the recorder and the actual pitch measurements taken at room temperature, the Dewar was raised and bolted into place.

Prior to cryogen flow the entire test system including the transfer line was purged with helium gas for 900 seconds, then evacuated and purged again with helium. During the second purge gas samples were periodically taken and analyzed on a gas chromatograph. When the analysis indicated that all combustible and solid particles were removed, the cryogen was admitted into the Dewar.

A thermocouple located at the bottom of the Dewar indicated when the internal environment was capable of sustaining liquid cryogen. The liquid level sensor was located approximately 4 inches (10 cm) above the top end plate. The cryogen was allowed to flow until the sensor indicated that the level of the liquid was at the level of the sensor. At this point in the test the bellows position was again noted on the recorder and compared to the position at room temperature.

The change in position was due to contraction of the rod attached to the linear potentiometer and taken into consideration when over-extension into the range of incipient buckling was started.

The buckling pitch was determined by setting the bellows pitch at .56 inches (1.422 cm) and then proceeding in increments of .060 inches (.152 cm) until buckling was determined by visual inspection. After each .060 inch (.152 cm) increment the cryogen was purged and the Dewar lowered to allow visual inspection without endangering the personnel involved.

An unsilvered DeWar was used for the Bell-sponsored IR&D incipient buckling program at liquid nitrogen and room temperatures. This enabled trained personnel to safely observe the bellows extension until crippling buckles were detected. (See Figure 45).

Incipient Buckling Test Results

The results of the incipient buckling test with liquid hydrogen indicated that the maximum buckling pitch of the specimens is less than 0.81 inches (2.05 cm) and greater than 0.77 inches (1.778 cm). The room temperature buckling specimens indicated a buckling pitch average of 0.65 inches (1.651 cm). The obvious trend then of these specimens is that the buckling pitch increases as temperature decreases. See Table IX for the results of each individual test.

The microhardness test of the bellows in the buckled area did not indicate hardness readings in excess of that expected for a bellows which has been severely deformed as these have been. The area within the buckle, however, did indicate a harder type of micro-structure than the surrounding area which is to be expected since the buckle occurred in the hardest area of the convolute, i.e. the crest. Buckling occurs when the sidewall forces of the convolute overcome the hoop strength of the crest bend radii. The crest then forms longitudinal buckles across the crest, which if forced to renest can result in a crack.

Discussion of Results

While the buckling inception point is precisely defined by mathematics, it is exceedingly difficult to determine experimentally. By the time a buckle is visable on the convolution it is already well advanced. Fortunately, in an expulsion bellows a non-visable buckled condition is of academic interest only, since it will not affect bellows operation unless it becomes a crippling buckle such as shown in Figure 46, which is visable.

An analytical evaluation of the expected buckling pitch is necessary to assist in interpreting the test results. To accomplish this analysis a computer program developed under the Minute-

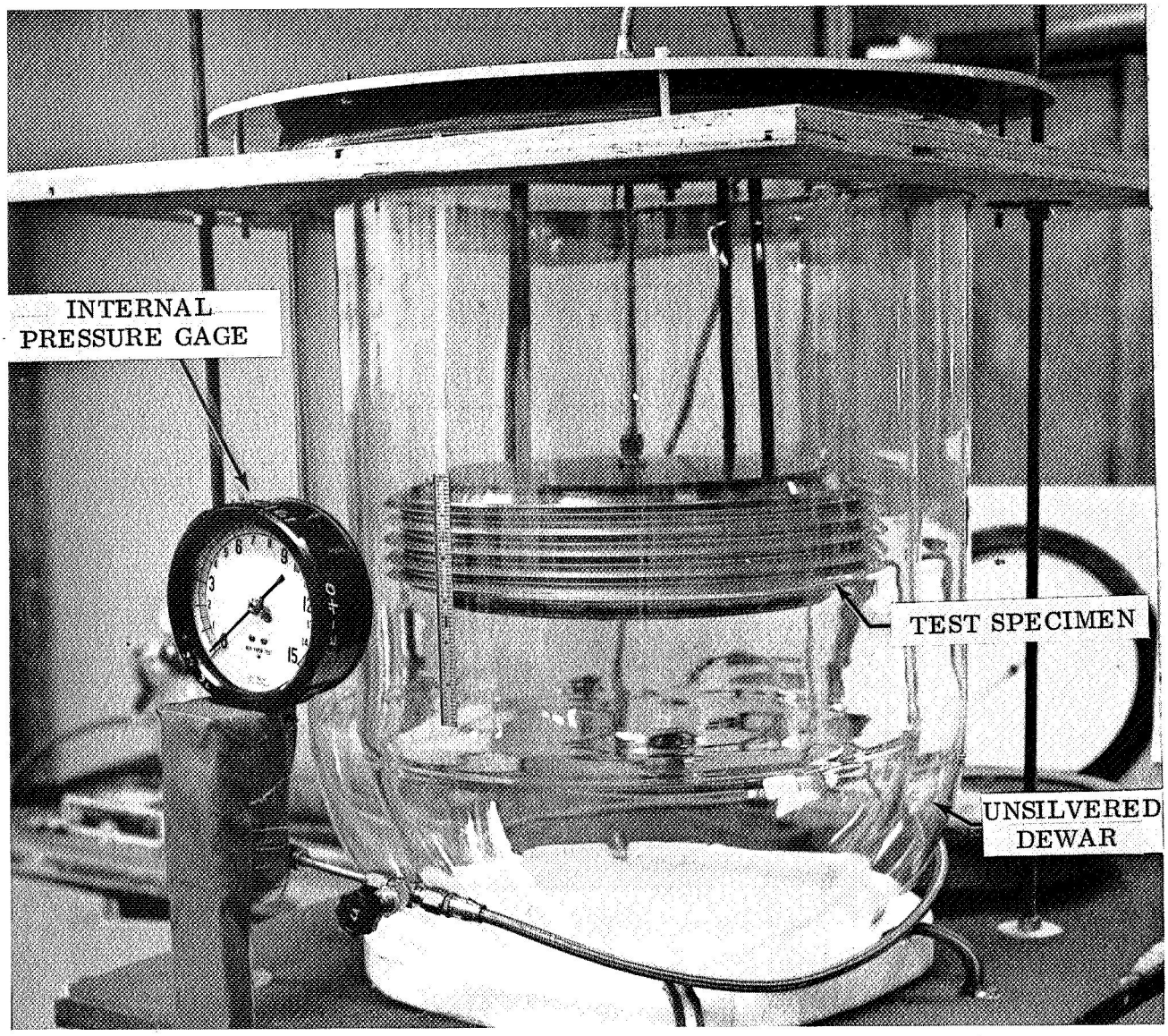

FIGURE 45. LIQUID NITROGEN INCIPIENT BUCKLING TEST APPARATUS

SPECIMEN		TEST TEMPERATURE						REMARKS
Part Number	Serial No.	20°K LH_2 Pitch (in/cm)		77°K LN_2 Pitch (in/cm)		530°K ambient Pitch (in/cm)		
		Actual	Predicted	Actual	Predicted	Actual	Predicted	
8606-471001-1	7	.83/2.108	.88/1.125					
8606-471001-1	32	.81/2.057	.88/2.235					
8477-471090-9	1			.70/1.778	.86/2.184			Bell IR&D Test Results
8477-471090-3	3			.70/1.778	.86/2.184			
8606-471001-1	3					.65/1.651	.64/1.626	

TABLE IX. BUCKLING TEST RESULTS

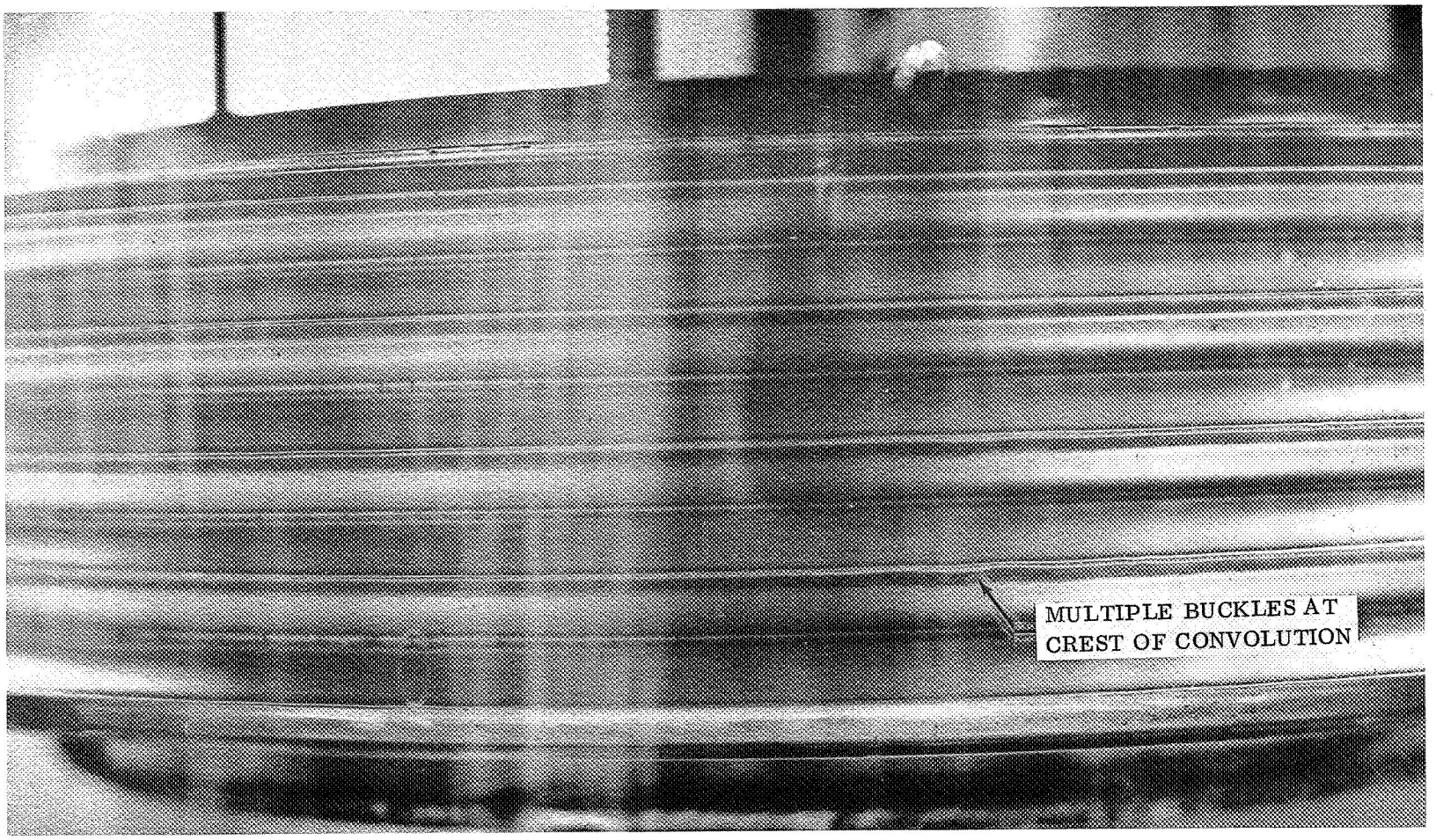

FIGURE 46. TEST SPECIMEN AT THE POINT OF INCIPIENT BUCKLING

man contract was used. The program and its theoretical foundation are discussed in Reference 7. Since the hoop stresses at buckling are in the plastic range, the analytically determined buckling pitch is governed by the material stress-strain curve for the temperature used. The stress-strain curves for the various temperatures used as inputs for the computer program are shown in Figure 47.

The analytical procedure involves finding the hoop strain at which buckling would occur from a linear increase in hoop strains existing at a particular extended pitch. As pitch is increased, however, the convolution shape changes as does the strain distribution. The buckling strain is determined as a separate steady state condition at a series of increased pitch values. The result of this procedure is a curve of buckling strain vs pitch, Figure 48 which intersects the curve of applied hoop strain vs pitch at the theoretical buckling pitch of the bellows. The deformed convolution shape and its corresponding hoop strain at each increased pitch value is supplied to the buckling program by the same nonlinear shell computer program as was previously described for expulsion cycle testing.

In general, the higher the yield point of the material, or the closer it approaches a purely elastic stress-strain relationship, the higher the buckling point becomes. Applying this to the stress-strain curves of Figure 47 it indicates that the buckling pitch increases as temperature decreases. The analytically derived results of Figure 48 and the empirically derived data of Table IX shows this to be the case. The buckling strain determination of Figure 48 was calculated for pitches up to .80 inches (2.03 cm) and extrapolated beyond. Table IX is a compilation of actual and predicted buckling pitches for each of the three cases tested.

A comparison of actual versus predicted buckling pitch is presented in Figure 49. This indicates that at ambient temperatures (300°K) good correlation exists, but at cryogenic temperatures the correlation is decreased.

There are many factors to be considered in comparing empirical and analytical results. Slight imperfections, critically located, can reduce the strain at which buckling occurs. Another factor is slight convolution shape variation from specimen to specimen which can have an effect at very large pitches. These factors along with the effect of neglecting the secondary plastic strain are probably the principal reasons why the actual values are lower than the analytical predictions. In general, however, the experimental results indicate the same trends predicted by the analysis in that the buckling pitch at cryogenic temperatures is greater than at ambient temperatures. This increased design margin can be used by the bellows designer to increase operating pitch or as additional design margin.

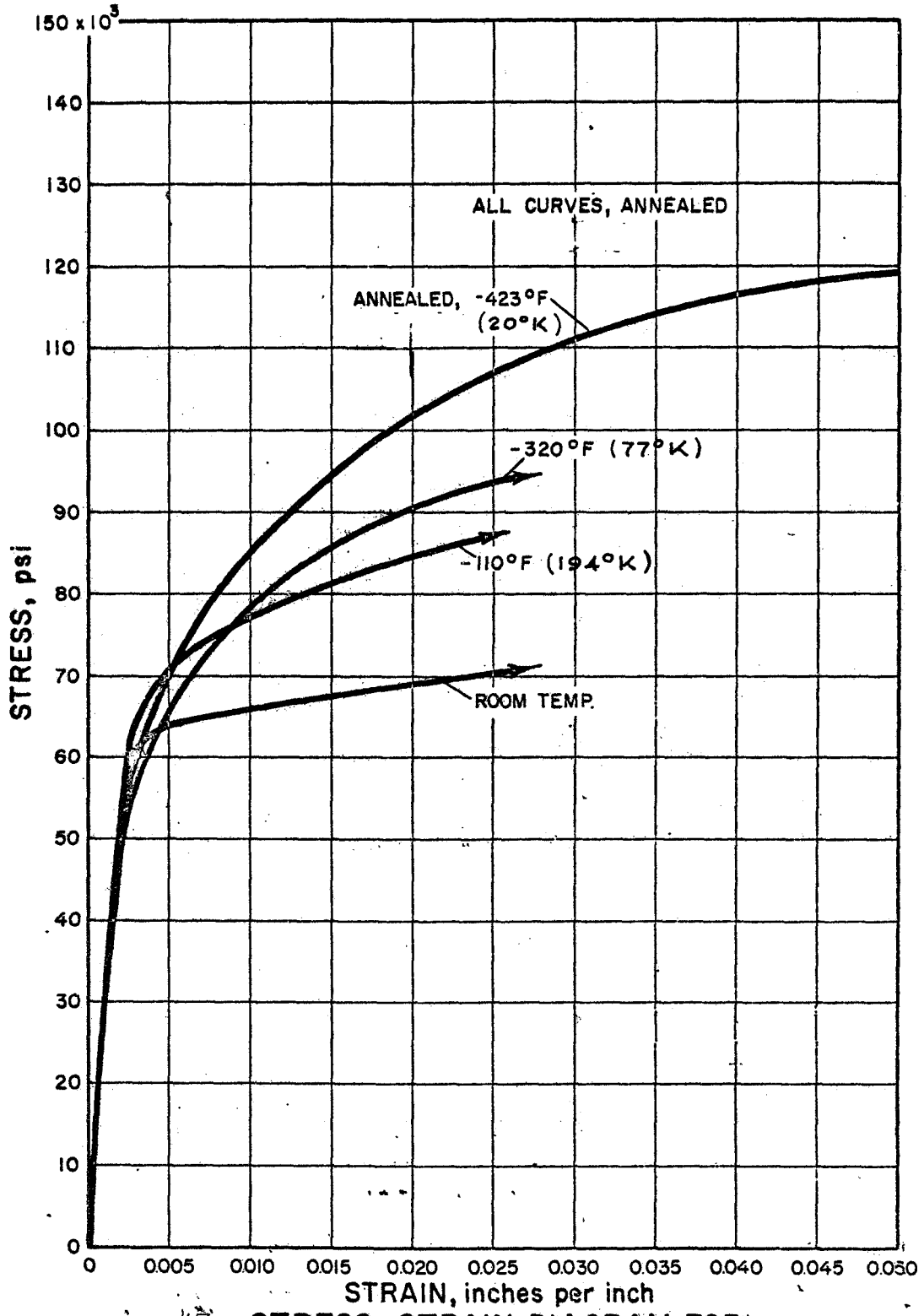

FIGURE 47 STRESS-STRAIN DIAGRAM FOR AISI 347 STAINLESS STEEL

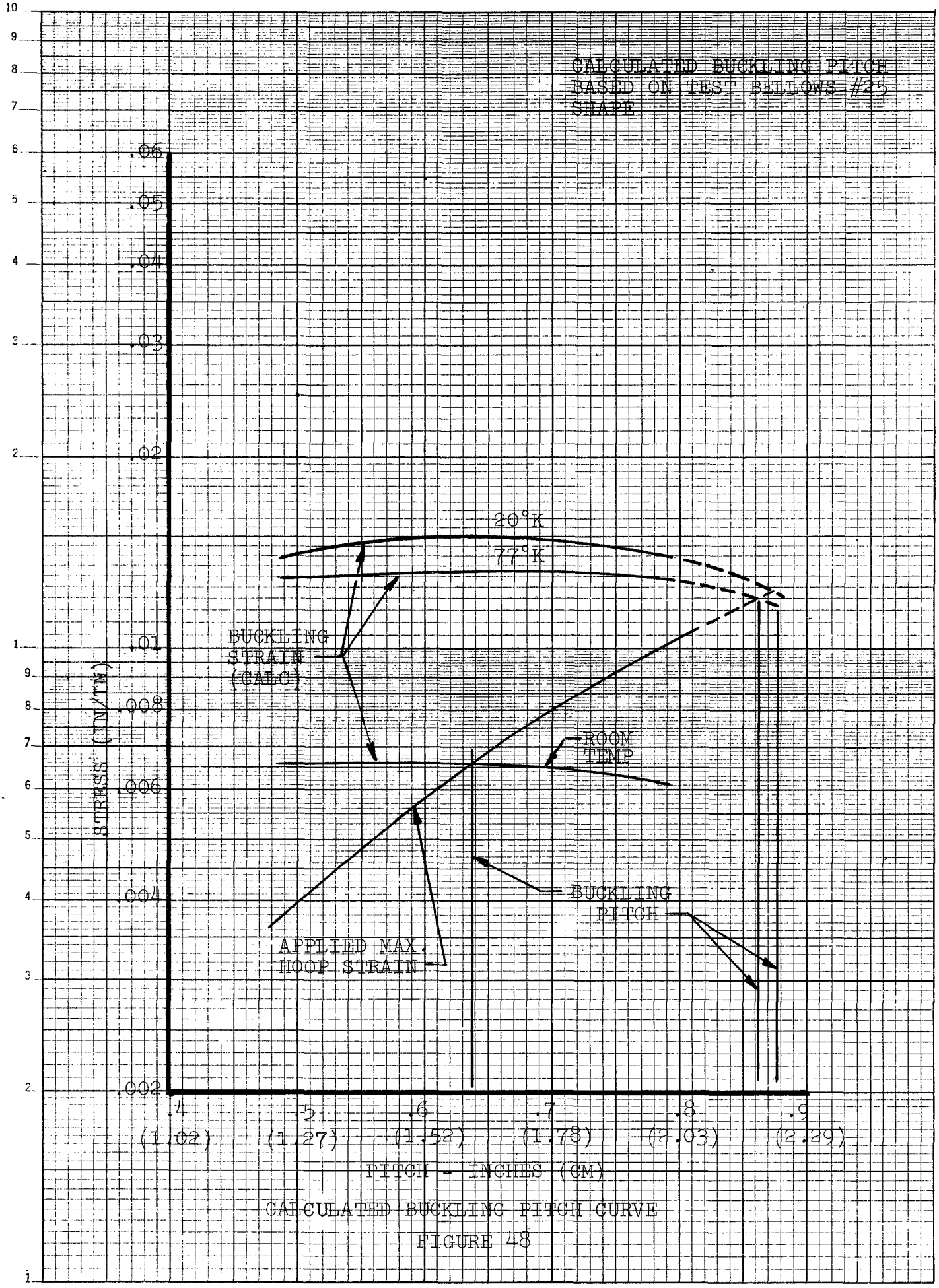

CALCULATED BUCKLING PITCH CURVE

FIGURE 48

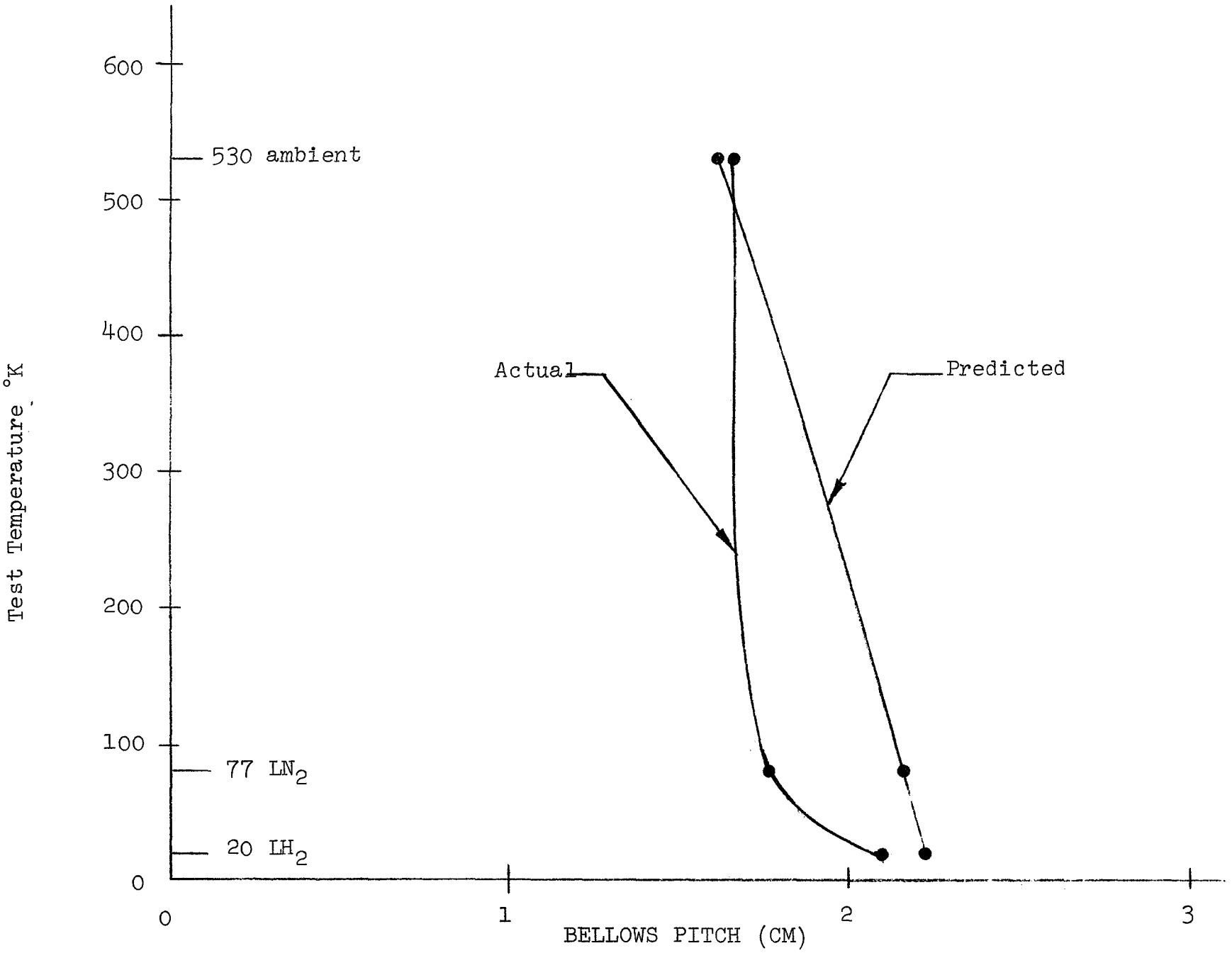

FIGURE 49. BUCKLING PITCH CORRELATION

The applied strain in the bellows is a function of the convolution motion and not the material properties. The stresses will be different for the same strain depending upon the stress-strain curve applied, but if the fundamental unit strain is used for buckling prediction the process is simplified. A completely rigorous analysis of buckling would include some second order effects of plastic strains which cause a slightly different deformed shape than produced by assuming a purely elastic strain condition. The errors involved in using the simplified elastic analysis are negligible at operating pitch, however, they become more significant at buckling pitch. The increased accuracy of the plastic analysis, however, is not warranted by the greatly increased cost since the test was conducted to determine gross effects only.

It is unknown if the test sequence of prestorage cycling and storage prior to the buckling test affected the results in any way since the sequence was not varied. The sequence did, however, simulate that to which a bellows is subjected in typical service. It is not expected that the cycling or storage altered the results to any significant degree since the strains imposed by buckling were far in excess of those imposed by pretest cycling and no change in natural properties were detected as a result of storage in any of the tests.

STORAGE TEST

The storage test was conducted with the test specimens exposed to liquid hydrogen only. Specimens exposed to liquid hydrogen, as part of the overall test matrix (Figure 8) were evaluated: (a) with 45-day conditioning in hydrogen at cryogenic temperatures prior to high stress level testing, (b) storage for 45 days in hydrogen at cryogenic temperatures after being exposed to high stress level testing and (c) a control specimen subjected only to 45 days storage.

Specimens were sectioned and metallurgically examined for indications of microstructural change, physical property deterioration and/or hydrogen embrittlement.

Test Equipment

The multi-purpose test apparatus includes the necessary equipment to perform the pre-storage or pre-vibration cycling, storage, expulsion cycling, cycling to failure, and incipient buckling tests.

Storage Test Dewar

The storage Dewar was previously described in the expulsion cycling test section.

Storage Test Fixture

The storage test fixture as shown in Figure 50 was a cylindrically shaped rack approximately 15.5 inches, 3937 cm in diameter and 34 inches, 86.36 cm long. (See Figure 50). The fixture positioned 10 specimens in a staggered manner providing a minimum height within the Dewar while maintaining specimen separation.

Instrumentation

The instrumentation for storage testing consisted of a liquid level sensor to control the height of the cryogen in the Dewar and a temperature sensor located at the bottom of the Dewar to indicate when it was empty.

Liquid Level

The germanium resistance thermometer used during storage testing was previously described in the expulsion cycling test section.

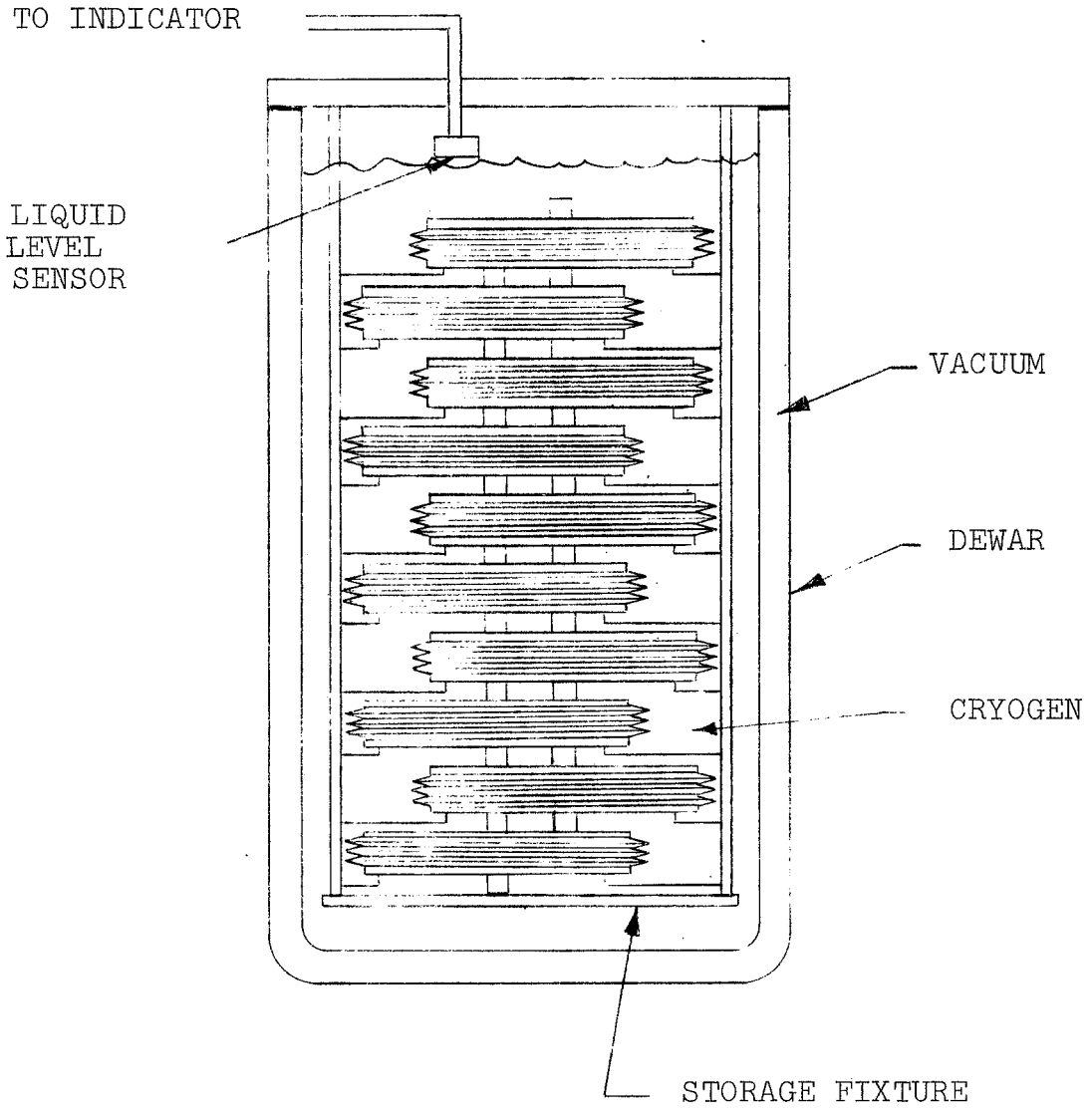

STORAGE TEST APPARATUS

FIGURE 50

Temperature

The Crygenic Linear Temperature Sensor (CLPS) was identical to that previously described in the expulsion cycling test section.

Storage Test Procedure

The 10 bellows specimens were stacked in the storage rack port side up with all ports open to insure exposure of the metal to the cryogen on both sides of the test specimen. When the Dewar was raised and bolted in place the entire test system, including the transfer line was purged with helium gas for 15 minutes, then evacuated and purged with helium again.

During the second purge, gas samples were periodically taken at the end of the purge system and analyzed on a gas chromatograph. When the analysis indicated that all combustible or noncompatible materials were purged from the system liquid cryogen was admitted into the Dewar. The liquid level sensor extended approximately 1.5 inches (3.81 cm) below the Dewar cover which provided a liquid level approximately 4 inches (10.16 cm) above the top bellows trunnion. Because of the long storage time the Dewar was filled on a periodic basis as determined from the first two days of storage. This insured that all specimens were immersed in the cryogen for the entire 45-day period. When the test was completed the cryogen was removed from the Dewar by pressurizing the Dewar and forcing the cryogen back through the transfer line and out the vent stack. Purging continued until the Dewar temperature reached -200°F (144°K) and a gas sample taken and analyzed. If the analysis of the gas sample showed a cryogen concentration of 1% or less, the Dewar was lowered to allow warming by exposure to ambient air.

Storage Test Results

The results of the liquid hydrogen storage test indicates that the bellows material (347 S.S.) is completely compatible with liquid hydrogen for the 45-day storage period. The specimens were free of any type of attack, hydrogen embrittlement, or corrosion of any kind. These bellows were in the same condition after the 45-day storage period as they were prior to the test in terms of microstructure and surface condition.

Although the Liquid Oxygen storage test was eliminated by program redirection, all the bellows tested in LO_2 were examined for evidence of corrosion. The results of this examination were negative in all cases without any indication of chemical attack, stress corrosion or corrosion of any kind.

CONCLUSIONS AND RECOMMENDATIONS

The Cryogenic Propellants Program subjected metallic positive expulsion bellows to a series of tests simulating the environment associated with spacecraft mission duty cycles. These operating parameters were evaluated in environments which included vibration, storage, expulsion life cycling, and incipient buckling.

Program Objectives:

1) Determine if service with cryogenic propellants imposes any limitations on bellows operating parameters, design margins or performance.

2) Revise existing design computer programs, as required, to incorporate characteristics associated with cryogenic propellants.

The most important conclusion provided by this program is that metallic positive expulsion bellows operating parameters are unimpaired by exposure to either liquid hydrogen or liquid oxygen and that ambient temperature design techniques apply. The program also indicated where certain areas of further investigation are required for more complete analysis of the mechanisms involved in bellows design. The following conclusions and recommendations for each primary test series is presented as a result of this program:

1) Expulsion Cycling

Conclusion - The bellows cycle life is improved at cryogenic temperature over ambient temperature and appeared to correlate with the fatigue life improvement associated with these temperatures.

Recommendation - It was impossible to determine the precise amount of fatigue life improvement or how this improvement affects the analysis because of the limited sample size and strain ranges. It is therefore recommended that a fatigue study be initiated that would subject an adequate sampling of both uni-axial and bi-axial specimens to a series of fatigue tests, varying the strain range and sequence of elastic and plastic strains at cryogenic temperatures, to quantitatively evaluate bellows fatigue life.

2) Vibration

Conclusion 1 - The same wear theory applies to all temperatures with the proper wear factor selected for temperature compensation.

Conclusion 2 - Bellows at cryogenic temperature exhibit greater resistance to wear than at ambient temperature in the general wear factor relationship established in Figure 43. Use of this wear factor should recognize the data scatter inherent in this type of test.

Recommendation - The wear theory developed is verified for Minuteman size bellows only. A study should be conducted to either verify for all sizes or establish scaling laws to be used for other size bellows.

3) Incipient Buckling

Conclusion - The incipient buckling pitch at cryogenic temperature was greater than at ambient temperature in relation to the yield strength improvement.

4) Compatibility

Conclusion - The bellows specimens were unaffected by the 45 day liquid hydrogen storage test or any other liquid hydrogen or liquid oxygen test. No indication of corrosion, chemical incompatibility or attack was detected in any of the test specimens.

5) Metallurgical

Conclusion 1 - Although the plastic working of the bellows resulted in the material becoming approximately 1/4 hard, there was no evidence of crystalline microstructural changes.

Conclusion 2 - The convolution roots and crests become harder through cold working than do the sidewalls.

Conclusion 3 - The majority of the work hardening occurs within the first 10 expulsion cycles with subsequent cycling adding little hardness.

6) Sequence

Conclusion - Variation in test sequence did not alter the results in any detectable manner.

REFERENCES

1. Sikorski, M. E., "Correlation of the Coefficient of Adhesion With Various Physical and Mechanical Properties of Metals", J. Basic Eng., Trans ASME, Series D, Vol. 85, No. 2, June 1963, pg 279.

2. Burwell, J. T. and Strang, C. D., "On the Empirical Law of Adhesive Wear", J. Appl. Phys. 23, 18 (1952).

3. "Designing for Zero Wear - Or a Predictable Minimum", Product Engineering, August 15, 1966, pg. 41.

4. Archard, J. F., "Single Contacts and Multiple Encounters", Jour. Appl. Phys., Vol. 32, No. 8, August 1961, pg 1420.

5. Bell Aerospace Company, "Study of Positive Expulsion Techniques, Design of Welded Bellows" - Final Report on NASA Contract NAS 7-149, Rep. No. 8230-933013, November 1966, unclassified.

6. Suly, F. B., and Smith, J. O., "Advanced Mechanics of Materials", 2nd Edition, New York, Wiley, 1952.

7. Bell Aerospace Company, "Minuteman III PBPS CDR Data Package", Section 4.1, Rep. No. 8477-950295, December 1967.

8. North American Rockwell Corp. STR 205, "MM III PBPS Bellows Dynamics Margin of Safety Report".

BELL AEROSYSTEMS COMPANY
DIVISION OF
BELL AEROSPACE CORPORATION
POST OFFICE BOX ONE . BUFFALO 5, NEW YORK

TECHNICAL DATA

CONTRACT NO. NAS-3-13327 NO. OF PAGES

REPORT NO. IMS 71-2 MODEL

CRYOGENIC TRANSDUCERS
CALIBRATION REPORT

BY L. Vito DATE 2/19/71
L. Vito

CHECKED _____ DATE _____

APPROVED R. Barton DATE 2/19/71
R. Barton

APPROVED W. W. Swenson DATE 2-19-71
W. W. Swenson

REVISIONS

DATE	PAGE NO.

Form 0304 Rev. 860

Bell Aerospace Company DIVISION OF textron
POST OFFICE BOX ONE . BUFFALO, NEW YORK 14240

1.0 INTRODUCTION:

Bell Aerospace Company is presently under contract with NASA/LeRC (NAS-3-13327) for testing Metallic Expulsion Bellows for Cryogenic Propellants. The specified cryogenic media for testing are Liquid Hydrogen (LH_2) and Liquid Oxygen (LOX).

To meet the testing requirements for this program, several items of instrumentation are required:

1. Linear Displacement Transducers - to monitor the movement of the bellows and plates for the proper pitch of the convolutions and to control the abrasion input level during vibration testing.

2. Pressure Transducers - to monitor the internal and external pressures of the bellows.

3. Accelerometers - to monitor the input/control and response acceleration during vibration testing of the bellows sample.

4. Cryogenic Linear Temperature Sensors - to measure temperature at various Bellows/Fixture and Cryostat locations.

Figure 1 is a photograph of the transducers.

All of the above transducers/sensors are required to operate at or about the test cryogen temperature. The cost and long procurement cycle precluded procurement of calibrated transducers. In most instances, the transducer manufacturer indicated they did not have the facilities for calibrating below liquid Nitrogen (LN_2) temperature.

Candidate transducers were selected based on knowledge of performance at LN_2 temperature and an analytical study of the design which gave a high degree of confidence that the performance would be adequate at LH_2 temperature.

Bell Aerospace Company DIVISION OF textron
POST OFFICE BOX ONE . BUFFALO, NEW YORK 14240

2.0 SUMMARY:

The following transducers were calibrated at cryogenic temperatures:

Qty.	Transducer	Manufacturer	Model
3	Pressure	MB/Alinco	172-DBA-1
3	LVDT	Shaevitz	477XS-Z1 (Modified)
8	Accelerometer	Kistler	808H
2	Temperature	Micro Measurements	CLTS

The results of the calibrations are presented in Tables 1 through 4.

In addition to the above instruments, two (2) Scientific Instrument LH_2 Liquid Level Sensors were checked for proper operation. Since these units are used for on-off control, no calibration data were obtained.

TABLE 1A

SYSTEM SENSITIVITIES IN VOLTS/PSI

TEMP.	S/N 54673	S/N 54678	S/N 54680
Ambient	-.0778	-.1221	-.1283
LN_2	-.0766	-.1209	-.1247
LN_e	-.0766	-.1162	-.1253

TABLE 1B

ZERO SHIFT IN PSIA

TEMP.	S/N 54673	S/N 54678	S/N 54680
Ambient	-	-	-
LN_2	+.0620	+.3536	-.0171
LN_e	+.1328	+.1701	-.1057

TABLE 1

MB/ALINCO MODEL 172-DBA-1 0-25 PSIA

Bell Aerospace Company DIVISION OF textron
POST OFFICE BOX ONE . BUFFALO, NEW YORK 14240

TABLE 2A

SYSTEM SENSITIVITIES IN VOLTS/INCH DEFLECTION

TEMP.	S/N 001	S/N 002	S/N 003
Ambient	-6.61	-6.93	-6.23
LN_2	-6.63	-7.40	-6.31
LN_e	-6.65	-7.28	-6.21

TABLE 2B

ZERO SHIFT IN INCHES

TEMP.	S/N 001	S/N 002	S/N 003
Ambient	-	-	-
LN_2	0.000	0.004	0.006
LN_e	0.000	0.005	0.003

TABLE 2

SCHAEVITZ MODEL 499XS-Z1 ±.5" LVDT

TABLE 3

ACCELEROMETERS

KISTLER MODEL 808H

ALL READINGS IN Pc/g

S/N	1857	1869	1991	1885	1892	1893	1894
Ambient	.911	.933	.922	.923	.982	.986	.958
LN_2	.933	.953	.958	.955	1.012	1.011	.989
LN_e	.938	.956	.961	.940	1.017	1.008	.989

Bell Aerospace Company DIVISION OF textron
POST OFFICE BOX ONE . BUFFALO, NEW YORK 14240

TABLE 4

M-M SURFACE LINEAR TEMPERATURE SENSORS (CLTS)

ERROR IN % DEVIATION FROM STANDARD TEMPERATURE

STANDARD TEMPERATURE ±.02°F	SENSOR #1	SENSOR #2
Ambient	0	0
ICE	-1.47	-1.16
-64.3°F	- .62	-1.40
LN_2	+1.75	+1.75
LN_e	+7.44*	+7.44*
LH_2	+1.63**	-

* This calibration point at LN_e was rejected because of striation temperature effect.

** Empirical data obtained during LH_2 bellows storage tests.

3.0 METHOD:

3.1 General: All calibrations were performed in the Instrumentation Lab of the Engineering Laboratories and Test Department. Since the actual test cryogens (LH_2 and LOX) are hazardous, it was decided that neither could be used safely in the Instrumentation Lab. Liquid Nitrogen (LN_2), which was readily available and safe to use in the Laboratory, was substituted for LOX. Liquid Neon (LN_e), an inert cryogen was substituted for LH_2. The following lists the boiling points for the calibration and test cryogens.

Cryogen	Temperature
LH_2	20.397°K (-422.955°F)
LN_e	27.102°K (-410.886°F)
LN_2	77.38 °K (-320.386°F)
LOX	90.188°K (-297.33 °F)

LN_e used in the calibration was transferred from the storage Dewar to a special 5 liter calibration Dewar. In order to conserve on LN_e, the more massive transducers (pressure, displacement) were first precooled in LN_2. The unit was then transferred to the LN_e dewar. Precooled nitrogen gas was used to insure no LN_2 was carried into the LN_e dewar.

The LN_e calibration dewar was placed on a scale so that an accurate account of the useage could be determined. In order to have uniformity of procedure and stability to cryogenic temperature, it was decided to keep the pressure transducers and LVDT's in the cryogen for 1 hour before any readings were taken.

3.2 Accelerometer Calibration

Kistler quartz accelerometer Model 808H is designed basically for high temperature use (+750°). The unit is heli-arc welded, hermetically sealed, and ceramic insulated. The manufacturer recommended temperature range (-450 to +750°F) and sensitivity .03%/°F makes unit suitable for cryogenic use.

Accelerometer calibrations were conducted in the accelerometer calibration room of the Instrumentation Laboratory using an MB Model C-12 vibration system as shown in Figure 2. Figure 3 is a schematic of the calibration system and Figure 4 is the calibration cryostat.

Insulated studs were used to attach the test accelerometer to the fixture. These studs are also used during actual test. The accelerometers and studs were torqued to 18 inch pounds.

Figure 3 is a schematic diagram of the setup for accelerometer sensitivity measurements. The output of the Test Accelerometer was fed to a CRL cathode follower and read on a Dana Digital AC Converter/Voltmeter. The input vibrator level was determined by a Kistler standard accelerometer/charge amplifier system, calibrated at Kistler in October 1970. The standard output was also read on a Dana Digital Converter/Voltmeter.

Each accelerometer was first calibrated within the cryostat fixture at room temperature. A special heating coil and thermocouple readout were installed at the bottom of the fixture to keep the temperature of the standard accelerometer constant during the calibration interval.

Following the room temperature test, LN_2 was added and allowed to stabilize. Four data frequency points (30 Hz, 50 Hz, 80 Hz, 100 Hz) at 5 G's vibration level were taken.

The LN_2 was quickly boiled out of the cryostat cup and LN_e was then transferred. This greatly reduced the initial boil off rate thus conserving LN_e. The four calibration points were then repeated for LN_e temperature.

The unit was recalibrated at room temperature to determine any changes in sensitivity.

3.3 Pressure Transducers

Model 172DBA-1 MB/Alinco Bonded Strain Gage Pressure Transducers are designed for measurement of pressure at cryogenic temperatures. The body and diaphragm are integral; machined from a solid piece of 17-4PH stainless steel. These units can be disassembled and cleaned for LOX usage.

For use on the cryogenic program, 0-25 psia units were purchased.

Each pressure system consisted of an MB cryogenic pressure transducer and one channel of a CEC System D carrier amplifier system. The output was read on a Honeywell Model 333 Digital Voltmeter. Figure 5 is a photograph of the calibration setup.

Three pressure measurement systems were calibrated at room temperature, LN_2 and LN_e temperatures. Each calibration consisted of 10 pressure points from 25 psia to vacuum and return.

The standard pressure system was calibrated by an Ideal Aerosmith Model DCNM-83-32 manometer. The standard system consisted of a Data Sensor Model PB923A-2 pressure transducer connected to a BF signal conditioner Model 1609. The output was read on a Cimeron Model 7650 Digital Voltmeter.

A static pressure system was constructed so that the pressure at room temperature would be the same at the standard transducer as the test transducer at cryogenic temperature. Gaseous H_e was used as the pressure media (see Figure 6).

3.4 Displacement Transducers

A special design cryogenic LVDT incorporating a spring loaded tip was manufactured at Schaevitz Engineering Company. The tip was sufficiently preloaded to follow vibration up to 20 G's acceleration at 100 Hz while being vibrated in a cross axis. A hardened steel tip provided the sliding contact.

Two basic calibrations were performed on each transducer. A special collar was manufactured at Bell to hold the moving element at the center of travel while the unit was emersed in the cryogen. This gave a zero shift due to temperature.

A second fixture was made from PVC plastic to determine the displacement sensitivity. The moving element of the LVDT was attached to a micrometer movement by means of a quartz rod (see Figures 7 and 8.)

The CEC system D was used to condition the LVDT output. A special calibration circuit was designed and incorporated into the electronics. All readings were taken on a Honeywell Model 333 Digital Voltmeter as shown in Figure 9.

Precooled gaseous nitrogen was used to "blow out" any remaining LN_2 within the LVDT while transferring it from LN_2 to LN_e.

After 1 hour stability time, thirteen calibration points were taken at room, LN_2 and LN_e temperatures. A second room temperature test was performed to determine any change in sensitivity.

The unit was placed in a vacuum chamber after being removed from the cryogen to prevent moisture buildup.

3.5 Temperature Sensors

The CLTS is a small (.430" long x .310" wide x .004" thick) Surface Thermometer Gage consisting of 3 thin foil sensing grids laminated in an epoxy resin matrix. Two alloys of special grades of nickel and maganese are processed for equal and opposite non-linearities in the resistance versus temperature characteristics. As a result, the composite sensor has an essentially linear change of resistance with temperature.

The CLTS also has a very low strain sensitivity (±1°F/1500 μE).

Two CLTS gages were bonded 90° from each other on a $1\frac{1}{2}$ x 1 x .020" sheet of 302 stainless steel using M-Bond 600 Adhesive.

CLTS matching networks were used to modify the sensor output to permit the use of the Budd Model A-110 Strain Indicator equipment to read temperature at 10 micro strain per degree Fahrenheit. A 3-wire system was used to decrease the error due to lead resistance (see Figure 10).

All dial settings on the Budd indicator were set to manufacturer's recommendations.

GF	=	2.00
Multiplier	=	X10
Bridge	=	half

The indicated output on the Budd indicator will be directly in °F.

Five temperature baths were established and allowed to stablize. The temperature of each bath was measured using a platinium resistance standard thermometer to ±.02°F. The CLTS was inserted in the bath and temperature read out on Budd indicator.

4.0 UNCERTAINTY MEASUREMENT:

Measurement uncertainty for acceleration pressure displacement measurements was determined from the following relationship.

$$(1)\quad W_R = \left[\left(\frac{\partial R}{\partial X_1} W_1\right)^2 + \left(\frac{\partial R}{\partial X_2} W_2\right)^2 + \cdots \left(\frac{\partial R}{\partial X_n} W_n\right)\right]^{1/2}$$

where:

$X_1, X_2, \ldots X_n$ = independent variables

$R = R(X_1, X_2, \ldots X_n)$

W_R = uncertainty in the result

$W_1, W_2, \ldots W_n$ = uncertainty in the independent variable

Each measurement will be treated independently and the results tabulated in Table 5.

Nomenclature for calculations:

E_T = Voltage output of test channel

E_S = Voltage output of standard channel

K = Cathode follower gain

g = Vibration level

S_T = Voltage sensitivity of test transducer

S_S = Voltage sensitivity of standard accelerometer system

Q_T = Charge sensitivity of test accelerometer

C_T = Total external capacitance

p = Pressure

D = Displacement

A. Acceleration

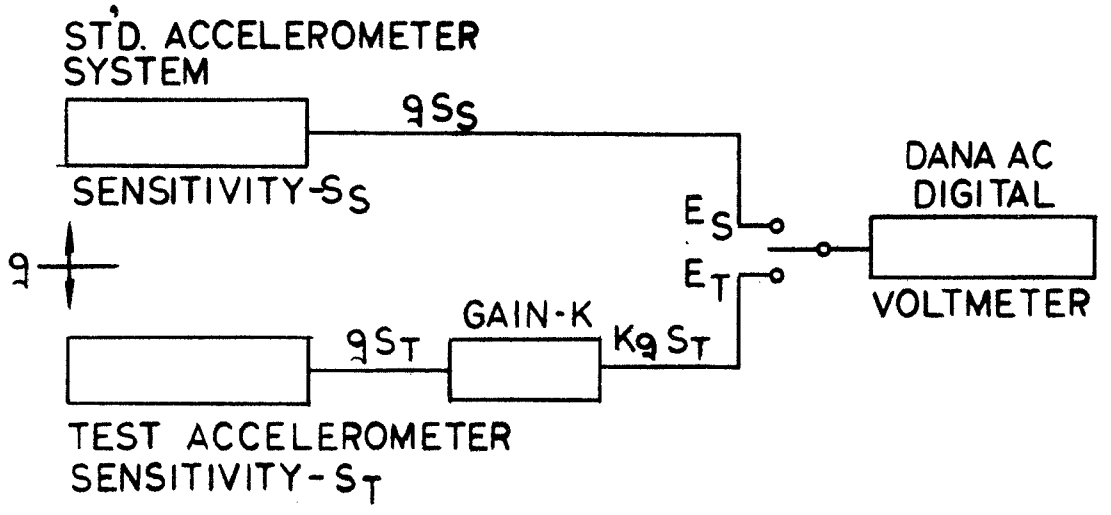

(1) $E_T = KgS_T$

(2) $E_S = g S_S$

(3) $Q_T = C_T S_T$

From equations (1), (2), and (3) the following form for Q_T is derived.

(4) $Q_T = C_T S_S \frac{E_T}{E_S}$

Applying equation (4) to uncertainty equation for W_R by setting Q = R

$$W_Q = \left[\left(\frac{\partial Q}{\partial C_T} W_{C_T} \right)^2 + \left(\frac{\partial Q}{\partial S_S} W_{S_S} \right)^2 + \left(\frac{\partial Q}{\partial E_T} W_{E_T} \right)^2 + \left(\frac{\partial Q}{\partial K} W_K \right)^2 + \left(\frac{\partial Q}{\partial E_S} W_{E_S} \right)^2 \right]^{1/2}$$

Let $P_1, P_2, \ldots P_n$ = Percentage uncertainty in each independent variable.

Let W'_Q = the total percentage uncertainty in Q

$$W'_Q = \frac{100 W_Q}{C_T \frac{S_S}{K} \frac{E_T}{E_S}} = \left[\left(P_{C_T} \right)^2 + \left(P_{S_S} \right)^2 + \left(P_{E_T} \right)^2 + \left(-P_K \right)^2 + \left(-P_{E_S} \right)^2 \right]^{1/2}$$

(5)

$P_{C_T} = .5$

$P_{S_S} = 1$

$P_{E_T} = .1$

$P_K = .2$

$P_{E_S} = .1$

$$\omega'_Q = \left[(.5)^2 + (1)^2 + (.1)^2 + (.2)^2 + (.1)^2\right]^{1/2} = 1.15$$

B. Pressure System

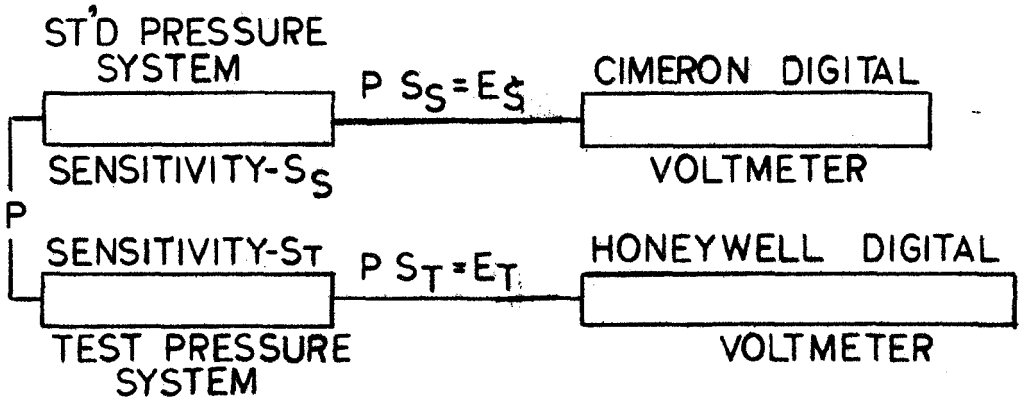

(1) $E_T = PS_T$

(2) $E_S = PS_S$

Solving (1) and (2) for S_T

(3) $S_T = S_S \frac{E_T}{E_S}$

Applying equation (3) to uncertainty equation W_R by setting $S_T = R$

$$\omega_{S_T} = \left[\left(\frac{\partial S_T}{\partial S_S}\omega_{S_S}\right)^2 + \left(\frac{\partial S_T}{\partial E_T}\omega_{E_T}\right)^2 + \left(\frac{\partial S_T}{\partial E_S}\right)^2\right]^{1/2}$$

Let $P_1, P_2, \ldots P_n$ = Percentage uncertainty in each independent variable.

Let W'_{S_T} = The total percentage uncertainty in W_{S_T}

$$W'_{S_T} = \frac{100 W_{S_T}}{S_S \frac{E_T}{E_S}} = \left[(P_{S_S})^2 + (P_{E_T})^2 + (P_{E_S})^2 \right]^{1/2}$$

$P_{S_S} = .05$

$P_{E_T} = .83$

$P_{E_S} = .005$

$$W'_{S_T} = \left[(.05)^2 + (.83)^2 + (.005)^2 \right] = 0.835$$

C. Displacement

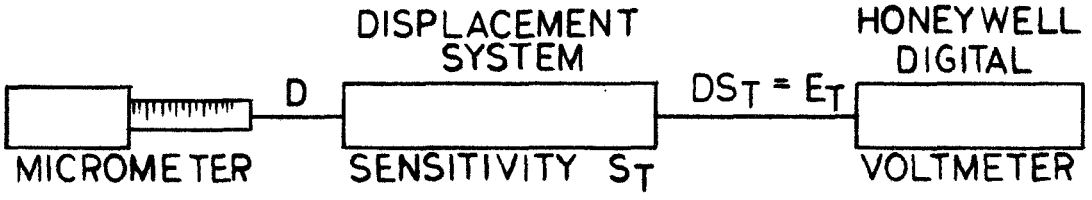

(1) $S_T = \frac{E_T}{D}$

Applying equation (1) to the uncertainty equation for W_R by setting $S_T = R$

$$W_{S_T} = \left[\left(\frac{\partial S_T}{\partial E_T} W_{E_T} \right)^2 + \left(\frac{\partial S_T}{\partial D} W_D \right)^2 \right]^{1/2}$$

Let $P_1, P_2, \ldots P_n$ = Percentage uncertainty in each independent variable.

Let W'_{S_T} = Total percentage uncertainty in W_{S_T}

$$W'_{S_T} = \frac{100\, W_{S_T}}{\frac{E_T}{D}} = \left[\left(P_{E_T} \right)^2 + \left(-P_D \right)^2 \right]^{1/2}$$

$P_D = .125$

$P_{E_T} = .83$

$$W'_{S_T} = \left[(.83)^2 + (.125)^2 \right]^{1/2} = 0.84$$

TABLE 5

	Acceleration	Pressure	Displacement
Uncertainty in %	1.15	.835	.840

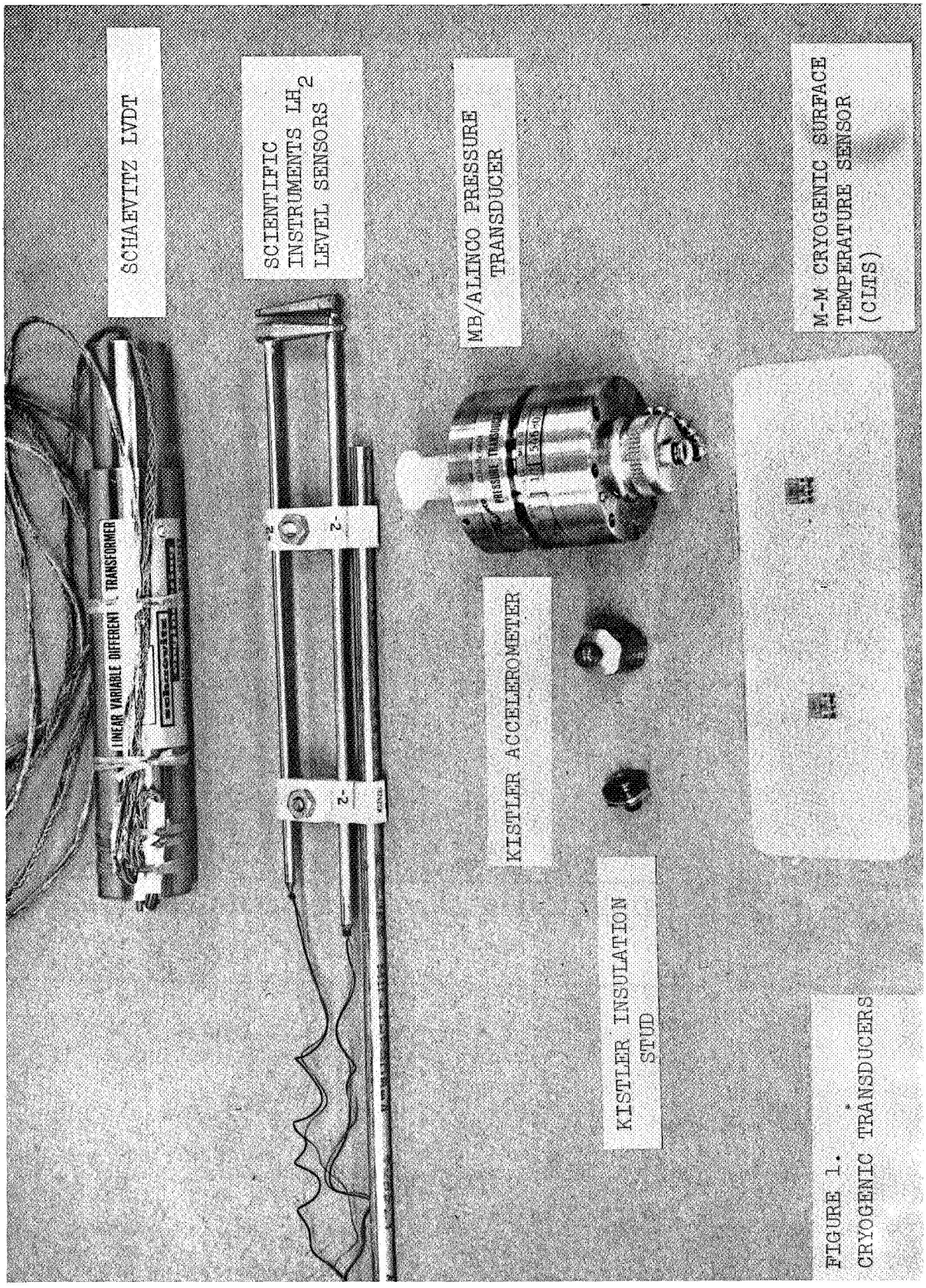

FIGURE 1. CRYOGENIC TRANSDUCERS

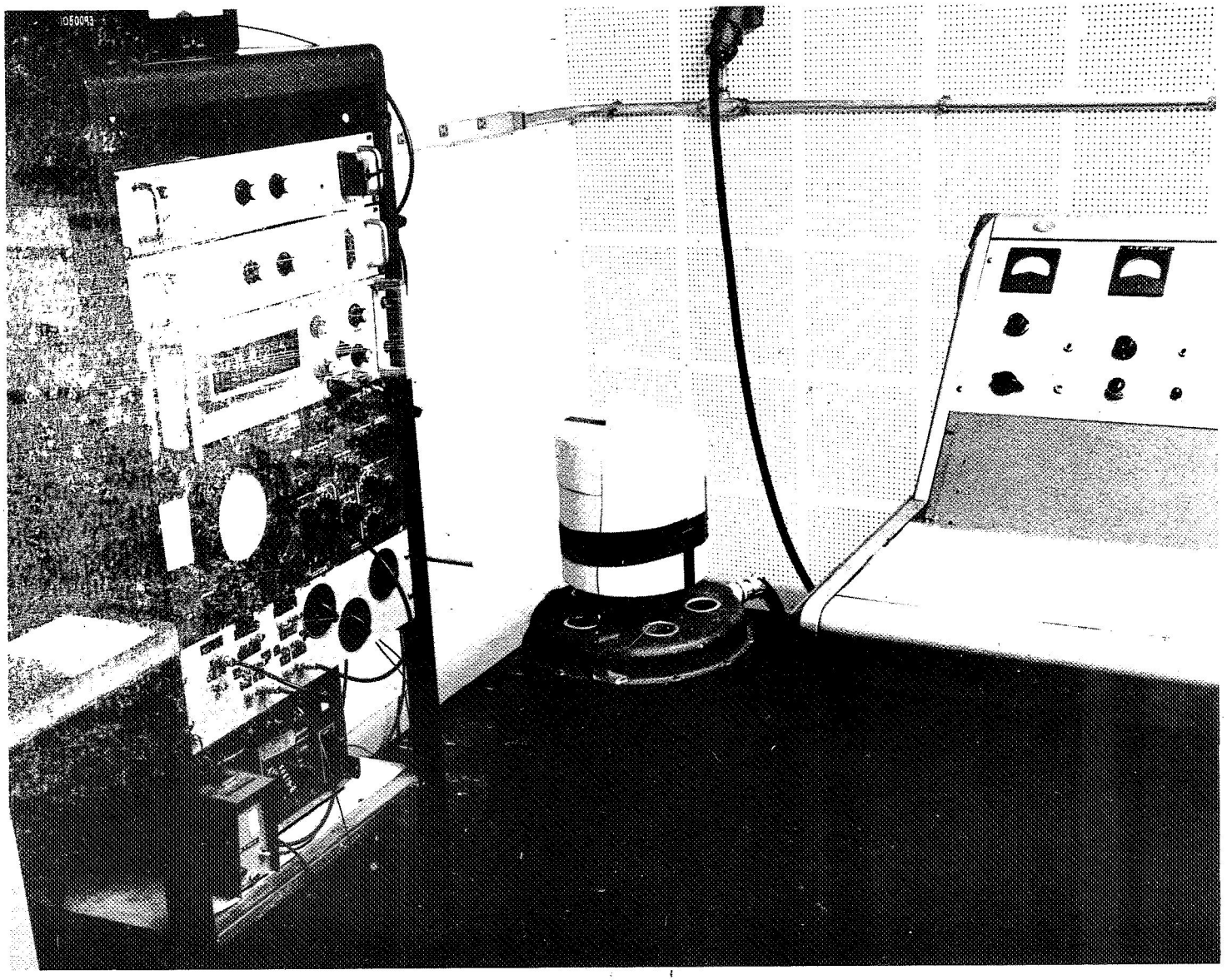

FIGURE 2. CRYOGENIC ACCELEROMETER CALIBRATION

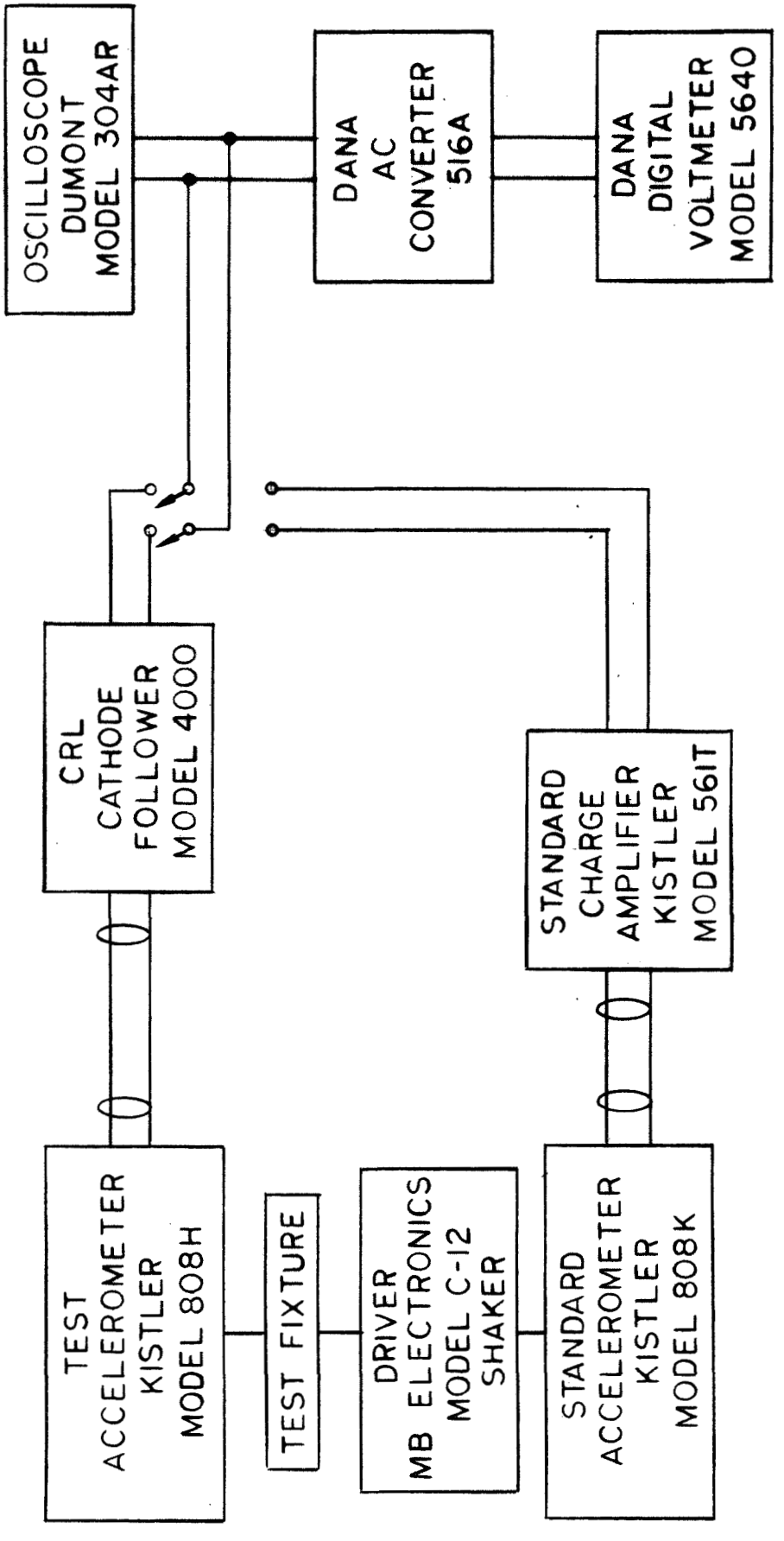

TEST SET-UP, BLOCK DIAGRAM - CRYOGENIC
VIBRATION CALIBRATION OF ACCELEROMETERS

FIGURE 3

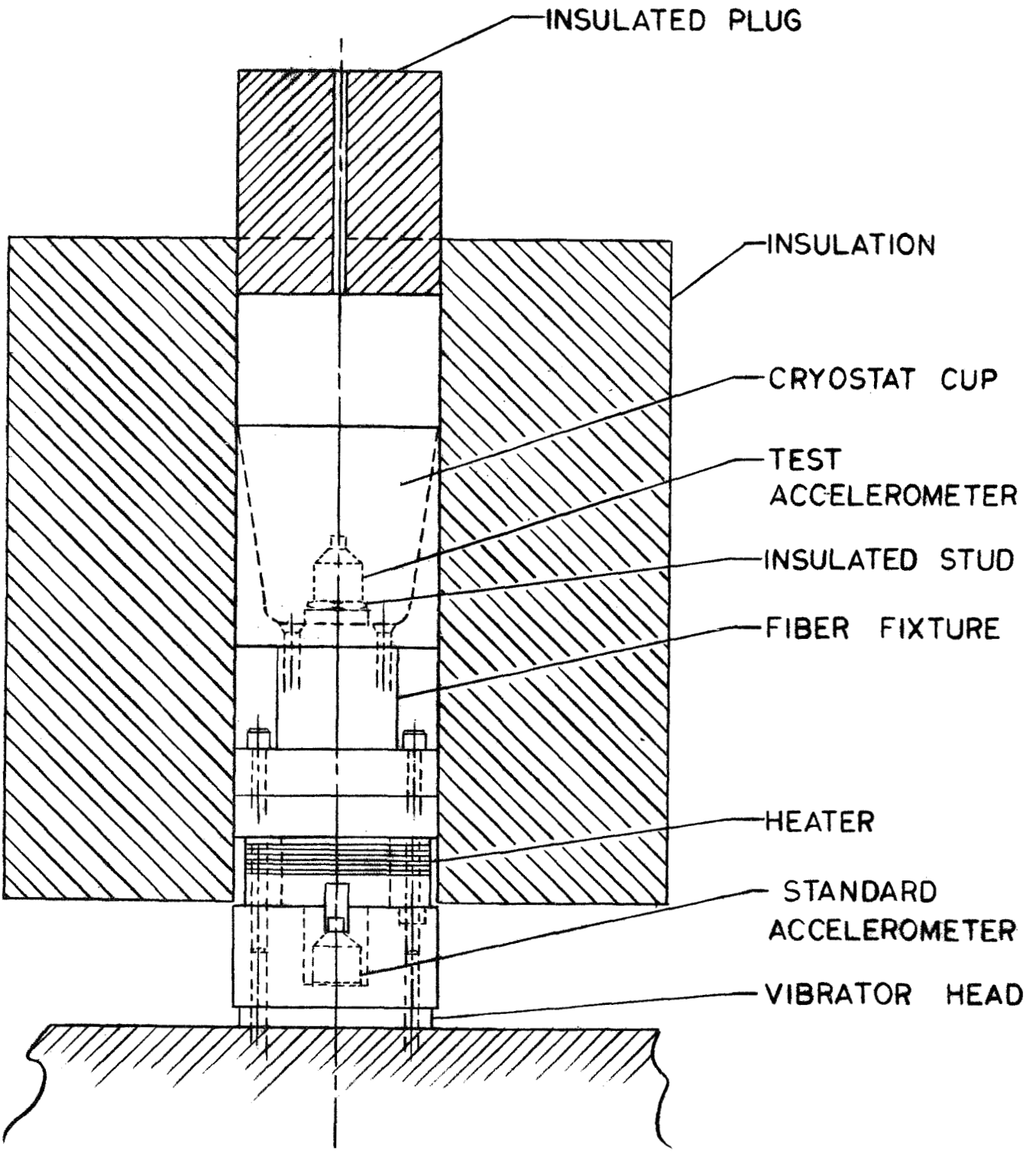

ACCELEROMETER CALIBRATION CRYOSTAT

FIGURE 4

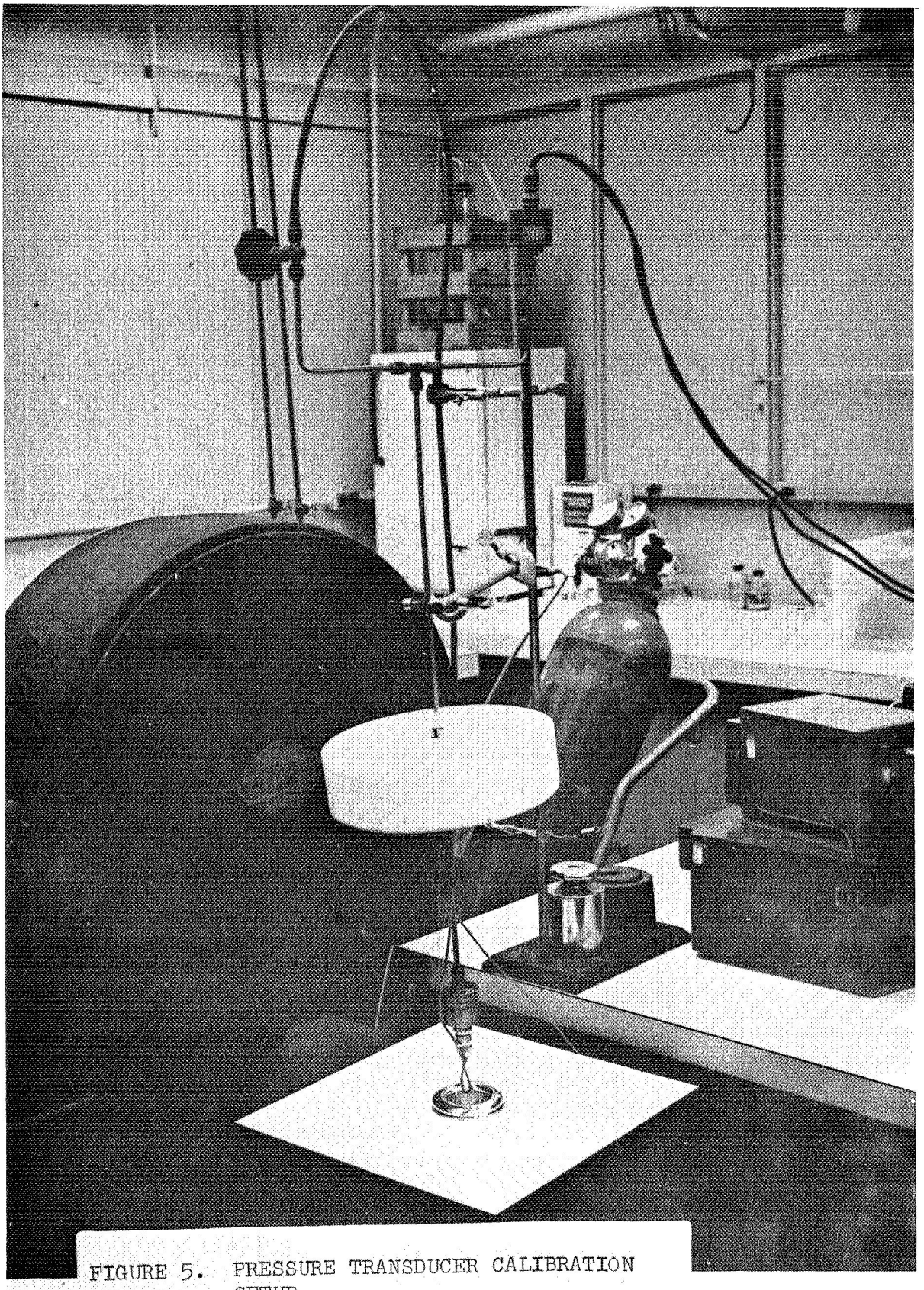

FIGURE 5. PRESSURE TRANSDUCER CALIBRATION SETUP

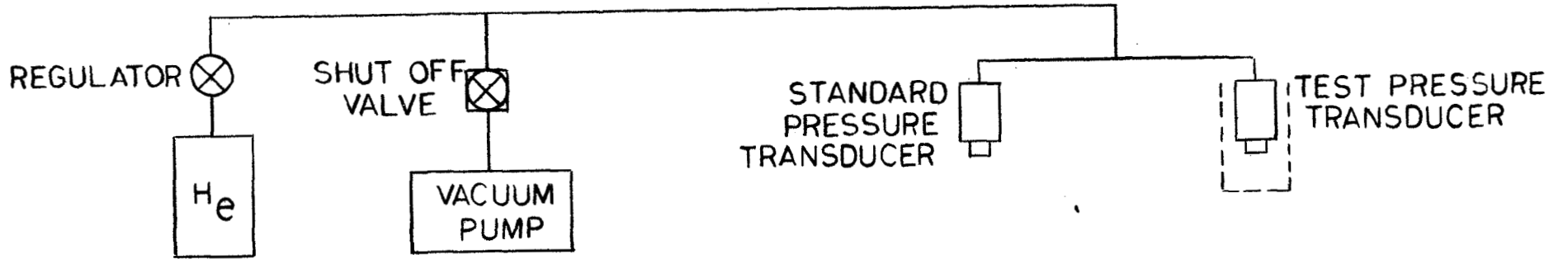

PRESSURIAZATION SYSTEM FOR CALIBRATION OF PRESSURE TRANSDUCER AT CRYOGENIC TEMP

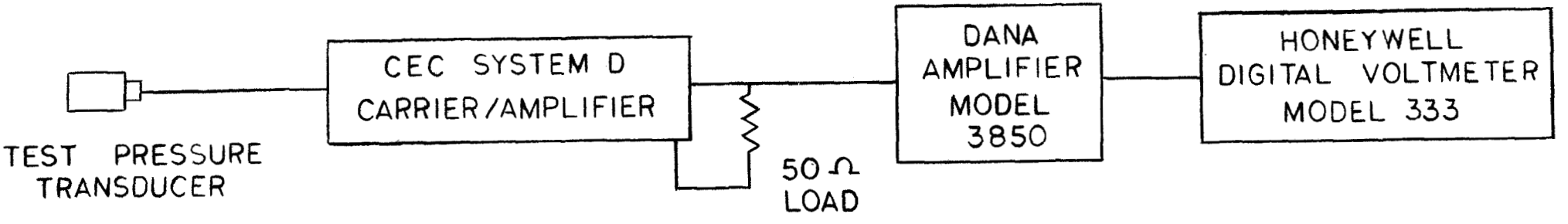

TEST PRESSURE TRANSDUCER SYSTEM

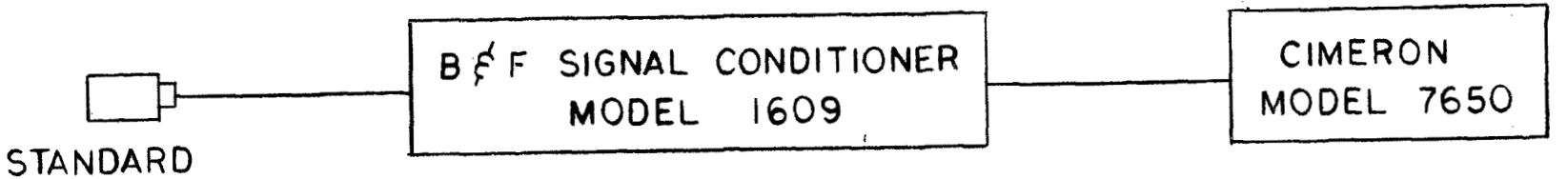

STANDARD PRESSURE TRANSDUCER SYSTEM

FIGURE 6

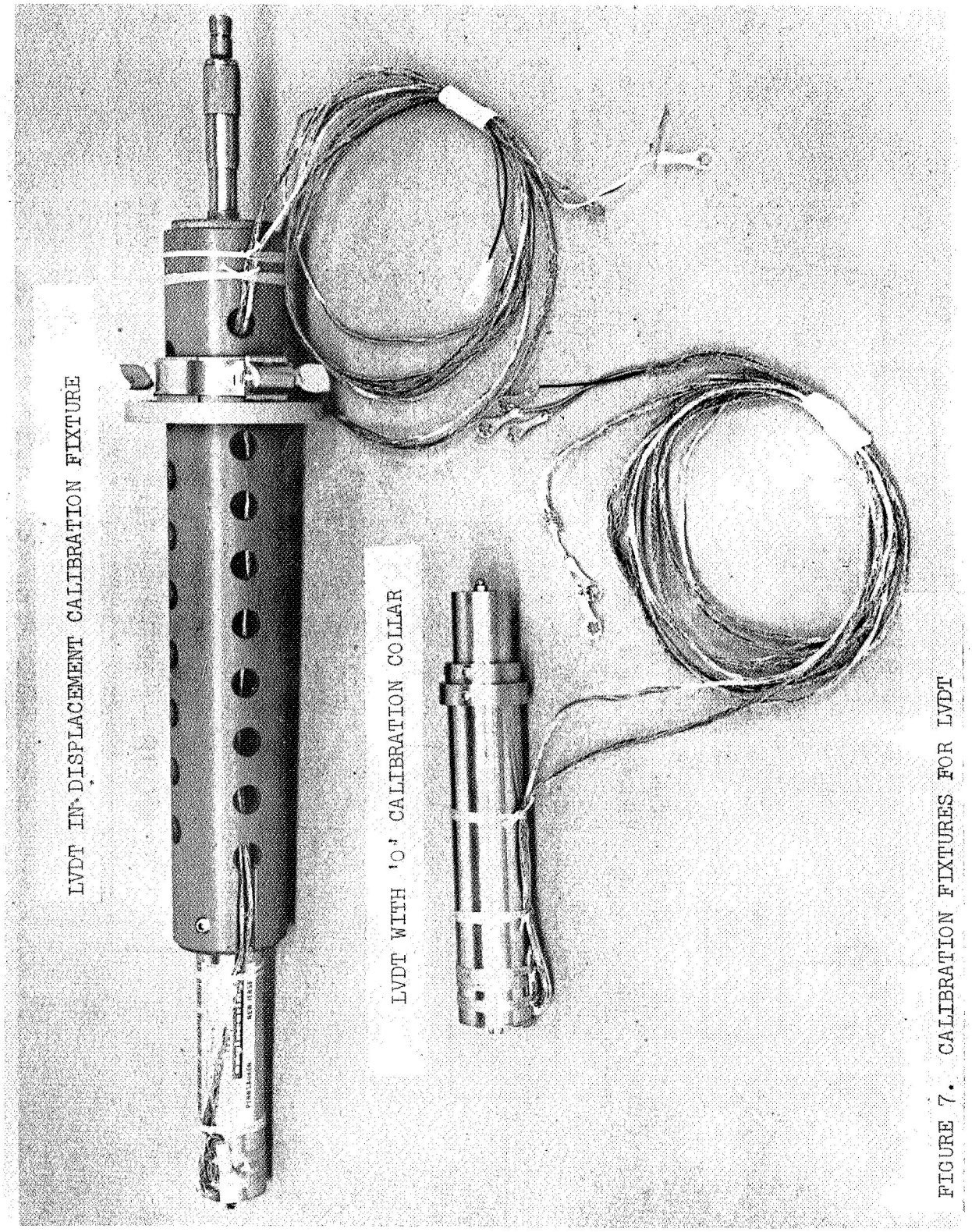

FIGURE 7. CALIBRATION FIXTURES FOR LVDT

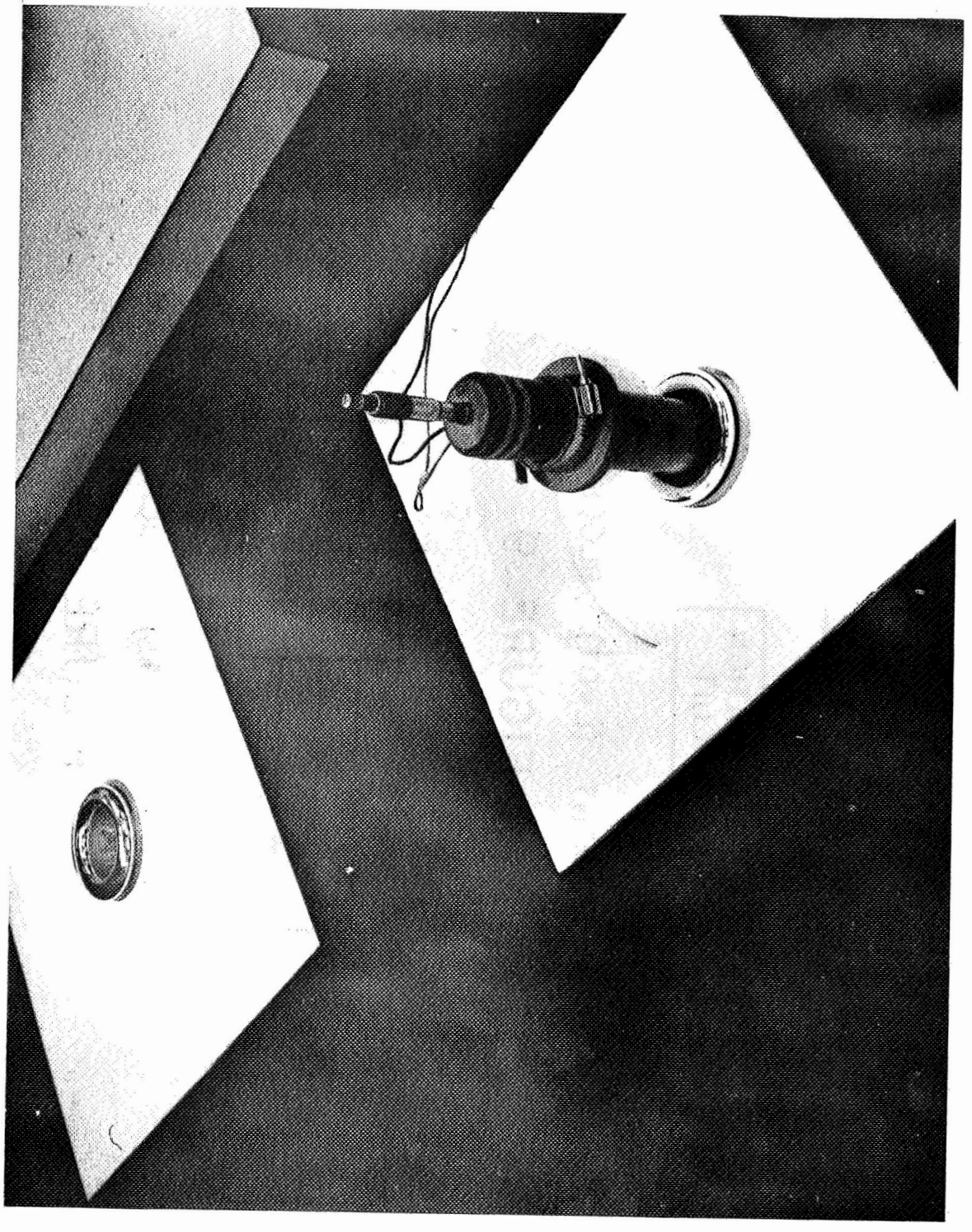

FIGURE 8. LVDT IN LN_2 PRECOOL BATH

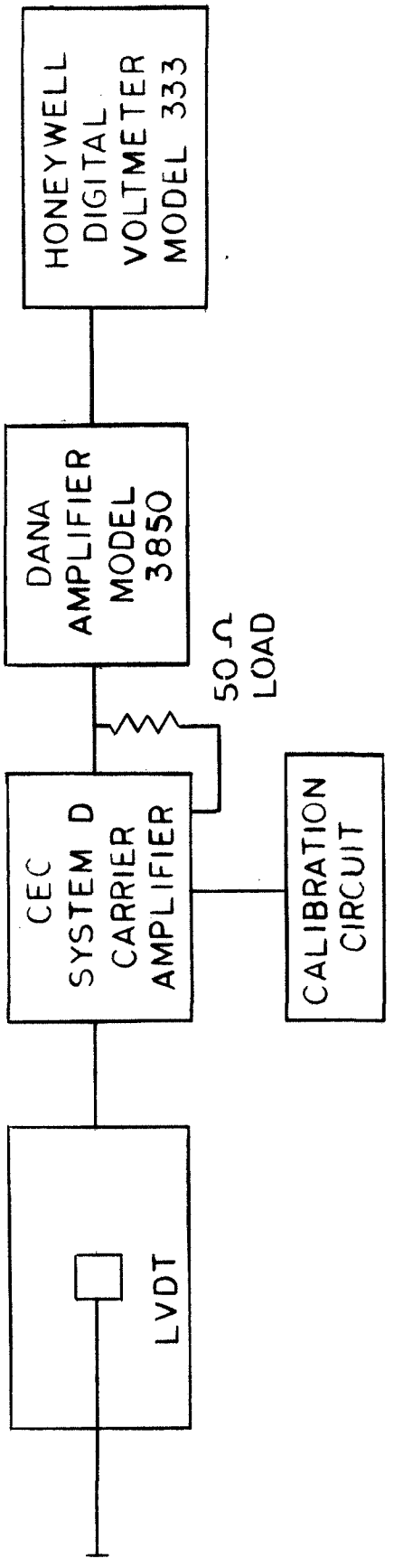

DISPLACEMENT (LVDT) BLOCK DIAGRAM

FIGURE 9

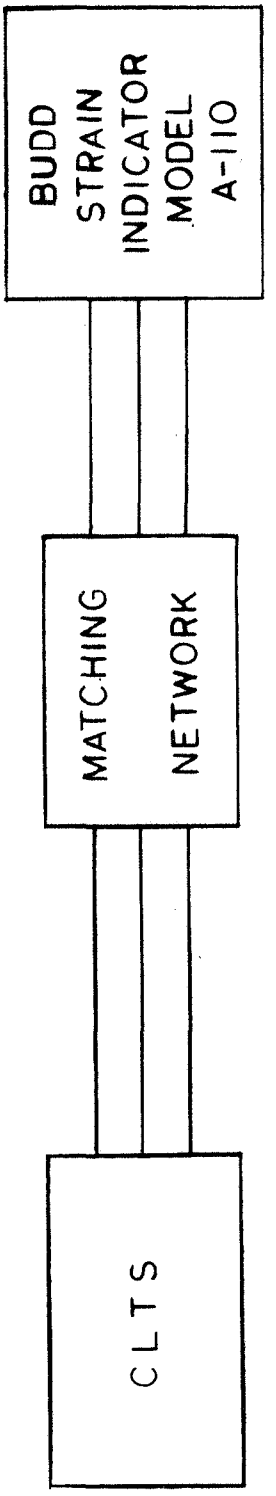

TEMPERATURE (CLTS) BLOCK DIAGRAM

FIGURE 10

APPENDIX B

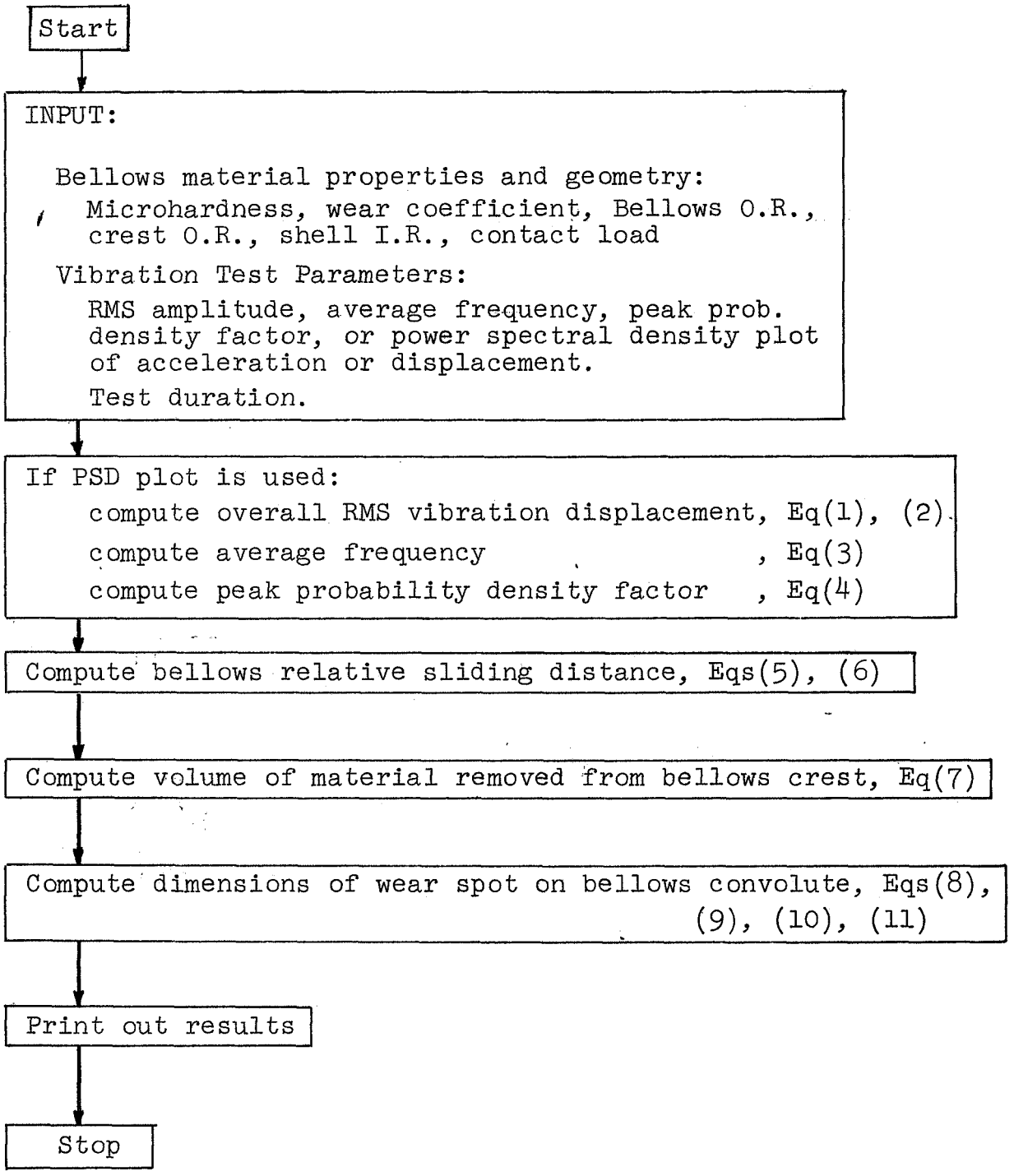

BLOCK DIAGRAM OF CRYOGENIC BELLOWS VIBRATION WEAR PROGRAM

If necessary, convert acceleration PSD to displacement PSD:

$$\text{inch}^2/\text{Hz} = 386^2 \cdot (g^2/\text{Hz})/(2\pi\omega)^4 \quad (1)$$

Equations used in computing overall RMS bellows displacement:

$$\left.\begin{aligned} DB &= \frac{10.0 \log\left(\psi_{i+1}/\psi_i\right)}{1.442 \ln\left(\omega_{i+1}/\omega_i\right)} \\ &\text{if } DB = -3.01 \\ G^2 &= \psi_{i+1} \cdot \omega_{i+1} \cdot \log\left(\frac{\omega_{i+1}}{\omega_i}\right) \\ &\text{if } DB \neq -3.01 \\ G^2 &= \frac{3.01\ (\psi_{i+1})}{(3.01 + DB)} \cdot \left(\omega_{i+1} - \omega_i \cdot \left(\frac{\omega_i}{\omega_{i+1}}\right)^{\left(\frac{DB}{3.01}\right)}\right) \\ \text{overall RMS} &= \sqrt{\Sigma G^2} \end{aligned}\right\} \quad (2)$$

$$\text{Average Zero Crossing Frequency} = \omega_1 \cdot \frac{\sqrt{\Sigma\left(\frac{\omega_i}{\omega_1}\right)\cdot\left(\frac{G_i^2}{G_1^2}\right)}}{\sqrt{\Sigma\left(G_i^2/G_1^2\right)}} = \bar{\omega} \quad (3)$$

$$\alpha = \frac{\left[1.0 + \Sigma_2\left(\frac{\omega_i}{\omega_1}\right)^2\left(\frac{G_i^2}{G_1^2}\right)\right]^2}{\left[1.0 + \Sigma_2\left(\frac{G_i^2}{G_1^2}\right)\right]\left[1.0 + \Sigma\left(\frac{\omega_i}{\omega_1}\right)^4\left(\frac{G_i^2}{G_1^2}\right)\right]} \quad (4)$$

$$\text{Distance} = \sum_{\sigma=0\to5}(4.0 \cdot \chi \cdot \bar{\omega} \cdot \text{Time} \cdot \rho(\chi) \cdot \delta\sigma) \quad (5)$$

$$\rho(\chi) = \frac{1-\alpha^2}{\sqrt{2\pi}} e^{-\frac{1}{2}\left(\frac{\chi}{\sigma} - \sqrt{\alpha}\right)^2} + \alpha^2 \left\{\frac{\left(\frac{\chi}{\sigma} - 1 - \sqrt{\alpha}\right) + \left|\frac{\chi}{\sigma} + 1 - \sqrt{\alpha}\right|}{2}\right\} e^{-\frac{1}{2}\left(\frac{\chi}{\sigma} + 1 - \sqrt{\alpha}\right)^2} \quad (6)$$

$$V = \frac{k.P.\text{Distance}}{3.0\ H_M\ g} \quad (7)$$

Bellows crest (torus) equations:

$$\left[(X-d)^2 + Y^2 + Z^2 - (R_B^2 + r^2)\right]^2 = 4 R_B^2 (r^2 - Y^2) \quad (8)$$

Shell equation:

$$X^2 + Z^2 = R_S^2 \quad (9)$$

Solve Bellows-Shell equations iteratively until enclosed volume = wear volume → yields wear depth.

$$\text{Wear spot width} = 2.0\sqrt{r^2 - (R_S - d - R_B)^2} \quad (10)$$

$$\text{Wear spot chord} = 2.0\sqrt{R_S^2 - \left(\frac{(R_B+r)^2 - R_S^2 - d^2}{2d}\right)^2} \quad (11)$$

NOMENCLATURE:

ω	=	frequency
ψ	=	power spectral density
DB	=	local slope of P.S.D. plot
χ	=	peak displacement
σ	=	RMS displacement
k	=	wear coefficient
P	=	Bellows - shell normal force
H_M	=	Bellows microhardness
R_S	=	Inside radius of shell
R_B	=	Outside radius of Bellows
r	=	Bellows crest outside radius
d	=	Bellows centerline offset in direction of worn spot
Y	=	axis of centerline of shell
X	=	"vertical" axis of bellows & shell (wear occurs on "bottom" of X axis)
Z	=	" horizontal" axis
g	=	acceleration of gravity

APPENDIX C

DISTRIBUTION LIST

REPORT COPIES R	REPORT COPIES D	RECIPIENT	DESIGNEE
		National Aeronautics & Space Administration Lewis Research Center 21000 Brookpark Road Cleveland, Ohio 44135	
1		Attn: Contracting Officer, MS 500-313	
5		Liquid Rocket Technology Branch, MS 500-209	
1		Technical Report Control Office, MS 5-5	
1		Technology Utilization Office, MS 3-16	
2		AFSC Liaison Office, 501-3	
2		Library	
1		Office of Reliability & Quality Assurance, MS 500-111	
1		D. L. Nored, Chief, LRTB, MS 500-209	
5		R. E. Grey, Project Manager, MS 500-209	
1		E. W. Conrad, MS 500-204	
1		J. W. Gregory, MS 500-209	
2		Chief, Liquid Experimental Engineering, RPX Office of Advanced Research & Technology NASA Headquarters Washington, D. C. 20546	
2		Chief, Liquid Propulsion Technology, RPL Office of Advanced Research & Technology NASA Headquarters Washington, D. C. 20546	
1		Director, Launch Vehicles & Propulsion, SV Office of Space Science & Applications NASA Headquarters Washington, D. C. 20546	
1		Chief, Environmental Factors & Aerodynamics Code RV-1 Office of Advanced Research & Technology NASA Headquarters Washington, D. C. 20546	
1		Chief, Space Vehicles Structures Office of Advanced Research & Technology NASA Headquarters Washington, D. C. 20546	

REPORT COPIES R	REPORT COPIES D	RECIPIENT	DESIGNEE
1		Director, Advanced Manned Missions, MT Office of Manned Space Flight NASA Headquarters Washington, D. C. 20546	
6		NASA Scientific & Technical Information Facility P.O. Box 33 College Park, Maryland 20740	
1		Director, Technology Utilization Division Office of Technology Utilization NASA Headquarters Washington, D. C. 20546	
1		National Aeronautics & Space Administration Ames Research Center Moffett Field, California 94035 Attn: Library	Hans M. Mark Mission Anal. Division
1		National Aeronautics & Space Administration Flight Research Center P.O. Box 273 Edwards, California 93523 Attn: Library	
1		National Aeronautics & Space Administration Goddard Space Flight Center Greenbelt, Maryland 20771 Attn: Library	Merland L. Moseson, Code 620
1		National Aeronautics & Space Administration John F. Kennedy Space Center Cocoa Beach, Florida 32931 Attn: Library	Dr. Kurt H. Debus
1		National Aeronautics & Space Administration Langley Research Center Langley Station Hampton, Virginia 23365 Attn: Library	E. Cortwright Director
3		National Aeronautics & Space Administration Manned Spacecraft Center Houston, Texas 77001 Attn: Library Charles Yodzis Code EP-2 Henry Pohl Code EP-4	J.G.Thiobodaux, Jr., Chief, Propulsion & Power Division

REPORT COPIES R	D	RECIPIENT	DESIGNEE
4		National Aeronautics & Space Administration George C. Marshall Space Flight Center Huntsville, Alabama 35812 Attn: Library Jerry Thomson, PD-RV John McCarty, R-P&VE Charlie Johnston, PD-RV-V	Hans G. Paul Leon J.Hastings James Thomas Dale Burrows I. G. Yates Clyde Nevins J. Blumrich
1		Jet Propulsion Laboratory 4800 Oak Grove Drive Pasadena, California 91103 Attn: Library	Henry Burlage,Jr. Duane Dipprey
1		Defense Documentation Center Cameron Station Building 5 5010 Duke Street Alexandria, Virginia 22314 Attn: TISIA	
1		Office of the Director of Defense Research & Engineering Washington, D. C. 20301 Attn: Office of Asst. Dir. (Chem. Technology)	
1		RTD (RTNP) Bolling Air Force Base Washington, D. C. 20332	
1		Arnold Engineering Development Center Air Force Systems Command Tullahoma, Tennessee 37389 Attn: Library	Dr. H.K.Doetsch
1		Advanced Research Projects Agency Washington, D. C. 20525 Attn: Library	
1		Aeronautical Systems Division Air Force Systems Command Wright-Patterson Air Force Base, Dayton, Ohio Attn: Library	D. L. Schmidt Code ARSCNC-2
1		Air Force Missile Test Center Patrick Air Force Base, Florida Attn: Library	L. J. Ullian
1		Air Force Systems Command Andrews Air Force Base Washington, D. C. 20332 Attn: Library	Capt. S. W. Bowen SCLT

REPORT COPIES R	D	RECIPIENT	DESIGNEE
2		Air Force Rocket Propulsion Laboratory (RPR) Edwards, California 93523 Attn: Library Tom Waddell RPRPD	Robert Wiswell W. W. Wells
1		Air Force Rocket Propulsion Laboratory (RPM) Edwards, California 93523 Attn: Library	
1		Air Force FTC (FTAT-2) Edwards Air Force Base, California 93523 Attn: Library	Donald Ross
1		Air Force Office of Scientific Research Washington, D. C 20333 Attn: Library	SREP, Dr. J. F. Masi
1		Director (Code 6180) U. S. Naval Research Laboratory Washington, D. C. 20390 Attn: Library	H. W. Carhart J. M. Krafft
1		Picatinny Arsenal Dover, New Jersey 07801 Attn: Library	I. Forsten
1		Air Force Aero Propulsion Laboratory Research & Technology Division Air Force Systems Command United States Air Force Wright-Patterson AFB, Ohio 45433 Attn: APRP (Library)	R. Quigley C.M.Donaldson
1		Electronics Division Aerojet-General Corporation P.O. Box 296 Azusa, California 91703 Attn: Library	W. L. Rogers
1		Space Division Aerojet-General Corporation 9200 East Flair Drive El Monte, California 91734 Attn: Library	S. Machlawski
1		Aerojet Ordnance and Manufacturing Aerojet-General Corporation 11711 South Woodruff Avenue Fullerton, California 90241 Attn: Library	

REPORT COPIES R	D	RECIPIENT	DESIGNEE
1		Aerojet Liquid Rocket Company P. O. Box 15847 Sacramento, California 95813 Attn: Technical Library 2484-2015A	R. Stiff C. W. Williams
1		Aeronutronic Division of Philco Ford Corp. Ford Road Newport Beach, California 92663 Attn: Technical Information Department	Dr. L.H.Linder
1		Space & Missile Systems Organization Air Force Unit Post Office Los Angeles, California 90045 Attn: Technical Data Center	
1		Office of Research Analyses (OAR) Holloman Air Force Base, New Mexico 88330 Attn: Library RRRD	
1		U. S. Air Force Washington, D. C. Attn: Library	Col. C. K. Stambaugh, Code AFRST
1		Commanding Officer U. S. Army Research Office (Durham) Box CM, Duke Station Durham, North Caroline 27706 Attn: Library	
1		U. S. Army Missile Command Redstone Scietific Information Center Redstone Arsenal, Alabama 35808 Attn: Document Section	Dr. W. Wharton
1		Bureau of Naval Weapons Department of the Navy Washington, D. C. Attn: Library	J. Kay, Code RTMS-41
1		Commander U. S. Naval Missile Center Point Mugu, California 93041 Attn: Technical Library	
1		Commander U. S. Naval Weapons Center China Lake, California 93557 Attn: Library	

REPORT COPIES R	D	RECIPIENT	DESIGNEE
1		Bellcomm 955 L'Enfant Plaza, S.W. Washington, D. C. Attn: Library	H. S. London C. Bendersky
1		Boeing Company Space Division P.O. Box 868 Seattle, Washington 98124 Attn: Library	J. D. Alexander C. F. Tiffany
1		Boeing Company 1625 K Street, N.W. Washington, D. C. 20006	
1		Boeing Company P.O. Box 1680 Huntsville, Alabama 35801	Ted Snow
1		Chemical Propulsion Information Agency Applied Physics Laboratory 8621 Georgia Avenue Silver Spring, Maryland 20910	Tom Reedy
1		Chrysler Corporation Missile Division P.O. Box 2628 Detroit, Michigan Attn: Library	John Gates
1		Chrysler Corporation Space Division P.O. Box 29200 New Orleans, Louisiana 70129 Attn: Librarian	
1		Curtiss-Wright Corporation Wright Aeronautical Division Woodridge, New Jersey Attn: Library	G. Kelley
1		University of Denver Denver Research Institute P.O. Box 10127 Denver, Colorado 80210 Attn: Security Office	
1		Fairchild Stratos Corporation Aircraft Missiles Division Hagerstown, Maryland Attn: Library	

REPORT COPIES R D	RECIPIENT	DESIGNEE
1	Commanding Officer Naval Research Branch Office 1030 E. Green Street Pasadena, California 91101 Attn: Library	
1	Aerospace Corporation 2400 E. El Segundo Blvd. Los Angeles, California 90045 Attn: Library-Documents	J. G. Wilder W. Wetmore
1	Arthur D. Little, Inc. 20 Acorn Park Cambridge, Massachusetts 02140 Attn: Library	A. C. Tobey
1	Astropower Laboratory McDonnell-Douglas Aircraft Company 2121 Paularino Newport Beach, California 92163 Attn: Library	
1	ARO, Incorporated Arnold Engineering Development Center Arnold AF Station, Tennessee 37389 Attn: Library	
1	Susquehanna Corporation Atlantic Research Division Shirley Highway & Edsall Road Alexandria, Virginia 22314 Attn: Library	
1	Beech Aircraft Corporation Boulder Facility Box 631 Boulder, Colorado Attn: Library	Douglas Pope
1	Bell Aerospace Company P.O. Box 1 Buffalo, New York 14240 Attn: Library	T. Reinhardt J. R. Flanagan
1	Instruments & Life Support Division Bendix Corporation P.O. Box 4508 Davenport, Iowa 52808 Attn: Library	W. M. Carlson

REPORT COPIES R	D	RECIPIENT	DESIGNEE
1		Research Center Fairchild Hiller Corporation Germantown, Maryland Attn: Library	Ralph Hall
1		Republic Aviation Fairchild Hiller Corporation Farmington, Long Island New York	
1		General Dynamics/Convair P.O. Box 1128 San Diego, California 92112 Attn: Library	Frank Dore R. Nau
1		Missiles and Space Systems Center General Electric Company Valley Forge Space Technology Center P.O. Box 8555 Philadelphia, Pa. 19101 Attn: Library	A. Cohen F. Schultz
1		General Electric Company Flight Propulsion Lab. Department Cincinnati, Ohio Attn: Library	D. Suichu Leroy Smith
1		Grumman Aircraft Engineering Corporation Bethpage, Long Island, New York Attn: Library	Joseph Gavin R. Grossman
1		Hercules Powder Company Allegheny Ballistics Laboratory P.O. Box 210 Cumberland, Maryland 21501 Attn: Library	
1		Honeywell, Inc. Aerospace Division 2600 Ridgeway Road Menneapolis, Minnesota Attn: Library	
1		IIT Research Institute Technology Center Chicago, Illinois 60616 Attn: Library	C. K. Hersh
1		Kidde Aer-Space Division Walter Kidde & Company, Inc. 367 Main Street Belleville, New Jersey 07107	R. J. Hanville

REPORT COPIES R	D	RECIPIENT	DESIGNEE
1		Ling-Temco-Vought Corporation P.O. Box 5907 Dallas, Texas 75222 Attn: Library	
1		Lockheed Missiles and Space Company P.O. Box 504 Sunnyvale, California 94087 Attn: Library	W. Sterbentz
1		Lockheed Propulsion Company P.O. Box 111 Redlands, California 92374 Attn: Library	H. L. Thackwell
1		Marquardt Corporation 16555 Saticoy Street Box 2013 - South Annex Van Nuys, California 91409	Irv Glasser T. Hudson
1		Radio Corporation of America Astro-Electronics Products Princeton, New Jersey Attn: Library	Y. Brill
1		Rocket Research Corporation Willow Road at 116th Street Redmond, Washington 98052 Attn: Library	F. McCullough, Jr.
1		Stanford Research Institute 333 Ravenswood Avenue Menlo Park, California 94025 Attn: Library	Dr. Gerald Marksman
1		Thiokol Chemical Corporation Redstone Division Huntsville, Alabana Attn: Library	John Goodloe
1		TRW Systems, Inc. 1 Space Park Redondo Beach, California 90278 Attn: Tech. Lib. Doc. Acquisitions	D. H. Lee
1		TRW TAPCO Division 23555 Euclid Avenue Cleveland, Ohio 44117	P. T. Angell

REPORT COPIES R	D	RECIPIENT	DESIGNEE
1		United Aircraft Corporation 400 Main Street East Hartford, Connecticut 06108 Attn: Library	Dr. David Rix Erle Martin Frank Owen Wm. E. Taylor
1		United Aircraft Corporation Pratt & Whitney Division Florida Research & Development Center P.O. Box 2691 West Palm Beach, Florida 33402 Attn: Library	R. J. Coar Dr. Schmitke Paul Nappi
1		Martin-Marietta Corporation (Baltimore Div.) Baltimore, Maryland 21203 Attn: Library	
1		Denver Division Martin-Marietta Corporation P.O. Box 179 Denver, Colorado 80201 Attn: Library	Dr. Morganthaler F. R. Schwartzber J. McCown
1		Orlando Division Martin-Marietta Corporation Box 5827 Orlando, Florida Attn: Library	J. Fern
1		Western Division McDonnell Douglas Astronautics 5301 Bolsa Ave. Huntington Beach, California 92647 Attention: Library	R. W. Hallet C. W. Burge P. Klevatt R. J. Gunkel
1		McDonnell Douglas Aircraft Corporation P. O. Box 516 Lambert Field, Missouri 63166 Attn: Library	R. A. Herzmark D. Stone
		Rocketdyne Division North American Rockwell Inc. 6633 Canoga Avenue Canoga Park, California 91304 Attn: Library, Department 596-306	Dr. R. J. Thompso S. F. Iacobellis S. Domokos
1		Space & Information Systems Division North American Rockwell 12214 Lakewood Blvd. 12214 Lakewood Blvd. Downey, California Attn: Library	Dr. L. A. Harris

REPORT COPIES R	D	RECIPIENT	DESIGNEE
1		Northrop Space Laboratories 3401 West Broadway Hawthorne, California Attn: Library	Dr. William Howard
1		Purdue University Lafayette, Indiana 47907 Attn: Library (Technical)	Dr. Bruce Reese
1		United Aircraft Corporation United Technology Center P. O. Box 358 Sunnyvale, California 94038	Dr. David Altman
1		Vickers Incorporated Box 302 Troy, Michigan	
1		Vought Astronautics Box 5907 Dallas, Texas Attn: Library	
1		McDonnell-Douglas Astronautics Co. Eastern Division P.O. Box 5491 Berkley, Missouri 63134 Attn: R. Quest	J. B. Fleming
1		Garrett Corporation AiResearch Division Phoenix, Arizona 85036 Attn: Library	
1		Garrett Corporation AiResearch Division Los Angeles, California Attn: Library	